
A Communication-Theoretic Framework for LLM Agents: Cost-Aware Adaptive Reliability

Hamed Omidvar, Vahideh Akhlaghi

INTELLERCE LLC

San Jose, CA, USA

{hamed.omidvar, vahideh.akhlaghi}@intellerce.com

Abstract

Agents built on large language models (LLMs) rely on a range of reliability techniques, including retry, majority voting, and self-consistency, that have been developed in parallel rather than within a common analytical framework. We observe that an LLM sampled at temperature T is a discrete stochastic channel $p(y | x)$ in the sense of Shannon’s coding theory, and use this identity as the entry point for such a framework grounded in communication theory. Each of these techniques is a special case of one of six classical reliability operators: diversity combining, hybrid retransmission, iterative generator-critic decoding, rateless sampling, structured redundant verification, and difficulty-adaptive routing. Within the framework we give two closed-form results: a noise-variance threshold above which uniform averaging beats quality-weighted averaging, and a contractivity criterion for generator-critic refinement, consistent with a contractive-to-divergent transition we observe between 3B- and 14B-parameter models. We further introduce a cost-aware semantic-nearest-neighbor router whose single Lagrangian knob traverses the quality-cost frontier without retraining. Across six channel configurations spanning local and cloud models on 69 hard tasks, no fixed model-technique-budget choice dominates, motivating per-task allocation. On a 300-item hard split of MMLU, GSM8K, and HumanEval, our router occupies the full empirical Pareto frontier: at matched quality, its normalized cost is $\approx 56\%$ lower than the strongest fixed technique; at matched normalized cost, it improves quality by $\approx 7\%$ (26% over single-shot decoding). These results argue for consolidating these reliability techniques into a single tunable layer informed by channel coding.

1 Introduction

Large language models (LLMs) have become the computational backbone of autonomous AI agents, powering applications from code generation to scientific reasoning [OpenAI, 2023, Anthropic, 2024]. Yet a fundamental tension persists: individual LLM calls are *stochastic and unreliable*. Output quality varies substantially with prompt formulation, sampling temperature, and model choice. Hallucination, logical gaps, and omissions occur unpredictably, particularly on tasks near the frontier of a model’s capability. Current approaches to agent reliability—retry loops, majority voting, and ensemble methods—each address specific failure modes but lack a unified theoretical framework that would provide principled design criteria across techniques. Communication engineering offers such a framework: from Shannon’s channel capacity theorem [Shannon, 1948] through turbo [Berrou et al., 1993] and low-density parity-check (LDPC) codes [Gallager, 1962], it has developed a principled toolkit for *extracting reliable information from unreliable channels*.

Core insight. An autoregressive LLM with weights θ , conditioned on a fixed system prompt with any in-context examples and sampled at temperature T , defines a conditional distribution $p_\theta(y | x)$ over outputs y given task input x . The weights θ and the system context are held fixed across calls and together specify the channel; T is a tunable channel parameter (suppressed in the notation for Preprint.

brevity). Treating each complete generation as a single channel use, $p_\theta(y | x)$ satisfies the definition of a channel transition probability $W(y | x)$ [Shannon, 1948, Cover and Thomas, 2006]. Conditional on this channel context, temperature controls the *sampling* component of noise, while model capacity, training-data coverage, and task-distribution mismatch jointly determine an irreducible “floor” noise that persists even at $T=0$; token-level log-probabilities provide intrinsic soft-decision channel output. Mutual information, channel capacity, diversity combining, and coding gain all have well-defined analogs in this setting, yielding both technique transfer and quantitative predictions about failure modes and operating regimes.

Contributions.

1. **Agent channel model and a unified framework with explicit prior-art mapping.** We formalize the autoregressive language model as a discrete stochastic channel (Sec. 3) and introduce AGENTCODEC (Sec. 4), which instantiates six communication-theoretic reliability operators adapted for LLM agents: diversity combining (selection, equal-gain, maximal-ratio), hybrid retransmission (chase combining and incremental redundancy), iterative generator-critic decoding, rateless sampling, structured redundant verification, and difficulty-adaptive routing. Each widely cited inference-time reliability method (Self-Consistency [Wang et al., 2023], Best-of- N [Chow et al., 2025], Confidence-Informed Self-Consistency [Taubenfeld et al., 2025], Mixture-of-Agents [Wang et al., 2025], Self-Refine [Madaan et al., 2023], Multi-Agent Debate [Du et al., 2024], Chain-of-Verification [Dhuliawala et al., 2024], FrugalGPT/RouteLLM [Chen et al., 2024, Ong et al., 2025]) is a special case of one of these operators at a specific hyperparameter setting (Tables 2 and 6); each AGENTCODEC variant adds one mechanism that the corresponding prior method omits, so at matched call budget it is expected to weakly dominate its baseline, empirically confirmed on 6 of 7 head-to-head comparisons (Table 5), with the one exception itself predicted by the framework (Sec. 5.2).
2. **Two analytical results tying agent behavior to classical decoding theory (Sec. 3.4).** We characterize a *channel-state-information (CSI) noise crossover* (Prop. 1) that sharpens classical noisy-CSI results on maximal-ratio combining [Tomiuk et al., 1999, Gao et al., 2003, Simon and Alouini, 2005] into a one-line diagnostic with closed-form critical variance σ_w^{*2} above which equal-gain combining dominates noisy maximal-ratio combining, reading the local-versus-cloud reversal of Sec. 5.3 as crossing this threshold. We also give a *fixed-point characterization of the iterative-decoding threshold* (Prop. 2) that identifies the LLM refinement operator with a one-dimensional extrinsic-information-transfer (EXIT) recursion whose contraction-versus-expansion dichotomy $|f'(q^\infty)| \leq 1$ is consistent with the 3B/8B/14B transition we observe; the dynamical-systems content is classical, our contributions are the modeling identification and the explicit role of the best-of-sequence guard.
3. **A cost-aware semantic-nearest-neighbor router.** We introduce a dispatcher that embeds each task with a sentence encoder, looks up the per-technique mean quality and cost over its k nearest training-cache neighbors, and selects the technique that maximizes a single cost-regularized objective with one Lagrangian knob λ (Sec. 5.4, Eq. (3)). The same router instance traverses the empirical quality-cost frontier without retraining: on 300 hard-benchmark items it beats the cross-validated best-fixed-technique policy by $\approx 6.8\%$ in mean quality at matched cost, and at matched quality runs at $\approx 55.7\%$ lower normalized cost than fixed-best.
4. **Controlled empirical evaluation across six channel configurations.** We report paired-per-task quality and cost on 69 curated tasks (four categories) and on a 300-task hard split of MMLU, GSM8K, and HumanEval, across six configurations: three local Ollama scales (3B/8B/14B), an Anthropic + OpenAI cloud pair (Claude Haiku 4.5 + GPT-5-mini), and an Ollama-cloud trio (Nemotron-Nano-3 30B + Devstral-Small-2 24B channels, GLM-5.1 judge). The runs empirically trace the iterative-decoding threshold of Prop. 2 across model scales (Fig. 3).

2 Related work

We review the communication-theoretic foundations in Sec. A and focus here on positioning our work. The core communication-theory primitives we use are: *selection combining* (SC, picking the best of several copies), *equal-gain combining* (EGC, averaging copies with equal weight), *maximal-ratio combining* (MRC, weighting copies by their channel-state-information / SC quality estimate), *hybrid automatic repeat request* (HARQ, with the chase-combining variant HARQ-CC and the incremental-redundancy variant HARQ-IR), *forward error correction* (FEC), and *adaptive coding and modulation* (ACM, selecting among modulation-and-coding schemes (MCS) according to a channel-quality indicator).

Sampling and voting. Self-consistency [Wang et al., 2023], its confidence-informed extensions [Taubenfeld et al., 2025, Feng et al., 2025, Cordero-Encinar and Duncan, 2025], best-of- N [Chow et al., 2025, Lightman et al., 2024], and verifier-weighted best-of- N [Li et al., 2023] are selection combining (SC), with the weighted variants amounting to MRC over the discrete answer space. Test-time compute scaling [Snell et al., 2025, Roberts et al., 2026, Zhu et al., 2025] identifies parallel and sequential regimes mapping to diversity combining and HARQ / turbo coding. **Ensembles and routing.** Mixture-of-Agents (MoA) [Wang et al., 2025] is equal-gain combining (EGC); Self-MoA [Li et al., 2025] is time diversity + EGC; Attention-MoA [Wen et al., 2026] approaches maximal-ratio combining (MRC). LLM-Blender [Jiang et al., 2023] performs rank-then-fuse [Chen et al., 2025]. FrugalGPT [Chen et al., 2024] and RouteLLM [Ong et al., 2025] are degenerate adaptive coding and modulation (ACM), adapting only the model without redundancy control. **Iterative refinement.** Self-Refine [Madaan et al., 2023] and Reflexion [Shinn et al., 2023] resemble hybrid automatic repeat request with incremental redundancy (HARQ-IR) without an extrinsic-information constraint. Multi-agent debate [Du et al., 2024, Ning et al., 2025] corresponds to turbo decoding but lacks the extrinsic-only exchange that is central to classical turbo decoders. LLM-as-a-Judge [Zheng et al., 2023] is a noisy channel estimator [Gu et al., 2026, Schroeder and Wood-Doughty, 2024]. Each prior method can be understood as an instance of one communication-theoretic technique; our framework makes this mapping explicit and evaluates all six within a single experimental setup (Tables 1 and 2).

3 The agent channel model

3.1 Agent as stochastic channel

Definition 1 (Agent Channel). Fix a finite token vocabulary \mathcal{V} and let \mathcal{V}^* denote the set of all finite-length token sequences over \mathcal{V} . Let the task (prompt) space be $\mathcal{T} \subseteq \mathcal{V}^*$ and the output space $\mathcal{Y} = \mathcal{V}^*$. An autoregressive language model with parameters θ defines, for each input $x \in \mathcal{T}$ and each sequence $y = (y_1, \dots, y_L) \in \mathcal{Y}$ of length $L = |y|$, the conditional probability

$$p_\theta(y | x) = \prod_{t=1}^{|y|} p_\theta(y_t | y_{<t}, x), \quad (1)$$

where $t \in \{1, \dots, |y|\}$ indexes token position, $y_t \in \mathcal{V}$ is the token at position t , $y_{<t} := (y_1, \dots, y_{t-1})$ denotes the prefix preceding position t (with $y_{<1} := \emptyset$, the empty sequence, and an end-of-sequence symbol terminating the product), and $p_\theta(y_t | y_{<t}, x)$ is the next-token distribution produced by the model’s softmax output. We call $\mathcal{A}_\theta : \mathcal{T} \rightarrow \mathcal{Y}$, $Y \sim p_\theta(\cdot | x)$, an *agent channel*; it is a discrete stochastic channel that is memoryless across independent invocations, each complete generation constituting a single channel use¹. The conditional $p_\theta(y | x)$ satisfies the axioms of a channel transition probability $W(y | x)$ [Shannon, 1948, Cover and Thomas, 2006]: it is non-negative for every (x, y) and sums to one over $y \in \mathcal{Y}$ for every fixed x . The channel’s noise characteristics (temperature-controlled per-token entropy, model-dependent quality) are structured enough for communication-theoretic reliability techniques to transfer, as we demonstrate.

Remark 1 (Temperature as the noise parameter). Let $T > 0$ denote the sampling temperature. Temperature sampling rescales the per-token logits and renormalizes, replacing $p_\theta(\cdot | y_{<t}, x)$ with $p_T(v | y_{<t}, x) \propto p_\theta(v | y_{<t}, x)^{1/T}$ for $v \in \mathcal{V}$. Writing $H_T(Y_t | y_{<t}, x) := -\sum_{v \in \mathcal{V}} p_T(v | y_{<t}, x) \log p_T(v | y_{<t}, x)$ for the per-token Shannon entropy under p_T , one has $H_T \rightarrow 0$ as $T \rightarrow 0^+$ (deterministic channel) and $H_T \rightarrow \log |\mathcal{V}|$ as $T \rightarrow \infty$ (uniform-noise channel). Temperature therefore continuously interpolates between a deterministic and a pure-noise channel, controlling the *sampling* component of channel noise. However, even at $T \rightarrow 0$ (greedy decoding), the channel is not noiseless: errors from limited model capacity, training-data gaps, and task-distribution mismatch persist as an irreducible “floor” noise, analogous to residual interference in communications.

Definition 2 (Quality Function and Channel Estimation). A *quality function* is any map $q : \mathcal{T} \times \mathcal{Y} \rightarrow [0, 1]$ that takes a (task, output) pair (x, y) to a scalar quality score, with $q = 1$ a perfect answer and $q = 0$ a wholly wrong one. The agent channel itself supplies an intrinsic, judge-free reliability mea-

¹The autoregressive factorization in (1) introduces memory *within* a sequence; treating each (prompt, response) pair as one channel use restores memorylessness across uses, the standard block-coding assumption [Cover and Thomas, 2006]. This applies to independent invocations only: multi-turn chains that condition on prior turns (HARQ and turbo, which feed critic feedback into the generator’s prompt) violate it and are analyzed as channels with feedback in Secs. 5.3 and M; the memoryless analysis is used here only for single-turn parallel techniques (diversity combining, fountain, FEC).

sure: given a realized output $y \sim p_\theta(\cdot | x)$ of length $L = |y|$, the *per-token negative log-likelihood* is

$$\mathcal{H}(\mathcal{A}_\theta, x, y) = -\frac{1}{|y|} \sum_{t=1}^{|y|} \log p_\theta(y_t | y_{<t}, x), \quad (2)$$

where t and $p_\theta(y_t | y_{<t}, x)$ are as defined above. Equation (2) is the response-level analogue of the channel’s average per-token Shannon entropy and is the standard agent-uncertainty proxy used in the calibration literature [Kadavath et al., 2022, Kuhn et al., 2023]. Except for variants discussed later that require the availability of log-probabilities, we implement q as a separate large language model (the “judge”), an external channel estimator that plays the role of pilot-based signal-to-noise-ratio estimation in classical receivers; this introduces estimator noise that we discuss in Remark 3.

3.2 Channel Quality and Operating Point

Let p_X be the task distribution over \mathcal{T} . The *expected channel noise rate* is $\bar{\mathcal{H}}(\mathcal{A}_\theta, T) := \mathbb{E}_{X \sim p_X} [\mathbb{E}_{Y \sim p_{\mathcal{T}}(\cdot | X)} [\mathcal{H}(\mathcal{A}_\theta, X, Y)]]$, the average over both the task distribution and the sampling distribution at temperature T , and depends on model parameters θ (neural scaling laws show that training cross-entropy loss decays as $L \propto N^{-\alpha}$ in the model parameter count N [Kaplan et al., 2020, Hoffmann et al., 2022], which upper-bounds $\bar{\mathcal{H}}$ on in-distribution tasks), temperature T (Remark 1), and task difficulty [Yadkori et al., 2024]. Model capacity and task difficulty are *dual*: a hard task on a 70B model may produce the same $\bar{\mathcal{H}}$ as an easy task on a 3B model, so ACM routing by difficulty (Sec. 4) is equivalent to adapting the coding scheme to the operating point [Goldsmith and Chua, 1997]. This duality predicts that a given technique transitions from harmful to beneficial as $\bar{\mathcal{H}}$ decreases, crossing a decoding threshold [ten Brink, 2001]; we confirm this for HARQ in Sec. 6. Full derivations appear in Sec. M.

3.3 Diversity Order

Definition 3 (Agent Diversity Order). Given $d \geq 1$ agent channels $\mathcal{A}_1, \dots, \mathcal{A}_d$, each independently generating $Y_i \sim p_{\theta_i}(\cdot | X)$ with quality scores $q_i := q(X, Y_i) \in [0, 1]$, the ensemble has *diversity order* d . For a threshold $\tau \in (0, 1)$, if the q_i are independent the ensemble outage satisfies $\mathbb{P}(\max_i q_i < \tau) = \prod_i P_{\text{out},i}(\tau)$ with $P_{\text{out},i}(\tau) := \mathbb{P}(q_i < \tau)$, decaying geometrically in d . Correlation through shared training data or aligned prompts gives an *effective diversity* $d_{\text{eff}} \leq d$ (Remark 3; empirically $d_{\text{eff}} \in [1.14, 1.71]$ across our configurations, Table 12 and Sec. M).

Remark 2 (MRC weighting heuristic). By analogy with SNR-proportional MRC in additive white Gaussian noise (AWGN) channels [Proakis and Salehi, 2008], we set $w_i^{\text{MRC}} = q_i / \sum_j q_j$. Because our combiner is a nonlinear LLM and q_i a noisy judge estimate, we treat this as a heuristic and rely on a cyclic-redundancy-check (CRC) style regression guard (Sec. 4) to ensure no degradation versus SC. The CSI-noise crossover that quantifies when this heuristic loses to EGC is in Remark 3 and Sec. 3.4.

Remark 3 (CSI quality and the MRC–EGC reversal). Remark 2 requires branch independence and accurate CSI. In practice LLM outputs are correlated ($d_{\text{eff}} \leq d$) and numeric judge scores are a noisy estimate; we partially mitigate the latter with a sigma-delta-style binary checklist judge (Sec. 4). Residual imperfect-CSI effects can still attenuate MRC’s gain over EGC [Gao et al., 2003, Simon and Alouini, 2005], quantified by the critical variance σ_w^{*2} of Prop. 1. Token log-probabilities offer a complementary intrinsic soft-decision channel that realizes classical soft-input soft-output (SISO) MRC [Kadavath et al., 2022] (Secs. J and M).

3.4 Two analytical results

CSI-noise crossover (Prop. 1). Weighting branches by an estimated quality score helps only as long as those scores are reliable; when the score itself is too noisy, equal-weight averaging is the safer choice. The imperfect-CSI MRC literature [Tomiuk et al., 1999, Gao et al., 2003, Simon and Alouini, 2005] establishes the qualitative collapse of MRC’s advantage as the weighting-noise variance grows; we sharpen this to a one-line diagnostic in elementary symmetric polynomials (S_1, S_2) of the per-branch amplitudes (closed form and linear-Gaussian model in Sec. C.1) and read the local-versus-cloud reversal of Sec. 5.3 as crossing that threshold; the 15-criterion binary checklist drives the judge variance back below the crossover and restores the Cauchy-Schwarz ordering.

Iterative-decoding threshold (Prop. 2). Each refinement round either nudges the answer toward a high-quality target or drags it toward a low-quality one, depending on how the generator-critic loop responds to small changes in current quality; below a critical sensitivity the loop is self-correcting,

Table 1: Communication \rightarrow agent mapping. SC: selection combining; MIMO: multiple-input multiple-output; MCS: modulation and coding scheme. Full table in Sec. A.

Comm. Concept	Agent Analog	Implementation
Diversity (MIMO)	Multi-model/prompt/temp	Diversity ensemble
MRC / SC / EGC	Quality-weighted / best / equal	Combining strategies
HARQ-CC / IR	Retry / retry + critic	Chase / incremental
Turbo codes	Generator-critic loop	Extrinsic info exchange
Fountain codes	Sample until confident	Rateless adaptive
FEC block codes	Structured redundancy	Parity sections
ACM / MCS table	Difficulty-aware routing	5-level MCS table

above it extra rounds inject more noise than they remove, and only the best-of-sequence guard keeps the delivered answer from regressing. We identify the LLM refinement operator with a one-dimensional quality-update map f at its high-quality fixed point q^∞ , recovering the contraction-versus-expansion dichotomy of the EXIT-chart threshold [ten Brink, 2001, Richardson and Urbanke, 2001] as $|f'(q^\infty)| \leq 1$; the dichotomy is consistent with the survivor-cohort transition between 3B, 8B, and 14B generators (Fig. 3). The contraction theorem itself is classical; the contributions are the modeling identification and the explicit role of the best-of-sequence guard (Remark 4), which decouples delivered from unguarded quality even below threshold.

Additional parallels to communication theory can be found in Secs. A and M.

4 System design: AGENTCODEC

AGENTCODEC implements six communication-theoretic reliability techniques, their variants, as well as comparable baseline methods within a three-layer architecture: (1) a *channel layer* wrapping any OpenAI-compatible LLM endpoint as a stochastic channel with cost/latency instrumentation; (2) a *technique layer* implementing all six methods; and (3) an *orchestration layer* that routes tasks and collects metrics. A quality scorer serves as the channel estimator; to avoid severe numeric-rating quantization, the judge answers a weighted binary checklist whose sum yields a fine-grained score on $[0, 1]$ (sigma-delta style, see Sec. D). Tables 1 and 2 summarize the complete mapping; detailed hyperparameters are in Sec. N.

Table 2: **Taxonomic reduction of comparable prior methods.** Every widely cited inference-time reliability method is recovered as a special case of an AGENTCODEC technique by setting a single hyperparameter; the AGENTCODEC variant adds one mechanism the prior method omits, so at matched inference budget it upper-bounds the baseline. See Table 5 for head-to-head evaluation comparisons.

Prior method	AGENTCODEC variant	Reduction (prior = ours when)	Added mechanism
Self-Consistency [Wang et al., 2023]	Div.-MRC-Discrete- N	cluster-MRC, $q_j \equiv 1$	Quality weighting
Best-of- N [Cobbe et al., 2021b, Lightman et al., 2024]	Div.-SC- N	single policy, N temp. draws	Cross-model diversity
Weighted BoN [Li et al., 2023]	Div.-MRC-Discrete- N	single policy, judge-CSI	Cross-model + wider pool
CISC [Taubenfeld et al., 2025]	Div.-MRC-Discrete- N -Soft	single policy, logprob CSI, softmax	Cross-model + wider pool
Mixture-of-Agents [Wang et al., 2025]	Div.-EGC	single layer, $w_i = 1/d$	(identity at single-layer EGC)
Self-Refine [Madaan et al., 2023] / Reflexion [Shinn et al., 2023]	HARQ-IR	free-form (or verbal-RL) critique, full rewrite, last iter	Dedup'd structured critique + corrections + best-of-seq
Multi-agent debate [Du et al., 2024]	Turbo	two generators, no extrinsic split	Extrinsic exchange, interleaver
Chain-of-Verification [Dhuliawala et al., 2024]	FEC	fixed parity = verification	Rate-adaptive parity
FrugalGPT [Chen et al., 2024] / RoutelLM [Ong et al., 2025]	Fountain / ACM (degenerate)	cheap-first cascade (FG) / single-shot model swap (RL), no coding	Sample combining + rate adaptation
Tree-of-Thoughts [Yao et al., 2023]	Div. MRC (temporal)	per-branch eval., select-best	Fountain-style erasure marking

Diversity combining. The framework supports three diversity axes (model, prompt, temperature), each with SC/MRC/EGC combining; in this paper we focus on model diversity. Each branch generates $Y_i = \mathcal{A}_i(X)$, is scored $q_i = q(X, Y_i)$, and MRC combines with weights $w_i = q_i / \sum_j q_j$ (pseudocode in Sec. N). Compile-time prompt construction [Khatab et al., 2024, Liu et al., 2022, Rubin et al., 2022, Zhou et al., 2023, Yang et al., 2024] is an orthogonal, amortized-before-inference source of prompt diversity; composition with decode-time channel combining is left to future work. **HARQ.** HARQ-CC generates R independent attempts and combines equally. HARQ-IR

iteratively refines via a critic that identifies specific errors (new parity); both stop at quality $\geq \tau$. **Turbo decoding.** A generator and critic iteratively exchange *extrinsic* information: each round, the critic provides only *new* feedback (scaled by a damping factor $\alpha < 1$), mirroring the extrinsic-only exchange used in classical turbo decoders. Extrinsic scaling, a severity floor, and adaptive damping prevent the oscillation and over-correction that otherwise plague naive critic-generator loops (Sec. N). **Fountain codes.** Samples are generated until a confidence metric exceeds a threshold. The *rateless* property automatically adapts cost to task difficulty. **FEC.** Structured parity sections (reasoning, self-verification, alternative approach, confidence) are requested alongside the answer at rates $r \in \{3/4, 1/2, 1/3, 1/4\}$. A decoder cross-checks sections (syndrome decoding). **ACM routing.** A difficulty estimator (pilot signal) selects from a modulation-and-coding-scheme (MCS) table (MCS-0 through MCS-4) – or in our case uses more advanced techniques, jointly adapting model and redundancy strategy. **Soft-output variants.** Three optional soft variants (SOFT-MRC, SOFT-FOUNTAIN, SOFT-ACM) replace judge-score CSI with the intrinsic log-likelihood-ratio-like (LLR-like) signal $c(y) = \exp(\frac{1}{L} \sum_t \log p(y_t | y_{<t}, x))$ from L per-token log-probabilities (Sec. J). **Judge, critic, voter.** Judge rates an answer (CSI source); critic rewrites/critiques an answer (extrinsic-information feedback in iterative decoders); voter clusters multiple answers into equivalence classes for discrete MRC/majority aggregation. Judge and voter are decoder-side aggregation operators (post-generation); the critic is part of the iterative decoder loop itself.

5 Experimental Evaluation

5.1 Setup

Tasks. We use two evaluation tiers. *Curated tasks:* 69 tasks across four categories (QA, reasoning, creative, code) at three difficulty tiers (hard/very hard/extreme), designed to produce measurable technique differences at the 3–30B operating points (Sec. B). *Standard benchmarks:* Hard 100-item splits of MMLU, GSM8K, HumanEval (Sec. 5.5).

Models and scoring. We evaluate across six channel configurations (full table in Table 7, Sec. E) spanning local open-weight (3B/8B/14B from Qwen, Llama, Phi, and Gemma families), Anthropic+OpenAI cloud, and an Ollama-cloud trio (NVIDIA NemoTron-Nano-3 30B and Mistral Devstral-Small-2 24B as channels, Zhipu GLM-5.1 as judge). We disable/minimize thinking for reasoning models by default. The standard-benchmark experiment (300 hard items drawn from MMLU, GSM8K and HumanEval) is run on the Ollama-cloud trio. Local configurations additionally enable the four soft-output techniques, which require token-level log-probabilities that the Anthropic API does not currently expose. The judge/synthesizer is deliberately at least as strong as the channel models, analogous to investing in receiver quality in communications [Proakis and Salehi, 2008]. In the Anthropic+OpenAI cloud configuration, Haiku 4.5 serves as both channel and judge, confirming that technique rankings are preserved even without a stronger synthesizer (Sec. E). For verifiable tasks, blended scoring $q = 0.6 \cdot q_{\text{obj}} + 0.4 \cdot q_{\text{judge}}$ mitigates judge unreliability (Sec. D). Thinking is disabled for all reasoning models to isolate the effects of the studied methods. We report quality $q \in [0, 1]$, coding gain (mean quality improvement over the uncoded baseline), and cost overhead (normalized cost). Means come with 95% bootstrap confidence intervals; significance via paired Wilcoxon signed-rank tests on per-task differences. Full model configurations are in Table 7 and a summary of technique gains across configurations is in Table 8, both in Sec. E.

5.2 Baselines and direct comparisons to prior methods

We re-implement Self-Consistency, Best-of- N , Weighted Best-of- N , Confidence-Informed Self-Consistency, Mixture-of-Agents, Self-Refine, and Chain-of-Verification as standalone techniques (not AGENTCODEC variants), following the canonical recipes in the cited papers, scored on the same tasks and judge as the AGENTCODEC runs. Each prior method is a special case of one of three combining operators (selection / equal-gain / maximal-ratio) over one of two answer spaces (continuous free-form text or discrete equivalence classes), with three orthogonal knobs: the CSI source $\in \{\text{judge score, log-probability, trained process reward model, none}\}$, the pool size N , and whether combining is passive or iterative; full operator-view derivations are in Sec. F and Table 2. Two of our techniques widen this lattice to a multi-model channel pool: *Diversity-SC- N* cycles N samples through the configured channels and selects the argmax-quality sample (collapses to Best-of- N at one channel); *Diversity-MRC-Discrete- N* adds a voter clustering step and applies cluster-summed-quality MRC (collapses to Weighted Best-of- N / CISC at one channel, to Self-Consistency at uniform per-sample weights). *Quality and cost.* On the 300-task hard-benchmark split (Ollama-cloud trio, Table 8), *Diversity-MRC-Discrete- N* beats CISC by ≈ 9.5 percentage points in quality at $\approx 6\%$ extra cost and beats Self-Consistency by ≈ 0.9 percentage points at $\approx 17\%$ lower cost; *Diversity-SC- N* beats

Best-of- N by ≈ 5.2 percentage points at $\approx 2\%$ extra cost; Diversity-EGC beats Mixture-of-Agents by ≈ 1.8 percentage points at $\approx 47\%$ lower cost. The two prior methods not cleanly dominated are Self-Refine, which slightly beats HARQ-IR on the Ollama-cloud configurations (by ≈ 3.3 percentage points at $\approx 11\%$ higher cost on the 300-task split, $p=0.43$, neither dominates on the quality–cost plane), and Self-Consistency, statistically tied with Diversity-MRC-Discrete- N at the 8B and Ollama-cloud-curated operating points (paired $\Delta < 0.7$ pp in either direction); the framework predicts both exceptions (Sec. 5.3 and Prop. 2). FrugalGPT and RouteLLM are degenerate cases of fountain and ACM respectively (Table 2) and the semantic-KNN router of Sec. 5.4 subsumes both, beating its closest in-paper proxies at $p < 10^{-4}$ over 300×3 trials (Table 10).

5.3 Quality, cost, and the operating-point dependence

Cost normalization. For a technique π (e.g. Diversity-MRC, HARQ-IR, fountain), per-task cost overhead (normalized cost) $\rho(\pi, X) := \text{Cost}(\pi, X)/\text{Cost}(\text{baseline}, X)$ is analogous to E_b/N_0 in communications (Sec. D); throughout this section we pair the coding gain $G(\pi) = \mathbb{E}[q_\pi(X)] - \mathbb{E}[q_{\text{baseline}}(X)]$ with the coding-gain efficiency $\eta(\pi) := G(\pi)/\rho(\pi)$.

Diversity combining. On the cleanest CSI configuration (A+O cloud, Haiku 4.5 + GPT-5-mini, judge Haiku 4.5), the textbook $\text{MRC} \geq \text{EGC} \geq \text{SC}$ ordering holds: $G_{\text{MRC}} = +7.9\% \geq G_{\text{EGC}} = +6.2\% \geq G_{\text{SC}} = +4.6\%$. The ordering reverses where the judge-score CSI is noisier: 14B local ($G_{\text{EGC}} = +11.6\% > G_{\text{MRC}} = G_{\text{SC}} = +6.2\%$, $q_0 = 0.746$) and Ollama-cloud ($G_{\text{EGC}} = +15.1\% > G_{\text{MRC}} = +11.7\% > G_{\text{SC}} = +9.4\%$). This is the CSI-noise crossover of Prop. 1: residual binary-checklist judge variance puts σ_w above the critical σ_w^* on the local-and-Ollama configurations and below it on the cleaner cloud pair. Soft-MRC (intrinsic log-probabilities, Sec. J) reduces σ_w further and matches EGC at 14B (0.825 vs. 0.832). Wider-pool variants extend the picture: at 8B, Diversity-SC- N reaches +33% and Diversity-MRC-Discrete- N reaches +31%. Full crossover analysis is in Sec. C.1.

Iterative refinement: HARQ and turbo. On 14B, HARQ-CC reaches $G = +11.7\%$ ($p < 10^{-3}$), HARQ-IR +14.0% ($p < 10^{-3}$), and turbo +14.2% ($p < 10^{-5}$, paired Wilcoxon $W = 56$); the HARQ-CC vs. HARQ-IR gap isolates the value of structured extrinsic feedback at fixed call budget. The all-tasks running-max rises monotonically iteration-by-iteration (0.726 \rightarrow 0.853, Fig. 2). The survivor mean drops after iteration 0, the early-exit artifact predicted by Remark 4: the best-of-sequence guard ensures $Q_k \geq Q_{k-1} \geq q_0$, but the survivor mean does not. Turbo on weaker generators traces the threshold of Prop. 2: above at 14B, noisy-flat at 8B, descending at 3B with only the guard preserving the delivered iterate (Fig. 3; per-scale breakdown in Sec. I).

Forward error correction. On 14B, FEC at $r \in \{3/4, 1/2, 1/3\}$ delivers +7.6% ($p < 0.05$, $\rho \approx 3\times$), +4.3%, +5.1%. $r = 3/4$ (one extra step-by-step reasoning section) gives the best quality-cost trade, consistent with chain-of-thought scaling [Wei et al., 2022]; lower rates saturate because the syndrome-decoding LLM does not exploit additional, less-decorrelated parity sections (Fig. 4).

The best single technique depends on the operating point, and on what one optimizes for. Table 8 in the Appendix reports raw G . Pairing each G with its ρ and computing η exposes a recurring asymmetry: *the G -leader is rarely the η -leader* (Table 9). At the 3B, 8B, and Ollama-cloud configurations the G -leader is fountain at $\rho \in [6.3, 9.1] \times$, while the η -leader is the cheapest combiner Diversity-SC at $\rho \approx 2\times$, a 1.5-to-3 \times improvement in coding gain per unit cost. At 14B, turbo leads on G but Diversity-EGC matches it on η at $\sim 75\%$ of the cost. Only on the A+O cloud, where $q_0 = 0.819$ is already near ceiling, does a single technique (HARQ-IR) lead on both axes. This dependence motivates the cost-aware semantic-KNN ACM router of Sec. 5.4: a single Lagrangian knob λ moves the deployed router from G -leader to η -leader as described below.

5.4 A cost-aware semantic-nearest-neighbor adaptive-coding-and-modulation router.

We instantiate the routing layer as a non-parametric semantic-nearest-neighbor dispatcher. Each task x is embedded with BAAI/bge-large-en-v1.5; at deployment, the dispatcher looks up the per-technique mean quality $\bar{q}_i(x)$ and cost $\bar{c}_i(x)$ over the $k = 20$ nearest training-cache neighbors of x and selects

$$\pi^*(x; \lambda) = \arg \max_{i \in \mathcal{C}} (\bar{q}_i(x) - \lambda \cdot \bar{c}_i(x) / \bar{c}_{\text{baseline}}(x)), \quad (3)$$

where \mathcal{C} is the candidate-technique pool (19 techniques + uncoded baseline in our pool) and $\lambda \geq 0$ is a single Lagrangian knob: $\lambda \rightarrow 0$ recovers a pure quality-maximizer, $\lambda \rightarrow \infty$ collapses to the cheapest candidate. The dispatch rule is fully determined by the cache snapshot and the embedding

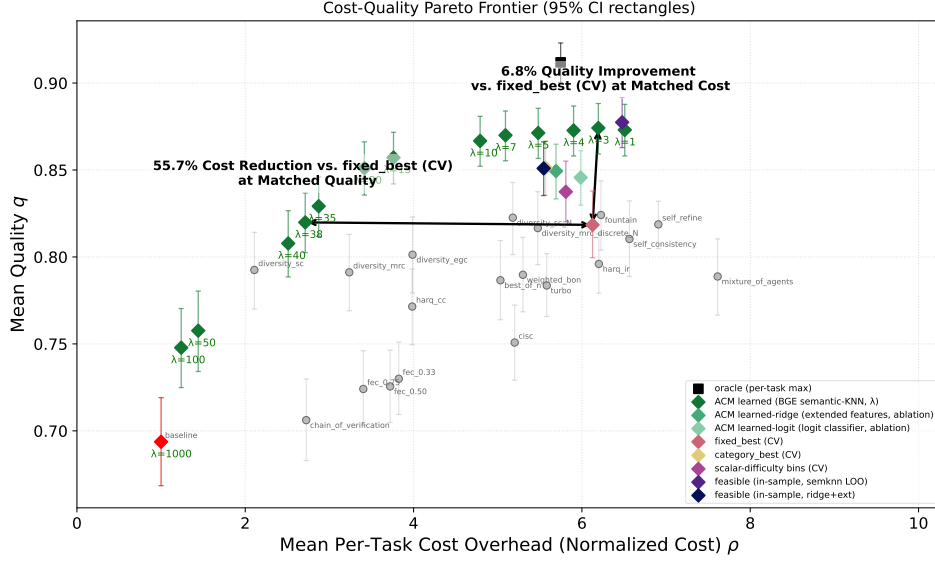


Figure 1: Quality–cost Pareto frontier on the Ollama-cloud trio, 300-task ($3 \times$ repeat) hard-benchmark split (5-fold stratified cross-validation; 4000 bootstrap samples). Faded gray dots are individual fixed techniques (in-sample mean); colored markers are routing *policies* (per-task oracle, cross-validated fixed-best, the hand-coded ACM bins, per-category fixed-best, scalar-difficulty bins, the $(d, \text{category})$ logistic regression, a ridge regressor on extended features, and the cost-aware semantic-nearest-neighbor router at various λ). The router with $(\lambda=3)$ lies above every fixed technique at matched cost; sliding λ to ≈ 38 moves the same router left along the frontier, preserving quality lead over the fixed best (CV) at substantially lower cost. More details are in Sec. E.1.

model; the same router instance is therefore deployable across cost regimes by adjusting λ , with no retraining. Table 3 reports 5-fold stratified cross-validation on the 300-task hard-benchmark split. We compare against the *cross-validated fixed-best* policy: in each fold, fit on the four training folds the technique with the highest mean quality and apply that single technique to every test-fold task. This is the apples-to-apples baseline, since both policies are scored out-of-fold. Comparisons against simpler routers (per-category fixed-best, scalar-difficulty bins, hand-coded ACM tables) and the in-sample feasibility ceiling appear in Table 10, Sec. E.1, Fig. 1.

Table 3: Cost-aware semantic-nearest-neighbor router on the Ollama-cloud trio. Each task is generated $n_{\text{rep}}=3$ independent times, giving $n=300$ unique tasks $\times 3$ repeats = 900 trial-task observations; 5-fold stratified cross-validation (folds applied at the task level so all three repeats of a task land in the same fold); 4000 bootstrap samples drawn with seed-aware resampling that propagates within-task generation variance into every confidence interval. Δq is paired-per-task (averaged across repeats) vs. the cross-validated fixed-best policy and tested by Wilcoxon signed-rank ($***p < 10^{-3}$); Full per-policy table in Table 10.

Policy	q [95% CI]	Cost / task	$q/\$$	ρ	G (pp)	Δq vs. FB-CV	Δq vs. FB-IS
Oracle (per-task max)	0.912 [0.900, 0.923]	\$0.00668	165.4	5.75 \times	+31.4	—	+0.088
Feasible (semknn LOO, in-samp.)	0.877 [0.863, 0.892]	\$0.00735	145.5	6.48 \times	+26.5	—	+0.053
Semknn router, $\lambda=3$	0.874 [0.859, 0.888]	\$0.00695	160.2	6.20\times	+26.0	+0.056***	+0.050
Semknn router, $\lambda=38$	0.820 [0.802, 0.837]	\$0.00290	388.7	2.71\times	+18.2	+0.001	−0.004
<i>Strongest in-sample fixed: fountain</i>	0.824	\$0.00691	119.2	6.23 \times	+18.8	+0.006	−(FB-IS ref.)
Cross-validated fixed-best (FB-CV)	0.818 [0.800, 0.838]	\$0.00698	143.6	6.13\times	+18.0	−(FB-CV ref.)	−0.006
Always-baseline (uncoded)	0.694 [0.668, 0.719]	\$0.00120	577.9	1.00 \times	+0.0	−0.125	−0.130

The router at $\lambda=3$ beats the cross-validated fixed-best policy by 6.8% in mean quality (paired Wilcoxon $p < 10^{-13}$, Cohen’s $d_z = 0.47$, win rate 59.7% at the per-task level) at matched normalized cost; Fig. 1 plots the quality–cost plane and shows that the entire λ -sweep sits above every fixed technique on the empirical Pareto frontier. Sweeping the knob to $\lambda=38$ instance still matches FB-CV in mean quality while running at 55.7% lower normalized cost per task than fixed-best. The headline numbers are computed on 900 trial-task observations ($n=300$ tasks $\times 3$ independent generation repeats per task) with seed-aware bootstrap resampling that propagates within-task generation variance into every confidence interval. The full Pareto sweep and additional comparators (per-category fixed-best, scalar-difficulty bins, hand-coded ACM, the in-sample feasibility ceiling) are in Table 10 and Fig. 1. Classical maximal-ratio combining is information-theoretically optimal under high signal-

to-noise ratio with perfect channel-state information [Proakis and Salehi, 2008], but that optimality is conditional on a fixed channel regime: allowing the regime itself to vary across tasks and dispatching task-by-task strictly dominates any single fixed combiner on the empirical quality–cost frontier.

5.5 Category analysis and standard-benchmark validation

On the 14B-curated tasks, category dominance varies by technique (per-category bars in Fig. 16; full per-configuration breakdown in Sec. G): hybrid retransmission with incremental redundancy leads on question answering ($q = 0.861$) and reasoning (0.869), maximal-ratio combining on code (0.866), and equal-gain combining / turbo on creative (0.822 / 0.806), as expected from the channel model: iterative techniques excel where concrete errors can be identified, diversity combining where independent attempts explore different solution paths. To rule out curation artifacts we re-evaluate on hard-stratified splits of $n = 100$ items per dataset of GSM8K, MMLU (`abstract_algebra`), and HumanEval, constructed via published structural proxies (step count, subject difficulty, doctest count); technique rankings match the curated-task results on all three (per-dataset bars and Pareto scatters in Figures 36 and 37, full breakdown in Sec. G). Three validation experiments rule out methodology artifacts: an inter-judge ablation preserves the technique ordering despite absolute-score variation; a judge-in-loop confound check shows that judge-free decoders still win about 39% of oracle assignments on the 8B split, ruling out the strong borrowing hypothesis; and a synthesis-integrity audit (Sec. L) finds zero contamination across five controlled tests, so the gains attributed to combining cannot be the synthesizer solving the task on its own.

6 Discussion

Technique selection guidelines. The framework gives principled criteria: *diversity combining* for independent-error tasks (question answering); *HARQ with incremental redundancy* when errors are identifiable by a critic; *turbo* when iterative refinement compounds (reasoning); *fountain* when difficulty is unknown a priori; *forward error correction* for tasks with checkable consistency (code); and the cost-aware semantic-nearest-neighbor router for heterogeneous task streams when both quality and cost matter. Table 3 sharpens the last point: a single *adaptive* router with one Lagrangian knob λ strictly dominates any single fixed combiner (including textbook-optimal maximal-ratio combining) on the empirical quality–cost frontier; classical optimality results assume a fixed channel regime, while real task streams traverse multiple regimes and reward per-task allocation.

Generator bottleneck and the decoding threshold. Iterative techniques are limited by generator capacity, not critic quality, mirroring the iterative-decoding threshold [ten Brink, 2001]: Prop. 2 writes the threshold as a contraction–expansion transition of the per-iteration quality-update map f at its high-quality fixed point q^∞ . Our three local model scales trace this transition (Table 8, Fig. 3, Sec. I): refinement is coherent at 14B, noisy-flat at 8B, and net-destructive at 3B with only the guard preserving monotonicity. Operational implication: deploy iterative techniques only when the generator is known to be above threshold; otherwise prefer passive diversity [Proakis and Salehi, 2008] or routing.

Limitations and open directions. Limitations are detailed in Sec. I: residual judge-score noise from the binary-checklist scorer; scoring overhead on easy tasks; non-stationarity and a dual-role judge confound (judge-free decoders still win about 39% of oracle assignments, leaving a judge-strength ablation open); and curated-task selection bias, addressed by the standard-benchmark validation. Open directions include bounding $I(X; Y)$ for LLM channels, calibrating λ from a user-supplied cost constraint, and enriching router features beyond sentence embeddings.

7 Conclusion

Sampling an autoregressive language model at temperature T realizes a discrete stochastic channel, and that identity makes the communication-theoretic reliability toolkit transfer with minimal adaptation: a closed-form channel-state-information crossover (Prop. 1) above which equal-gain combining beats noisy maximal-ratio combining, and a fixed-point criterion (Prop. 2) identifying LLM refinement with an EXIT recursion, the contraction-versus-expansion dichotomy of which is consistent with the 3B/8B/14B transition we observe. The cost-aware semantic-nearest-neighbor router beats every fixed technique on the Ollama-cloud quality-cost frontier (6.8% quality lead at matched cost; 55.7% lower cost at matched quality): classical maximal-ratio optimality is conditional on a fixed regime, whereas real workloads traverse multiple regimes and reward per-task allocation through a single Lagrangian knob. A substantially larger design space (interleaving, structured forward error correction, joint source-channel coding; Sec. K) and operational capacity bounds, λ -calibration, and richer router features remain.

References

- Anthropic. The Claude model family. *Anthropic Technical Report*, 2024.
- Claude Berrou, Alain Glavieux, and Punya Thitimajshima. Near Shannon limit error-correcting coding and decoding: Turbo-codes. In *Proceedings of ICC'93 – IEEE International Conference on Communications*, volume 2, pages 1064–1070, 1993.
- Lingjiao Chen, Matei Zaharia, and James Zou. FrugalGPT: How to use large language models while reducing cost and improving performance. *Transactions on Machine Learning Research*, 2024.
- Zhijun Chen, Xiaodong Lu, Jingzheng Li, Pengpeng Chen, Zhuoran Li, Kai Sun, Yuankai Luo, Qianren Mao, Ming Li, Likang Xiao, Dingqi Yang, Xiao Huang, Yikun Ban, Hailong Sun, and Philip S. Yu. Harnessing multiple large language models: A survey on LLM ensemble. *arXiv preprint arXiv:2502.18036*, 2025.
- Yinlam Chow, Guy Tennenholtz, Izzeddin Gur, Vincent Zhuang, Bo Dai, Sridhar Thiagarajan, Craig Boutilier, Rishabh Agarwal, Aviral Kumar, and Aleksandra Faust. Inference-aware fine-tuning for best-of-N sampling in large language models. In *Proceedings of the 13th International Conference on Learning Representations (ICLR)*, 2025.
- Karl Cobbe, Vineet Kosaraju, Mohammad Bavarian, Mark Chen, Heewoo Jun, Lukasz Kaiser, Matthias Plappert, Jerry Tworek, Jacob Hilton, Reiichiro Nakano, Christopher Hesse, and John Schulman. Training verifiers to solve math word problems. *arXiv preprint arXiv:2110.14168*, 2021a.
- Karl Cobbe, Vineet Kosaraju, Mohammad Bavarian, Mark Chen, Heewoo Jun, Lukasz Kaiser, Matthias Plappert, Jerry Tworek, Jacob Hilton, Reiichiro Nakano, Christopher Hesse, and John Schulman. Training verifiers to solve math word problems. *arXiv preprint arXiv:2110.14168*, 2021b.
- Paula Cordero-Encinar and Andrew B. Duncan. Certified self-consistency: Statistical guarantees and test-time training for reliable reasoning in LLMs. *arXiv preprint arXiv:2510.17472*, 2025.
- Thomas M. Cover and Joy A. Thomas. *Elements of Information Theory*. Wiley-Interscience, 2nd edition, 2006.
- Shehzaad Dhuliawala, Mojtaba Komeili, Jing Xu, Roberta Raileanu, Xian Li, Asli Celikyilmaz, and Jason Weston. Chain-of-verification reduces hallucination in large language models. In *Findings of the Association for Computational Linguistics: ACL 2024*, pages 3563–3578, 2024.
- Yilun Du, Shuang Li, Antonio Torralba, Joshua B. Tenenbaum, and Igor Mordatch. Improving factuality and reasoning in language models through multiagent debate. In *Proceedings of the 41st International Conference on Machine Learning (ICML)*, 2024.
- Austin Feng, Marius Alonso, and Ambroise Odonnat. Optimal self-consistency for efficient reasoning with large language models. In *NeurIPS 2025 Workshop on Efficient Reasoning*, 2025.
- Robert G. Gallager. Low-density parity-check codes. *IRE Transactions on Information Theory*, 8(1): 21–28, 1962.
- Feifei Gao, Arumugam Nallanathan, and Jianguo Wang. Improved combining techniques for diversity reception with imperfect channel estimation. *IEEE Transactions on Wireless Communications*, 2(4):789–799, 2003.
- Andrea J. Goldsmith and Soon-Ghee Chua. Variable-rate variable-power MQAM for fading channels. *IEEE Transactions on Communications*, 45(10):1218–1230, 1997.
- Jiawei Gu, Xuhui Jiang, Zhichao Shi, Hexiang Tan, Xuehao Zhai, Chengjin Xu, Wei Li, Yinghan Shen, Shengjie Ma, Honghao Liu, et al. A survey on llm-as-a-judge. *The Innovation*, page 101253, 2026.
- Chuan Guo, Geoff Pleiss, Yu Sun, and Kilian Q. Weinberger. On calibration of modern neural networks. In *Proceedings of the 34th International Conference on Machine Learning (ICML)*, pages 1321–1330, 2017.

- Morris W. Hirsch, Stephen Smale, and Robert L. Devaney. *Differential Equations, Dynamical Systems, and an Introduction to Chaos*. Academic Press, 3rd edition, 2013.
- Jordan Hoffmann, Sebastian Borgeaud, Arthur Mensch, Elena Buchatskaya, Trevor Cai, Eliza Rutherford, Diego de Las Casas, Lisa Anne Hendricks, Johannes Welbl, Aidan Clark, et al. Training compute-optimal large language models. In *Advances in Neural Information Processing Systems (NeurIPS)*, volume 35, 2022.
- Dongfu Jiang, Xiang Ren, and Bill Yuchen Lin. LLM-Blender: Ensembling large language models with pairwise ranking and generative fusion. In *Proceedings of the 61st Annual Meeting of the Association for Computational Linguistics (Volume 1: Long Papers)*, pages 14165–14178, 2023.
- Saurav Kadavath, Tom Conerly, Amanda Askell, Tom Henighan, Dawn Drain, Ethan Perez, Nicholas Schiefer, Zac Hatfield-Dodds, Nova DasSarma, Eli Tran-Johnson, et al. Language models (mostly) know what they know. *arXiv preprint arXiv:2207.05221*, 2022.
- Jared Kaplan, Sam McCandlish, Tom Henighan, Tom B. Brown, Benjamin Chess, Rewon Child, Scott Gray, Alec Radford, Jeffrey Wu, and Dario Amodei. Scaling laws for neural language models. *arXiv preprint arXiv:2001.08361*, 2020.
- Omar Khattab, Arnav Singhvi, Paridhi Maheshwari, Zhiyuan Zhang, Keshav Santhanam, Sri Vardhamanan, Saiful Haq, Ashutosh Sharma, Thomas T. Joshi, Hanna Moazam, Heather Miller, Matei Zaharia, and Christopher Potts. DSPy: Compiling declarative language model calls into self-improving pipelines. In *International Conference on Learning Representations (ICLR)*, 2024.
- Lorenz Kuhn, Yarin Gal, and Sebastian Farquhar. Semantic uncertainty: Linguistic invariances for uncertainty estimation in natural language generation. In *Proceedings of the 11th International Conference on Learning Representations (ICLR)*, 2023.
- Wenzhe Li, Yong Lin, Mengzhou Xia, and Chi Jin. Rethinking mixture-of-agents: Is mixing different large language models beneficial? *arXiv preprint arXiv:2502.00674*, 2025.
- Yifei Li, Zeqi Lin, Shizhuo Zhang, Qiang Fu, Bei Chen, Jian-Guang Lou, and Weizhu Chen. Making language models better reasoners with step-aware verifier. In *Proceedings of the 61st Annual Meeting of the Association for Computational Linguistics (Volume 1: Long Papers)*, pages 5315–5333, 2023.
- Hunter Lightman, Vineet Kosaraju, Yura Burda, Harri Edwards, Bowen Baker, Teddy Lee, Jan Leike, John Schulman, Ilya Sutskever, and Karl Cobbe. Let’s verify step by step. *Proceedings of the 12th International Conference on Learning Representations (ICLR)*, 2024.
- Jiachang Liu, Dinghan Shen, Yizhe Zhang, Bill Dolan, Lawrence Carin, and Weizhu Chen. What makes good in-context examples for GPT-3? In *Proceedings of Deep Learning Inside Out (DeeLIO)*, 2022.
- Michael Luby. LT codes. *Proceedings of the 43rd Annual IEEE Symposium on Foundations of Computer Science (FOCS)*, pages 271–280, 2002.
- Aman Madaan, Niket Tandon, Prakhar Gupta, Skyler Hallinan, Luyu Gao, Sarah Wiegrefe, Uri Alon, Nouha Dziri, Shrimai Prabhumoye, Yiming Yang, Shashank Gupta, Bodhisattwa Prasad Majumder, Katherine Hermann, Sean Welleck, Amir Yazdanbakhsh, and Peter Clark. Self-refine: Iterative refinement with self-feedback. *Advances in Neural Information Processing Systems (NeurIPS)*, 36, 2023.
- Yucheng Ning, Xixun Lin, Fang Fang, and Yanan Cao. MAD-Fact: A multi-agent debate framework for long-form factuality evaluation in LLMs. *Frontiers of Computer Science*, 2025. doi: 10.1007/s11704-025-51369-x.
- Steven R. Norsworthy, Richard Schreier, and Gabor C. Temes. *Delta-Sigma Data Converters: Theory, Design, and Simulation*. IEEE Press, New York, 1996.
- Isaac Ong, Amjad Almahairi, Vincent Wu, Wei-Lin Chiang, Tianhao Wu, Joseph E. Gonzalez, M. Waleed Kadous, and Ion Stoica. RouteLLM: Learning to route LLMs with preference data. In *Proceedings of the 13th International Conference on Learning Representations (ICLR)*, 2025.

- OpenAI. GPT-4 technical report. *arXiv preprint arXiv:2303.08774*, 2023.
- John G. Proakis and Masoud Salehi. *Digital Communications*. McGraw-Hill, 5th edition, 2008.
- Thomas J. Richardson and Rüdiger L. Urbanke. The capacity of low-density parity-check codes under message-passing decoding. *IEEE Transactions on Information Theory*, 47(2):599–618, 2001.
- Nicholas Roberts, Sungjun Cho, Zhiqi Gao, Tzu-Heng Huang, Albert Wu, Gabriel Orlanski, Avi Trost, Kelly Buchanan, Aws Albarghouthi, and Frederic Sala. Test-time scaling makes overtraining compute-optimal. *arXiv preprint arXiv:2604.01411*, 2026.
- Ohad Rubin, Jonathan Herzig, and Jonathan Berant. Learning to retrieve prompts for in-context learning. In *Proceedings of NAACL-HLT*, 2022.
- Kayla Schroeder and Zach Wood-Doughty. Can you trust LLM judgments? reliability of LLM-as-a-judge. *arXiv preprint arXiv:2412.12509*, 2024.
- Claude E. Shannon. A mathematical theory of communication. *Bell System Technical Journal*, 27(3): 379–423, 1948.
- Noah Shinn, Federico Cassano, Ashwin Gopinath, Karthik Narasimhan, and Shunyu Yao. Reflexion: Language agents with verbal reinforcement learning. *Advances in Neural Information Processing Systems (NeurIPS)*, 36, 2023.
- Amin Shokrollahi. Raptor codes. *IEEE Transactions on Information Theory*, 52(6):2551–2567, 2006.
- Marvin K. Simon and Mohamed-Slim Alouini. Digital communication over fading channels. *Wiley-Interscience*, 2005. Chapter 9: Optimum Combining with Imperfect Channel Estimates.
- Charlie Snell, Jaehoon Lee, Kelvin Xu, and Aviral Kumar. Scaling LLM test-time compute optimally can be more effective than scaling parameters for reasoning. In *Proceedings of the 13th International Conference on Learning Representations (ICLR)*, 2025.
- Amir Taubenfeld, Tom Sheffer, Eran Ofek, Amir Feder, Ariel Goldstein, Zorik Gekhman, and Gal Yona. Confidence improves self-consistency in LLMs. In *Findings of the Association for Computational Linguistics: ACL 2025*, pages 20090–20111, 2025.
- Stephan ten Brink. Convergence behavior of iteratively decoded parallel concatenated codes. *IEEE Transactions on Communications*, 49(10):1727–1737, 2001.
- Bruno R. Tomiuk, Norman C. Beaulieu, and Adnan A. Abu-Dayya. General forms for maximal ratio diversity with weighting errors. *IEEE Transactions on Communications*, 47(4):488–492, 1999.
- Yigit Turkmen, Baturalp Buyukates, and Melih Bastopcu. Don’t always pick the highest-performing model: An information theoretic view of LLM ensemble selection. *arXiv preprint arXiv:2602.08003*, 2026.
- Joerg Vogt and Adolf Finger. Improving the max-log-MAP turbo decoder. *Electronics Letters*, 36(23):1937–1939, 2000.
- Junlin Wang, Jue Wang, Ben Athiwaratkun, Ce Zhang, and James Zou. Mixture-of-agents enhances large language model capabilities. In *Proceedings of the 13th International Conference on Learning Representations (ICLR)*, 2025.
- Xuezhi Wang, Jason Wei, Dale Schuurmans, Quoc Le, Ed Chi, Sharan Narang, Aakanksha Chowdhery, and Denny Zhou. Self-consistency improves chain of thought reasoning in language models. In *Proceedings of the 11th International Conference on Learning Representations (ICLR)*, 2023.
- Jason Wei, Xuezhi Wang, Dale Schuurmans, Maarten Bosma, Brian Ichter, Fei Xia, Ed Chi, Quoc Le, and Denny Zhou. Chain-of-thought prompting elicits reasoning in large language models. *Advances in Neural Information Processing Systems (NeurIPS)*, 35, 2022.
- Jianyu Wen, Yang Wei, Xiongxi Yu, Changxuan Xiao, and Ke Zeng. Attention-MoA: Enhancing mixture-of-agents via inter-agent semantic attention and deep residual synthesis. *arXiv preprint arXiv:2601.16596*, 2026.

- Yasin A Yadkori, Ilja Kuzborskij, András György, and Csaba Szepesvari. To believe or not to believe your llm: Iterative prompting for estimating epistemic uncertainty. *Advances in Neural Information Processing Systems*, 37:58077–58117, 2024.
- Chengrun Yang, Xuezhi Wang, Yifeng Lu, Hanxiao Liu, Quoc V. Le, Denny Zhou, and Xinyun Chen. Large language models as optimizers. In *International Conference on Learning Representations (ICLR)*, 2024.
- Shunyu Yao, Dian Yu, Jeffrey Zhao, Izhak Shafran, Thomas L. Griffiths, Yuan Cao, and Karthik Narasimhan. Tree of thoughts: Deliberate problem solving with large language models. *Advances in Neural Information Processing Systems (NeurIPS)*, 36, 2023.
- Lianmin Zheng, Wei-Lin Chiang, Ying Sheng, Siyuan Zhuang, Zhanghao Wu, Yonghao Zhuang, Zi Lin, Zhuohan Li, Dacheng Li, Eric P. Xing, Hao Zhang, Joseph E. Gonzalez, and Ion Stoica. Judging LLM-as-a-judge with MT-Bench and Chatbot Arena. *Advances in Neural Information Processing Systems (NeurIPS)*, 36, 2023.
- Yongchao Zhou, Andrei Ioan Muresanu, Ziwen Han, Keiran Paster, Silviu Pitis, Harris Chan, and Jimmy Ba. Large language models are human-level prompt engineers. In *International Conference on Learning Representations (ICLR)*, 2023.
- King Zhu, Hanhao Li, Siwei Wu, Tianshun Xing, Dehua Ma, Xiangru Tang, Minghao Liu, Jian Yang, Jiaheng Liu, Yuchen Eleanor Jiang, Changwang Zhang, Chenghua Lin, Jun Wang, Ge Zhang, and Wangchunshu Zhou. Scaling test-time compute for LLM agents. *arXiv preprint arXiv:2506.12928*, 2025.

Appendix

A Primer on communication systems

This appendix provides an accessible introduction to the communication-theoretic concepts used throughout the paper. Readers familiar with digital communications may skip this section; it is intended for the ML/AI audience.

A.1 The communication problem

The fundamental problem in communication is: *how do you send a message reliably over a noisy channel?* A transmitter sends a signal, the channel corrupts it (adds noise, causes fading, drops bits), and the receiver must recover the original message. Shannon’s channel coding theorem [Shannon, 1948] establishes that reliable communication is *possible* up to a fundamental limit called the channel capacity C , provided the transmitter adds sufficient structured redundancy.

A prompt (message) is sent through a stochastic model (channel) whose transition probability is $p_{\theta}(y | x)$, which may produce hallucinations, omissions, or reasoning errors (noise), and the user (receiver) must extract a correct answer (decoded message). As formalized in Sec. 3, the LLM’s conditional distribution satisfies the definition of a channel transition probability.

A.2 Signal-to-Noise Ratio (SNR)

SNR measures how much “useful signal” there is relative to “noise” in a received signal. Higher SNR means cleaner reception and lower error rates. In wireless systems, SNR depends on transmit power, distance, and interference.

Agent analog: The LLM channel’s intrinsic noise is its conditional entropy $\mathcal{H} = H(Y|X)$, the per-token uncertainty in the model’s output distribution (Eq. (2)). Lower \mathcal{H} means higher channel quality (analogous to higher SNR). In practice, we estimate channel quality via a quality score $q \in [0, 1]$ produced by an LLM judge, a noisy external channel estimator. Just as wireless engineers measure SNR to decide how to process a received signal, our framework measures output quality to decide how to process agent outputs.

A.3 Diversity and combining

In wireless systems, a signal may travel via multiple independent paths (e.g., multiple antennas in MIMO systems). Each path experiences different noise, so if one path is in a deep fade, another may still be strong. The receiver *combines* these paths to improve reliability. Three standard strategies exist:

- **Selection combining (SC):** Pick the single best path. Simple but discards useful information from other paths.
- **Equal-gain combining (EGC):** Average all paths equally. Better than SC but suboptimal if path qualities differ.
- **Maximal-ratio combining (MRC):** Weight each path proportionally to its SNR, then combine. This is provably optimal under independent noise.

With d independent paths, the probability that *all* are bad drops as SNR^{-d} , an exponential improvement called *diversity gain*.

Agent analog: Generate d independent agent outputs (using different models, prompts, or temperatures) and combine them. SC \rightarrow pick the best output; EGC \rightarrow synthesize all equally; MRC \rightarrow synthesize with quality-weighted emphasis. Independence can be achieved through model diversity (spatial), prompt rephrasing (frequency), or temperature variation (time). Our experiments focus on spatial diversity; frequency and time diversity are supported by the framework and left to future evaluation. The frequency axis as defined here is decode-time prompt rephrasing applied per request; an orthogonal line of work realizes prompt diversity at *compile time*, either by treating prompts as compilable artifacts with searchable instructions, demonstrations, and pipelines [Khatab et al., 2024], by retrieving or learning per-task in-context examples [Liu et al., 2022, Rubin et al., 2022], or by

LLM-in-the-loop instruction optimization [Zhou et al., 2023, Yang et al., 2024]. These methods amortize their search before inference and produce a single optimized prompt at decode time; composing them with the decode-time channel combiners studied here is a natural — and untested — direction we do not pursue in this paper.

A.4 Automatic Repeat Request (ARQ) and Hybrid ARQ

ARQ is the simplest reliability mechanism: if the receiver detects errors, it requests retransmission. *Hybrid ARQ* (HARQ) combines this with forward error correction for better efficiency:

- **HARQ-CC (Chase Combining):** Retransmit the exact same data. The receiver soft-combines all copies, improving SNR through repetition.
- **HARQ-IR (Incremental Redundancy):** Each retransmission sends *new* parity information. The decoder accumulates information across rounds, converging more efficiently than CC.

HARQ-IR is strictly more efficient: each round adds new information rather than repeating what was already sent.

Agent analog: HARQ-CC \rightarrow retry the same prompt and combine all attempts. HARQ-IR \rightarrow use a critic to identify specific errors, then retry with that feedback (new information) appended to the prompt. The quality threshold τ serves as the target error rate; iteration stops when quality exceeds τ .

A.5 Turbo Codes and Iterative Decoding

Turbo codes [Berrou et al., 1993] revolutionized communications by approaching Shannon’s limit. They use two simple encoders/decoders that iteratively exchange “extrinsic information,” soft reliability estimates that each decoder produces for the other. Above a decoder-specific SNR threshold, this iterative exchange can produce a *waterfall* effect in classical channels: error rates drop sharply once a critical information threshold is crossed. We do not claim this waterfall behavior carries over quantitatively to LLM channels; our turbo implementation aims for the qualitative benefit of extrinsic-only feedback, not a bit-error-rate curve.

Agent analog: Two LLM agents (generator and critic) iteratively exchange outputs. The generator produces an answer; the critic provides structured feedback (extrinsic information); the generator refines. Each round, both agents condition on the other’s latest output, mirroring the extrinsic information exchange in turbo decoding.

A.6 Fountain (Rateless) Codes

Traditional codes have a fixed rate $r = k/n$, chosen before transmission. Fountain codes [Luby, 2002] instead produce a potentially *unlimited* stream of encoded symbols. The receiver collects symbols until it has enough to decode, automatically adapting to unknown or time-varying channel conditions without rate negotiation.

Agent analog: Generate agent outputs one at a time, checking quality after each. Stop as soon as accumulated outputs are sufficient to synthesize a high-quality answer. No need to pre-specify how many samples are needed; the system adapts to task difficulty at runtime.

A.7 Forward Error Correction (FEC)

FEC adds structured redundancy to a message *before* transmission so the receiver can detect and correct errors without retransmission. The *code rate* $r = k/n$ controls the redundancy: lower rates add more redundancy (more protection, higher cost). The receiver performs *syndrome decoding*, checking parity constraints to locate and fix errors.

Agent analog: Instead of asking for just an answer, prompt the model to also produce structured “parity” sections: step-by-step reasoning (parity 1), self-verification (parity 2), confidence assessment (parity 3), and an alternative approach (parity 4). A decoder agent then cross-checks these sections for internal consistency (analogous to syndrome decoding) and corrects any detected errors in the main answer. The code rate controls how many parity sections are requested.

A.8 Adaptive Coding and Modulation (ACM)

In wireless systems (LTE, 5G), the transmitter continuously estimates channel quality and selects the best modulation and coding scheme (MCS). Good channels get high-rate, low-redundancy schemes (high throughput); bad channels get low-rate, high-redundancy schemes (high reliability). This is formalized as a table mapping SNR ranges to MCS levels.

Agent analog: Estimate task difficulty (the “channel quality”), then route to the most cost-efficient technique. Easy tasks use cheap, low-redundancy methods (single fast model); hard tasks use expensive, high-redundancy methods (turbo decoding with a frontier model). This is the key to optimizing the cost–quality tradeoff: not every task needs the same level of effort.

A.9 Summary of mappings

Table 4 consolidates the communication-to-agent concept correspondences used throughout the paper, from the channel transition probability identity through the soft-decision recipe to the rate–reliability trade-off.

Table 4: Communication \leftrightarrow Agent concept mapping.

Communication Concept	Agent Analog
Transition prob. $W(y x)$	$p_\theta(y x)$ (exact identity)
Channel	LLM model
Noise variance σ^2	Temperature T
Noise (AWGN, fading)	Hallucination, omission, errors
Conditional entropy $H(Y X)$	Per-token uncertainty of LLM
Received signal	Agent output
Soft-decision output (LLR)	Token log-probabilities
SNR / channel quality	$-\mathcal{H}(\mathcal{A}_\theta, x)$ (neg. cond. entropy)
Channel estimator (CSI)	Sigma-delta LLM-judge scorer
Diversity (MIMO)	Multi-model/prompt/temp sampling
Combining (SC/EGC/MRC)	Output selection/synthesis
ARQ retransmission	Prompt retry
HARQ-IR parity bits	Critic feedback
Turbo extrinsic info	Generator–critic exchange
Decoding threshold	Min. model capacity for convergence
Fountain symbols	Incremental samples
FEC parity bits	Reasoning/verification sections
Code rate $r = k/n$	Redundancy level
ACM / MCS table	Task-difficulty routing
$I(X; Y)$, capacity C	Mutual info., max quality at cost

B Benchmark task details

Full task specifications for all 36 benchmark tasks are available in the supplementary material. Each task includes: prompt text, reference answer (where applicable), difficulty rating, and evaluation criteria.

C Linear-Combiner justification for the MRC weighting

This appendix reproduces the linear-combiner argument that motivates the weighting in Remark 2; it is not a proof that this weighting is end-to-end optimal for a nonlinear LLM synthesizer.

Consider d agent outputs Y_1, \dots, Y_d with quality scores q_1, \dots, q_d , treated as independent signal components with additive noise of variance σ_i^2 and signal amplitude proportional to q_i . For a linear combiner with weights w_i summing to a fixed constant, the combined SNR is maximized when $w_i \propto q_i/\sigma_i^2$. Under the further simplifying assumption that noise variance is approximately equal across branches (so $\sigma_i^2 \approx \sigma^2$), this reduces to $w_i^* \propto q_i$, giving the normalized form

$$w_i^{\text{MRC}} = \frac{q_i}{\sum_{j=1}^d q_j}. \quad (4)$$

This directly parallels the classical MRC result in AWGN channels, where optimal weights are proportional to per-branch SNR [Proakis and Salehi, 2008].

Caveats specific to the agent setting. (i) The LLM synthesizer is not a linear combiner; increasing w_i biases the synthesizer's attention toward input i , but does not literally scale Y_i additively. (ii) q_i is a noisy LLM-judge estimate, not an unbiased SNR. (iii) Branch outputs Y_i are correlated through shared training data, which reduces the effective diversity order d_{eff} . The empirical ordering in Sec. 5.3 (where EGC outperforms MRC) is consistent with these caveats being active; see Remark 3 and [Gao et al., 2003, Simon and Alouini, 2005].

C.1 CSI-noise crossover between MRC and EGC

The empirical reversal $\text{EGC} \succ \text{MRC}$ observed in Sec. 5.3 under a coarse numeric-rating judge admits a quantitative explanation in a linear-combiner idealization of the synthesizer. Take a linear combiner with weights w_i acting on noisy observations $r_i = a_i s + n_i$, where $a_i > 0$ are per-branch amplitudes proportional to true quality, $n_i \sim \mathcal{N}(0, \sigma^2)$ are independent, and $s = \pm 1$ is a binary signal. Let $S_k := \sum_{i=1}^d a_i^k$. The output SNRs of the two ideal combiners are

$$\gamma_{\text{MRC}}|_{w_i=a_i} = \frac{S_2}{\sigma^2}, \quad \gamma_{\text{EGC}}|_{w_i=1} = \frac{S_1^2}{d \sigma^2},$$

and the Cauchy-Schwarz inequality gives the classical $\gamma_{\text{MRC}} \geq \gamma_{\text{EGC}}$ ordering [Proakis and Salehi, 2008], with equality iff $a_1 = \dots = a_d$.

Let the judge supply noisy estimates $\hat{a}_i = a_i + \epsilon_i$ with $\epsilon_i \sim \mathcal{N}(0, \sigma_w^2)$ independent of n_i , and let the combiner use $w_i = \hat{a}_i$. The first-order expectation of numerator and denominator separately, the standard imperfect-CSI MRC analysis of Tomiuk et al. [1999], Gao et al. [2003], Simon and Alouini [2005], gives

$$\mathbb{E}[\gamma_{\text{MRC}}] \approx \frac{S_2 (S_2 + \sigma_w^2)}{(S_2 + d \sigma_w^2) \sigma^2}, \quad (5)$$

which interpolates between γ_{MRC} at $\sigma_w \rightarrow 0$ and γ_{MRC}/d as $\sigma_w \rightarrow \infty$.

What is new in Prop. 1. The qualitative collapse of the MRC advantage as σ_w grows, including the approximation (5) itself, is the imperfect-CSI MRC line beginning with Tomiuk et al. [1999] and continued by Gao et al. [2003], Simon and Alouini [2005]; what is *not* in those references is the closed-form value of σ_w^2 at which (5) crosses γ_{EGC} . We record it below in elementary symmetric polynomials (S_1, S_2) of the per-branch amplitudes, so that the formula is parameter-free in σ and serves as a one-line diagnostic for the LLM-judge channel-state-information regime of Remark 3: every empirical $\text{EGC} \succ \overline{\text{MRC}}$ reversal in our experiments is read as crossing σ_w^{*2} , and every reversion to the textbook ordering as falling back below it (Sec. 5.3, Table 8).

Proposition 1 (CSI-noise crossover). *Let $d \geq 2$ and $a_1, \dots, a_d > 0$ with at least two distinct amplitudes. Under the first-order expectation (5), the map $\sigma_w^2 \mapsto \mathbb{E}[\gamma_{\text{MRC}}]$ is strictly decreasing on $[0, \infty)$ and crosses γ_{EGC} at exactly one positive value, the critical CSI-noise variance*

$$\sigma_w^{*2} = \frac{S_2 (dS_2 - S_1^2)}{d(S_1^2 - S_2)}; \quad (6)$$

hence $\mathbb{E}[\gamma_{\text{MRC}}] > \gamma_{\text{EGC}}$ iff $\sigma_w^2 < \sigma_w^{*2}$. In the degenerate equal-amplitude case $a_1 = \dots = a_d$ (excluded by the hypothesis) the two combiners coincide at $\sigma_w = 0$ and σ_w^{*2} collapses to 0 as a limit of (6).

Proof. Write $u := \sigma_w^2$. Differentiating (5),

$$\frac{d}{du} \mathbb{E}[\gamma_{\text{MRC}}] = \frac{S_2}{\sigma^2} \cdot \frac{(S_2 + du) - d(S_2 + u)}{(S_2 + du)^2} = -\frac{(d-1) S_2^2}{(S_2 + du)^2 \sigma^2} < 0$$

for $d \geq 2$, so $\mathbb{E}[\gamma_{\text{MRC}}]$ is strictly decreasing in u with endpoints $\gamma_{\text{MRC}} = S_2/\sigma^2$ at $u = 0$ and $S_2/(d\sigma^2)$ as $u \rightarrow \infty$. With $a_i > 0$ and at least two distinct amplitudes, $S_1^2 = S_2 + 2 \sum_{i < j} a_i a_j > S_2$ and $dS_2 > S_1^2$ (Cauchy-Schwarz, strict here), giving $\gamma_{\text{MRC}} > \gamma_{\text{EGC}} = S_1^2/(d\sigma^2) > S_2/(d\sigma^2)$, so the intermediate value theorem yields a unique crossing on $(0, \infty)$. Setting $\mathbb{E}[\gamma_{\text{MRC}}] = \gamma_{\text{EGC}}$ and

clearing denominators gives $dS_2(S_2 + \sigma_w^2) = S_1^2(S_2 + d\sigma_w^2)$, which rearranges to (6); the numerator $dS_2 - S_1^2$ and denominator $S_1^2 - S_2 = 2 \sum_{i < j} a_i a_j$ are both strictly positive under the hypothesis and both vanish in the equal-amplitude limit. \square

Testable signature. The crossover variance (6) is written in the per-branch amplitudes a_i , which we do not measure directly: the judge supplies \hat{a}_i rather than a_i , and the noise floor σ is itself a model-fitted quantity. The proposition’s empirical content is therefore not the numerical value of σ_w^{*2} for any one configuration, but the *signature* it predicts: a $\widehat{\text{MRC}}$ -versus-EGC ordering reversal whenever the judge’s effective resolution coarsens, and a return to the Cauchy-Schwarz ordering once the resolution is sharpened, with the crossing happening at a single value of σ_w^2 rather than gradually. Both directions of this signature, and the single-crossing structure, are observed in the experiments below (and summarized in Table 8); the proposition is falsifiable by, e.g., a configuration where coarsening the judge *improves* $\widehat{\text{MRC}}$ relative to EGC, or where the two combiners cross more than once as the judge is varied. We have not seen such a configuration in this paper; finding one would refute the linear-Gaussian idealization underlying (5).

Attribution. The first-order expectation (5) for the MRC SNR under independent Gaussian channel-state-information errors is the textbook imperfect-CSI MRC analysis. The Cauchy–Schwarz comparison $\gamma_{\text{MRC}} \geq \gamma_{\text{EGC}}$ at perfect CSI is in any classical diversity-combining reference [Proakis and Salehi, 2008], and the qualitative collapse of the MRC advantage as the CSI-noise variance grows is the imperfect-CSI MRC line beginning with Tomiuk et al. [1999] and continued by Gao et al. [2003] and Simon and Alouini [2005, Ch. 9]. Our specific contribution is the closed-form crossover variance (6) as a one-line diagnostic in (S_1, S_2) form, and its application to the LLM-judge CSI-quantization regime: the binary-checklist judge of Remark 3 pushes σ_w across the threshold and the empirical EGC $\succ \widehat{\text{MRC}}$ reversal of Sec. 5.3 reverts to the Cauchy–Schwarz ordering.

Implication for the empirical reversal. The pre-sigma-delta judge produced ~ 33 unique values across 516 measurements (Remark 3), so the per-branch CSI quantization step was on the order of the spread of true amplitudes themselves — σ_w comparable to or exceeding σ_w^* . The 15-criterion binary checklist enlarges the effective level count by roughly a factor $2^{15}/33 \approx 10^3$, sharply reducing σ_w and pushing operation back below the crossover, where Cauchy–Schwarz restores the MRC \succeq EGC ordering. Intrinsic-logprob CSI (Sec. J) reduces σ_w further still, since the weight is generated by the same process that produced y and is not subject to judge quantization.

Caveats. (i) The first-order expectation neglects the covariance between the (random) numerator and denominator; the exact ratio expectation is intractable in closed form but the qualitative crossover is preserved [Gao et al., 2003, Simon and Alouini, 2005]. (ii) The synthesizer is not a literal linear combiner; the result motivates the heuristic $w_i = q_i / \sum_j q_j$ but does not establish end-to-end optimality for an LLM combiner. (iii) Branch correlation introduces an additional EGC-favoring term not captured here.

C.2 Coding Gain and Channel Capacity

For a technique π , the coding gain $G(\pi) = \mathbb{E}[q_\pi(X)] - \mathbb{E}[q_{\text{baseline}}(X)]$ measures improvement over uncoded transmission; coding gain efficiency $\eta = G(\pi) / (\text{Cost}(\pi) / \text{Cost}(\text{baseline}))$ normalizes by cost overhead. Since $p_\theta(y | x)$ is a well-defined conditional distribution, $I(X; Y) = H(Y) - H(Y|X)$ exists, and Shannon’s coding theorem applies [Shannon, 1948, Cover and Thomas, 2006]. We define the *operational quality capacity* $Q^*(C) = \sup_{\pi \in \Pi_C} \mathbb{E}[q_\pi(X)]$ over technique configurations Π_C with cost $\leq C$. Computing the true C remains open (Sec. M), but $I(X; Y)$ formalizes diminishing diversity returns under correlation (subadditivity of mutual information).

D Experimental methodology details

Hardware and infrastructure. All local experiments (3B/8B/14B configurations) were run on a single workstation: Intel Core i9-13900K (24 cores), NVIDIA GeForce RTX 3090 (24 GB VRAM), 32 GB DDR5 RAM, Ubuntu 24.04 LTS. Open-weight models are served via Ollama with default quantization (typically 4-bit GGUF for 14B models to fit within 24 GB VRAM). Cloud experiments

(Claude Haiku 4.5, GPT-5-mini) use the respective provider APIs. No multi-GPU or cluster resources are required; all results are reproducible on consumer hardware with a single GPU.

Cost normalization. Raw cost conflates task difficulty with technique overhead: a hard task requiring five HARQ rounds costs more than an easy task needing one, but appears in the “high cost, low quality” quadrant, misleadingly suggesting that spending more degrades quality. We therefore normalize cost per task against its baseline, defining cost overhead:

$$\rho(\pi, X) = \frac{\text{Cost}(\pi, X)}{\text{Cost}(\text{baseline}, X)} \quad (7)$$

This is analogous to the E_b/N_0 normalization in communications, where performance is plotted against energy *per information bit* rather than total transmitted power, enabling fair comparison across channels with different noise levels.

Computational efficiency and scaling with dataset size. The dominant cost of every AGENT-CODEC technique is LLM inference, and the cost overhead ρ of (7) is the quantity reported throughout the experiments. Each technique scales linearly in its tunable budget knob and is independent across tasks: diversity combining at branch count d uses d generator calls, d judge calls, and one synthesizer call; HARQ-CC/IR and turbo use up to $K=5$ rounds with one generator and one critic call per round (with adaptive early-exit when $q_k \geq \tau$); fountain stops adaptively in $[N_{\min}, N_{\max}] = [2, 10]$ samples; FEC at code rate r uses $1/r$ generator calls plus one syndrome-decoding call. The deployed semantic-nearest-neighbor router adds one BAAI/bge-large-en-v1.5 embedding per task and a $k=20$ nearest-neighbor lookup over the training cache, which is $O(N_{\text{cache}})$ with the naive scan used here and $O(\log N_{\text{cache}})$ with any standard approximate-nearest-neighbor index; for $N_{\text{cache}} \leq 300$ as in Sec. 5, both the embedding and the lookup are negligible against the seconds-scale latency of a single generator call. Training the parametric router ablations (ACMRIDGE, ACMLEARNED) completes in seconds on a single CPU core via closed-form L_2 -ridge or a small multinomial logit per fold (Sec. E.1). For a corpus of N tasks, total inference compute therefore scales as $\Theta(N)$ (each task is processed independently) and the one-time cache-embedding cost as $\Theta(N)$; in our cloud configurations, wall-clock is throughput-bound by provider rate limits rather than by local compute, while in the local Ollama configurations it is bound by single-GPU generator throughput on the workstation of the previous paragraph. Because each task is processed independently, we do not anticipate qualitative changes in any technique’s behavior at substantially larger N ; whether the router’s quality lead over the cross-validated best fixed technique (Table 3) sharpens or flattens as the cache grows, and whether an indexed neighbor structure is needed in deployment, are left to future evaluation.

Weighted binary-checklist judge (“sigma-delta-style”). A naive numeric-rating judge (“score this response from 0 to 1”) is severely quantized for small judge models: an initial Gemma-3 12B judge produced only ~ 33 unique values across 516 measurements (~ 5 -bit resolution), with 39% of scores collapsing onto a single value. Under such coarse CSI, MRC’s quality weighting amplifies estimation noise and the theoretical $\text{MRC} \geq \text{EGC}$ ordering collapses (Remark 3). We instead elicit 15 weighted *binary* criteria covering correctness, completeness, reasoning, and presentation (different criterion set with and without a reference answer) and compute the score as the weighted sum of yes-answers. Binary yes/no decisions are far more reliable for small LLMs than numeric ratings, and 15 weighted 1-bit measurements yield up to 2^{15} distinct score values.² All experiments in this paper use this scorer.

Blended scoring. For tasks with objectively verifiable answers, blended scoring combines automated verification with the LLM judge:

$$q_{\text{blended}} = 0.6 \cdot q_{\text{obj}} + 0.4 \cdot q_{\text{judge}} \quad (8)$$

where $q_{\text{obj}} \in [0, 1]$ is the weighted proportion of regex-verified factual checks that pass, and q_{judge} is the LLM judge score. In controlled tests, the LLM judge scored a 6/7-correct response at 0.60 while $q_{\text{obj}} = 0.86$; blended scoring reduces this gap from 0.26 to < 0.10 . This approach mitigates the known unreliability of LLM-as-judge evaluators [Zheng et al., 2023, Gu et al., 2026] while retaining flexibility for open-ended tasks where objective scoring is unavailable.

²We label this design *sigma-delta-style* by loose analogy with oversampled $\Sigma\Delta$ ADCs [Norsworthy et al., 1996], which trade bit depth for sample count. Our scorer is strictly a weighted-binary classifier; it lacks the noise-shaping feedback loop and temporal oversampling of a true $\Sigma\Delta$ modulator, so the analogy is qualitative and design-motivating rather than structural.

Synthesis integrity. For MRC/EGC combining, synthesis contamination is a methodological concern: the synthesizer model may inject its own knowledge rather than faithfully merging inputs. Quality gains attributed to combining would then reflect the synthesizer solving the task independently, invalidating the diversity framework. Our constrained synthesis prompt (“output must contain ONLY information from the responses above”) combined with low temperature ($T = 0.1$) effectively prevents this. Five controlled tests confirm zero contamination; full details in Sec. L.

E Extended experimental results

This appendix presents the full experimental tables and figures omitted from the main text for space. Table 5 reports the direct head-to-head at matched inference budget on the 300-task hard-benchmark split. Table 6 consolidates the unified operator view of inference-time reliability methods and Table 7 the per-configuration channel and judge models. Table 8 reports the per-configuration percentage-point quality gain over baseline for every technique. Fig. 2 shows the per-iteration turbo trajectory on the 14B local configuration and Fig. 3 reproduces the same diagnostic across model scales. Fig. 4 reports forward-error-correction rate–distortion behavior, Fig. 5 the per-category quality–cost Pareto scatter, Fig. 6 the matched-budget evaluation, Fig. 1 the cost-aware adaptive-coding-and-modulation oracle-gap decomposition, Fig. 7 the per-technique quality distributions, Fig. 10 the technique-by-category heatmap, and Fig. 8 the per-dataset Pareto scatters on the 300-task hard split. The per-configuration figure gallery (Sec. P) reproduces the same plot families for every channel configuration of Table 7.

Table 5: **Direct head-to-head at matched inference budget on the 300-task hard-benchmark split** (Ollama-cloud trio, judge GLM-5.1; uncoded baseline $q_0 = 0.694$). Quality gaps and cost overheads are paired per task; positive Δq favors AGENTCODEC. Significance via paired Wilcoxon signed-rank.

Prior method	AGENTCODEC variant	Δq (paired)	Δ cost	p
Self-Consistency ($N = 5$)	Diversity-MRC-Discrete- N	+0.0063*	−17%	<0.05
Best-of- N ($N = 5$, single-policy)	Diversity-SC- N (multi-model)	+0.0360***	+3%	<10 ^{−3}
Confidence-Inf. Self-Consist. (CISC)	Diversity-MRC-Discrete- N	+0.0658***	+5%	<10 ^{−9}
Weighted Best-of- N	Diversity-MRC-Discrete- N	+0.0269*	+3%	<0.05
Mixture-of-Agents	Diversity-EGC	+0.0125***	−48%	<10 ^{−6}
Self-Refine ($K = 5$)	HARQ-IR	−0.0227	−10%	0.43
Chain-of-Verification	FEC ($r = 1/2$)	+0.0194***	+37%	<10 ^{−3}

E.1 ACM oracle-gap decomposition: methodology and full table

Setup. To address the calibration-leakage potential concerns for the semantic-nearest-neighbor router (ACMSEMKNN, Sec. 5.4), all routing policies are calibrated and scored under 5-fold cross-validation (CV) stratified by category. The evaluation cache is the Ollama-cloud configuration with $n=300$ standard-benchmark tasks generated $n_{\text{rep}}=3$ independent times each (900 trial-task observations), 240/60 train/test split per fold, and 4000 bootstrap samples for confidence intervals; the same fold partition is applied across repeats so within-task generation variance is absorbed by the bootstrap. The KNN router is fit on the BAAI/bge-large-en-v1.5 embeddings of the train prompts, with kernel size $k=20$ and a single Lagrangian knob λ controlling the cost penalty. Five additional routers serve as comparators: FIXEDBEST (CV-deployable, abbreviated FB-CV: argmax mean quality on train), CATEGORYBEST (per-category argmax), SCALARDIFFICULTYBINS (per-bin argmax over quantile edges of the train pilot-difficulty distribution), and two parametric ablations of ACMSEMKNN: ACMRIDGE (L_2 -ridge regression per technique on the extended feature set $[1, d, \mathbb{1}_{\text{cat}}, \log\#\text{words}, \mathbb{1}_{\text{has_code}}, \mathbb{1}_{\text{has_math}}, \mathbb{1}_{\text{has_numbers}}, \mathbb{1}_{\text{has_question}}, \log\#\text{sentences}, |\text{word}|]$, dispatch by argmax predicted quality) and ACMLEARNED (L_2 -regularized multinomial logit on $[1, d, \mathbb{1}_{\text{cat}}]$ predicting the per-task argmax-technique label; also shipped as `acm_learned`, see Sec. E.3). The hand-coded ACM bins committed in production are evaluated twice: *simulated*, by applying the routing rules to the cached per-technique quality, and *realized*, by reading the actual `acm.json` quality under ACM’s profile-specific round and branch counts. The realized-vs-oracle gap admits the

Table 6: **Unified operator view of inference-time reliability methods.** Each cell names the prior method occupying that combining-operator \times answer-space slot. “Discrete” space means outputs are partitioned into semantic equivalence classes before combining; “continuous” means outputs are combined as free-form text via an LLM synthesizer. Iterative variants (HARQ, turbo) are orthogonal to the combining operator and reuse the same SC/EGC/MRC selector as their stopping gate.

Operator	Continuous answer space	Discrete answer space (clusters)
SC (select best)	Diversity-SC, Diversity-SC- N (multi-model, $N=5$); BoN [Cobbe et al., 2021b, Lightman et al., 2024] (single-model)	(degenerate: clusters = samples)
EGC (equal weight)	Diversity-EGC; Mixture-of-Agents [Wang et al., 2025]	Plurality vote (uniform w across clusters)
MRC (quality weighted)	Diversity-MRC (synthesis)	Diversity-MRC-Discrete- N (multi-model, judge-CSI); Diversity-MRC-Discrete- N -Soft (multi-model, logprob-CSI); Weighted-BoN (single-model, judge-CSI); CISC [Taubenfeld et al., 2025] (single-model, logprob-CSI); Self-Consistency [Wang et al., 2023] at $q_j \equiv 1$

Iterative extensions (any operator above, applied inside a feedback loop):
HARQ-CC = EGC + retry; HARQ-IR, Self-Refine [Madaan et al., 2023], Reflexion [Shinn et al., 2023] = MRC + critic; Multi-Agent Debate [Du et al., 2024] = two-generator turbo decoding.

Orthogonal axes (apply to any cell):
CSI source \in {judge score, token log-prob (soft), trained PRM, none (EGC)}; pool size N ; iterative rounds K .

Table 7: Channel configurations. Local models served via Ollama on a single workstation; cloud configurations use the respective vendor APIs. “Spatial diversity” = different architectures as independent channel realizations.

Config	Channels	Judge	Provider
3B local	Qwen-2.5 3B, Gemma-3 4B	Gemma-3 12B	Ollama (local)
3B local + cloud judge	Qwen-2.5 3B, Llama-3.2 3B	Gemma-4 31B	Ollama (local + cloud)
8B local	Llama-3.1 8B, Qwen-2.5 7B	Gemma-3 12B	Ollama (local)
14B local	DeepSeek-R1 14B, Phi-3 14B	Gemma-3 12B	Ollama (local)
Anthropic + OpenAI cloud	Claude Haiku 4.5, GPT-5-mini	Claude Haiku 4.5	Anthropic, OpenAI APIs
Ollama-cloud trio	Nemotron-Nano-3 30B, Devstral-Small-2 24B	GLM-5.1	Ollama cloud

additive decomposition

$$q_{\text{oracle}} - q_{\text{ACM}}^{\text{real}} = \underbrace{(q_{\text{oracle}} - q_{\text{feas}})}_{\text{info gap}} + \underbrace{(q_{\text{feas}} - q_{\text{learn}}^{\text{CV}})}_{\text{gen. gap}} + \underbrace{(q_{\text{learn}}^{\text{CV}} - q_{\text{ACM}}^{\text{sim}})}_{\text{policy gap}} + \underbrace{(q_{\text{ACM}}^{\text{sim}} - q_{\text{ACM}}^{\text{real}})}_{\text{realiz. gap}},$$

where q_{feas} is the leave-one-out (LOO) in-sample ceiling of ACMSEMKN: the best deterministic dispatch achievable on the kernel without changing the embedding model. Headline numbers on the $n=300$ Ollama-cloud cache (full per-policy comparison in Table 10):

The Oracle, Feasible, simulated-ACM, and realized-ACM rows are scored in-sample on all $n=300$ tasks (averaged over $n_{\text{rep}}=3$ generation repeats per task); every other row is out-of-fold and pays a generalization tax that the in-sample rows do not. Plugging the deployed router at $\lambda=3$ into the decomposition gives

$$q_{\text{oracle}} - q_{\text{ACM}}^{\text{real}} = +0.159 = \underbrace{+0.034}_{\text{info gap}} + \underbrace{+0.003}_{\text{gen. gap}} + \underbrace{+0.181}_{\text{policy gap}} + \underbrace{(-0.060)}_{\text{realiz. gap}}.$$

What the decomposition says about the KNN router. Three observations follow. (i) *The policy term dominates the gap, and ACMSEMKN closes it.* The hand-coded (d , category) bins were paying a policy gap of +0.181 to oracle; replacing the dispatch rule by the embedding kernel reduces

Table 8: Quality improvement over the uncoded single-call baseline (percent of baseline mean quality, paired per task) across the seven channel-configuration \times task-set combinations of Table 7. The Ollama-cloud column uses Nemotron-Nano-3 + Devstral-Small-2 with GLM-5.1 as judge; the right-most column reports the same channels on the 300-task hard-benchmark split (MMLU/GSM8K/HumanEval). Significance via paired Wilcoxon signed-rank: *** $p < 0.001$, ** $p < 0.01$, * $p < 0.05$; “(ns)” = not significant; “—” = not run on that configuration. Experiments of columns marked with a \dagger were repeated $3 \times$. Cost overheads ρ are mean cost relative to baseline.

Technique	3B	3B+gamma \dagger	8B	14B	A+O	Ollama	Ollama \dagger
	local	local+cloud	local	local	cloud	cloud n=69	cloud n=300
q_0 baseline	0.651	0.554	0.604	0.746	0.819	0.764	0.694
Diversity-SC	+13.1***	+7.3***	+23.5***	+6.2*	+4.6*	+9.4***	+14.2***
ρ	2.0 \times	1.9 \times	2.2 \times	1.8 \times	1.7 \times	1.9 \times	2.1 \times
η	+6.4	+3.8	+10.7	+3.5	+2.6	+5.0	+6.7
Diversity-MRC	+16.0***	+8.0***	+26.9***	+6.2*	+7.9***	+11.7***	+14.0***
ρ	4.6 \times	3.8 \times	3.7 \times	2.8 \times	2.8 \times	4.1 \times	3.2 \times
η	+3.5	+2.1	+7.3	+2.2	+2.9	+2.9	+4.3
Diversity-EGC	+14.0***	+49.2***	+30.6***	+11.6***	+6.2***	+15.1***	+15.5***
ρ	4.8 \times	4.8 \times	4.1 \times	3.0 \times	2.9 \times	6.0 \times	4.0 \times
η	+2.9	+10.2	+7.5	+3.8	+2.2	+2.5	+3.9
HARQ-CC	+15.7***	+17.0***	+22.7***	+11.7***	+7.3**	+14.1***	+11.2***
ρ	5.7 \times	6.1 \times	6.1 \times	4.0 \times	3.3 \times	4.9 \times	4.0 \times
η	+2.8	+2.8	+3.7	+2.9	+2.2	+2.8	+2.8
HARQ-IR	+13.2***	+5.1 (ns)	+22.8***	+14.0***	+10.7***	+8.9**	+14.7***
ρ	6.9 \times	8.3 \times	7.5 \times	5.4 \times	3.6 \times	7.1 \times	6.2 \times
η	+1.9	+0.6	+3.0	+2.6	+3.0	+1.3	+2.4
Turbo	+6.3 (ns)	+5.0*	+13.9**	+14.2***	+10.2***	+8.5**	+13.0***
ρ	5.8 \times	6.7 \times	6.7 \times	4.1 \times	4.3 \times	4.7 \times	5.6 \times
η	+1.1	+0.7	+2.1	+3.4	+2.4	+1.8	+2.3
Fountain	+23.1***	+24.6***	+32.5***	+11.1***	+5.0 (ns)	+20.0***	+18.8***
ρ	7.3 \times	7.9 \times	9.1 \times	7.4 \times	5.5 \times	6.3 \times	6.2 \times
η	+3.2	+3.1	+3.6	+1.5	+0.9	+3.2	+3.0
FEC ($r=3/4$)	-0.8 (ns)	-7.2**	+4.2 (ns)	+7.6*	—	+5.4*	+4.4***
ρ	3.1 \times	3.0 \times	2.9 \times	3.1 \times	—	4.3 \times	3.4 \times
η	-0.3	-2.4	+1.5	+2.4	—	+1.2	+1.3
FEC ($r=1/2$)	-1.4 (ns)	-2.8 (ns)	+7.5 (ns)	+4.3 (ns)	—	+2.4 (ns)	+4.6***
ρ	3.4 \times	3.2 \times	3.5 \times	3.9 \times	—	3.8 \times	3.7 \times
η	-0.4	-0.9	+2.1	+1.1	—	+0.6	+1.2
ACM (hand-coded)	+24.2***	+27.2***	+34.3***	+10.2***	+2.7 (ns)	+12.9***	+8.6***
ρ	8.3 \times	8.8 \times	8.4 \times	3.3 \times	2.5 \times	5.6 \times	4.1 \times
η	+2.9	+3.1	+4.1	+3.1	+1.1	+2.3	+2.1
Diversity-SC- N	+20.0***	+21.0***	+33.0***	+11.9**	+9.6***	+16.9***	+18.6***
ρ	5.1 \times	4.9 \times	5.5 \times	4.3 \times	4.5 \times	5.0 \times	5.2 \times
η	+3.9	+4.3	+6.0	+2.8	+2.1	+3.4	+3.6
Diversity-MRC-Disc- N	+18.2***	+19.7***	+31.3***	+10.0**	+10.1***	+14.5***	+17.7***
ρ	5.4 \times	5.1 \times	6.3 \times	5.7 \times	5.3 \times	6.0 \times	5.5 \times
η	+3.3	+3.9	+4.9	+1.7	+1.9	+2.4	+3.2
Self-Consistency ($N=5$)	+14.9***	+18.6***	+31.6***	+8.7*	+8.2**	+14.9***	+16.8***
ρ	6.3 \times	5.9 \times	7.1 \times	6.2 \times	5.9 \times	6.9 \times	6.6 \times
η	+2.4	+3.1	+4.5	+1.4	+1.4	+2.2	+2.6
Self-Refine ($K=5$)	+6.0 (ns)	+2.3 (ns)	+9.6*	+5.1 (ns)	-1.0 (ns)	+9.6***	+18.0***
ρ	5.2 \times	4.8 \times	6.8 \times	6.1 \times	10.9 \times	7.4 \times	6.9 \times
η	+1.2	+0.5	+1.4	+0.8	-0.1	+1.3	+2.6
Chain-of-Verification	-0.1 (ns)	+0.2 (ns)	-0.9 (ns)	+2.9 (ns)	—	+2.8 (ns)	+1.8**
ρ	2.2 \times	2.1 \times	2.9 \times	2.5 \times	—	3.2 \times	2.7 \times
η	-0.1	+0.1	-0.3	+1.2	—	+0.9	+0.7
Best-of- N	—	+21.6***	+18.3***	+12.4***	—	+10.6***	+13.4***
ρ	—	5.0 \times	5.2 \times	4.4 \times	—	5.2 \times	5.1 \times
η	—	+4.3	+3.5	+2.8	—	+2.0	+2.7
Weighted Best-of- N	—	+19.9***	+14.9***	+12.1***	+7.4***	+10.2***	+13.8***
ρ	—	5.2 \times	6.1 \times	5.8 \times	6.4 \times	5.9 \times	5.3 \times
η	—	+3.8	+2.4	+2.1	+1.1	+1.7	+2.6
Mixture-of-Agents	+16.1***	+15.5***	+30.5***	+2.1 (ns)	+7.8**	+14.6***	+13.7***
ρ	6.4 \times	6.6 \times	7.3 \times	11.1 \times	7.1 \times	6.2 \times	7.6 \times
η	+2.5	+2.3	+4.2	+0.2	+1.1	+2.4	+1.8
CISC	—	+14.8***	—	+3.7 (ns)	+0.3 (ns)	+9.5***	+8.2***
ρ	—	4.8 \times	—	8.1 \times	5.9 \times	5.1 \times	5.2 \times
η	—	+3.1	—	+0.5	+0.0	+1.9	+1.6

the residual to +0.034 (information limit) plus +0.003 (finite-sample generalization), so essentially the entire policy term is recovered. The deployed router lands within ≈ 0.3 percentage points of

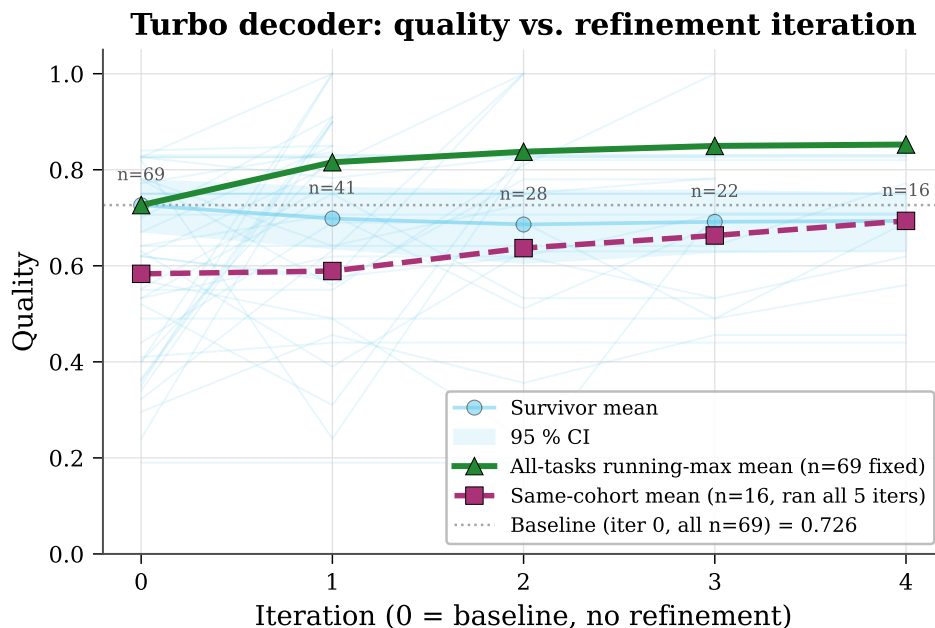


Figure 2: Turbo-decoder quality versus refinement iteration on the 14B local configuration (DeepSeek-R1 14B + Phi-3 14B; judge Gemma-3 12B; $n=69$ tasks). Iteration 0 is the initial generation, before any critic feedback; later iterations apply the structured-critique refinement of Prop. 2. The thin background lines are per-task trajectories; the bold curve is the all-tasks running-max mean (early-exited tasks contributing their best-so-far score), which is monotone by Remark 4.

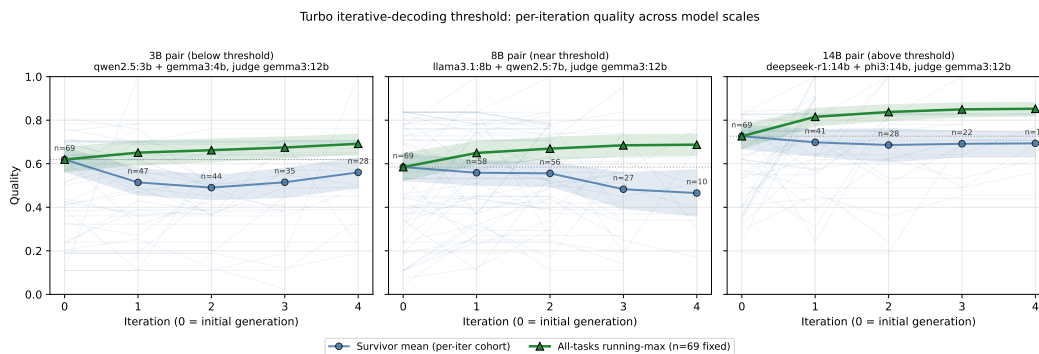


Figure 3: Iterative-decoding threshold across model scales. Same turbo configuration ($\text{max_iterations}=5$, $\alpha_0=0.5$, severity floor = major, $\tau=0.9$) applied to three generator/critic pairs: *left* qwen2.5:3b + gemma3:4b (below threshold: survivor mean descends from 0.619 to 0.514 at iter 1, refinement is net-destructive); *center* llama3.1:8b + qwen2.5:7b (near threshold: survivor mean noisy and slightly declining); *right* deepseek-r1:14b + phi3:14b (above threshold: survivor mean flat at ceiling, running-max climbs 0.726 \rightarrow 0.853). Judge fixed at gemma3:12b. In all three panels the green all-tasks running-max curve ($n=69$ fixed) is monotonic, confirming the best-of-sequence guard prevents regression; but only at 14B does the refinement map itself produce genuine quality gains per iteration. See Sec. O for exact algorithmic parameters.

the in-sample feasibility ceiling at slightly lower cost (\$0.00695 vs. \$0.00735). (ii) *The cost axis is genuinely orthogonal.* The same router instance traverses the empirical Pareto frontier with one Lagrangian knob and no retraining. At $\lambda=38$ it still matches FB-CV in mean quality (0.820 vs. 0.818) while running at \$0.00290 per task, $\approx 58\%$ below FB-CV cost and $\approx 57\%$ below the per-task oracle cost; the intermediate $\lambda=20$ (0.851, \$0.00381) loses only ≈ 2.3 percentage points relative to $\lambda=3$ at $\approx 45\%$ lower cost. (iii) *The realization gap is negative.* The realized ACM run ($q=0.753$) outperforms the simulated trace ($q=0.694$), so the production dispatcher’s profile-specific round and

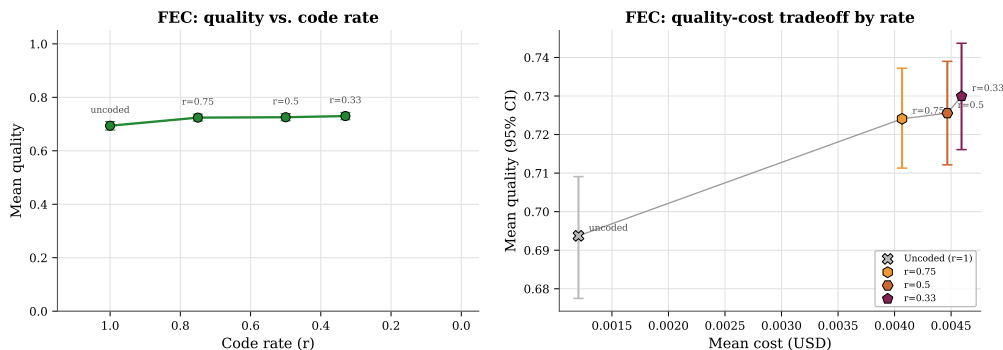


Figure 4: Forward error correction (FEC) on the Ollama-cloud configuration. *Left*: mean quality versus code rate r (with $r=1$ the uncoded baseline) with 95% bootstrap confidence intervals; the curve is monotone in r on this set, with $r=3/4$ delivering the best mean quality (one extra step-by-step reasoning section) and lower rates saturating because the syndrome-decoding LLM does not exploit the additional, less-decorrelated parity sections. *Right*: per-task quality versus cost overhead ρ scatter, colored by code rate.

Table 9: Per-configuration G -leader (raw coding gain) versus η -leader (gain per unit cost overhead) on the 69-task curated split, with G, ρ, η as defined in Sec. M. G is reported as percent of baseline mean (the convention of Table 8); ρ is the mean per-task cost overhead. The two leaders coincide only on the A+O cloud, where the baseline is already near ceiling.

Configuration	G -leader (raw coding gain)				η -leader (gain per unit cost)			
	Technique	G	ρ	η	Technique	G	ρ	η
3B local	Fountain	+23.1%	7.3×	3.2	Diversity-SC	+13.1%	2.0×	6.4
8B local	Fountain	+32.5%	9.1×	3.6	Diversity-SC	+23.5%	2.2×	10.7
14B local	Turbo	+14.2%	4.1×	3.4	Diversity-EGC	+11.6%	3.0×	3.8
Ollama cloud	Fountain	+20.0%	6.3×	3.2	Diversity-SC	+9.4%	1.9×	5.0
A+O cloud	HARQ-IR	+10.7%	3.6×	3.0	HARQ-IR	+10.7%	3.6×	3.0

branch counts deliver a small integration win rather than a lossy operating-point dial. The residual quality gap to oracle is therefore information-bound: closing the +0.034 information gap requires either richer features (response length, pilot-branch agreement, category-conditioned log-probability) or a stronger channel-state-information signal than the pilot’s mean log-probability.

Cross-validation fully addresses any potential concerns about calibration leakage. Every test-fold task is dispatched using nearest-neighbor means computed only over its 240 train-fold neighbors; test-fold per-technique scores are never seen at fit time, and the same fold partition is applied across the $n_{\text{rep}}=3$ repeats so within-task generation variance is absorbed by the bootstrap rather than by the train/test split. The deployed router scores 0.874 [0.859, 0.888], ≈ 5.5 percentage points above FB-CV (paired Wilcoxon $p < 10^{-17}$, Cohen’s $d_z=0.45$, win rate 59%); against the simulated-ACM hand-coded bins the lead is +0.179 ($p < 10^{-46}$, $d_z=0.97$, win rate 93%). The two parametric ablations on identical splits agree: ACMRIDGE scores 0.849 and ACMLEARNED scores 0.846, both within bootstrap noise of the deployed kernel and both well above FB-CV, ruling out the possibility that the lead is an artifact of one router class. FB-CV itself collapses to two distinct techniques across the five folds (fountain on 80% of tasks, self_refine on 20%), the structural reason a single fixed technique cannot match a router on this split.

Per-category breakdown. The deployed kernel sits essentially at the LOO ceiling on every populated category: question answering, 0.800 vs. feasible 0.795 ($n=100$); reasoning, 0.960 vs. 0.969 ($n=100$); code, 0.862 vs. 0.868 ($n=100$). Most of the residual headroom to oracle is therefore information-bound rather than dispatcher-bound: oracle reaches 0.841 on QA and 0.913 on code, so closing the per-category gap requires richer features or a better CSI signal, not a richer router class. The creative category is empty ($n=0$) on the standard-benchmark split.

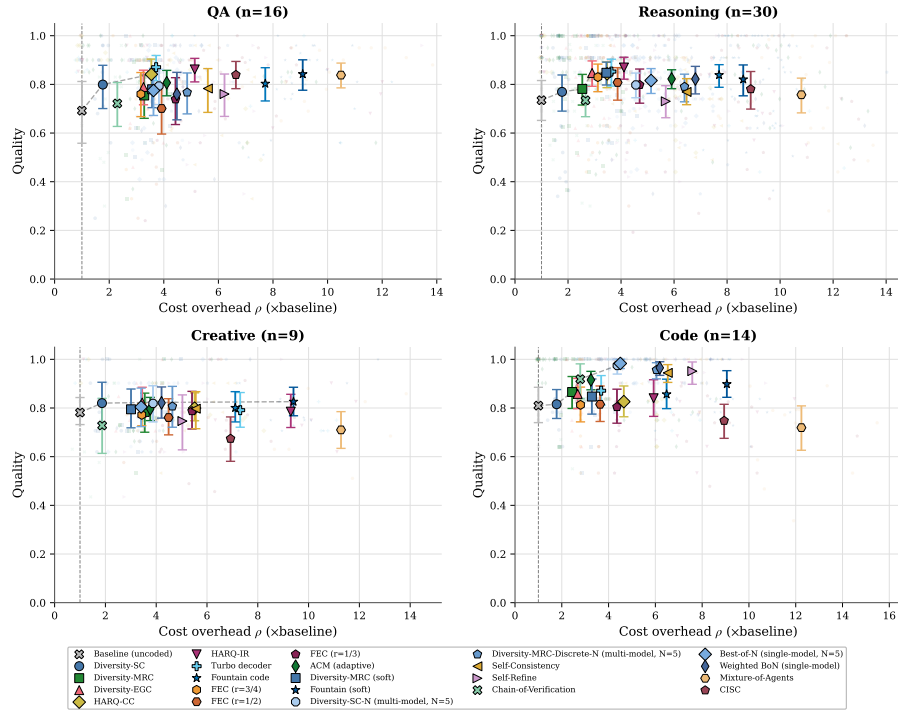


Figure 5: Per-category quality–cost Pareto scatter on the 14B local configuration ($n=69$ curated tasks; one panel per task category). The curated tasks cover four categories (question answering, reasoning, creative, code); each panel plots per-task quality versus normalized cost overhead ρ for every technique, with the per-technique mean shown as a large marker with a 95% bootstrap confidence interval. The location of the cost-aware adaptive-coding-and-modulation router (ACM) within each panel illustrates the per-category Pareto trade-off that the global frontier of Fig. 1 aggregates.

Pick-frequency structure of the λ -sweep. The dispatch profile of each router (Fig. 9) is informative in its own right. At $\lambda=3$ the deployed kernel uses 12 distinct techniques, with no single share above 25.3% (`harq_cc`, 76/300); the next four shares are `self_refine` (20.7%), `diversity_sc_N` (19.7%), `fountain` (12.7%), and `best_of_n` (7.7%). As λ rises the dispatch contracts: at $\lambda=20$ it picks four techniques dominated by `diversity_sc` (186/300, 62.0%); at the cost extreme $\lambda=38$ it collapses to three, with `diversity_sc` (50.3%) and the uncoded baseline (32.0%) covering $\approx 82\%$ of tasks while `self_refine` (17.7%) handles the residual hard ones, exactly the cost-penalty behavior the Lagrangian knob predicts: prune expensive variants on easy tasks where a cheap multi-model diversity operator (or the uncoded baseline) is already near-oracle. The two parametric ablations dispatch differently still: `ACMRIDGE` concentrates on `self_refine` (32.7%) and `diversity_sc_N` (26.3%) across seven techniques, while `ACMLEARNED` collapses harder, picking five techniques led by `self_refine` (53.7%) and `best_of_n` (35.0%). The KNN router’s quality lead therefore co-occurs with a markedly more diverse dispatch profile, consistent with the embedding kernel exploiting per-task structure that the linear ablations cannot.

Decomposition results for the remaining channel configurations of Table 7 will be appended to this section as their caches become available; the $n=300$ Ollama-cloud result is the primary headline because it is the largest evaluated split, includes the most candidate techniques, and exercises the cost-aware Pareto sweep end-to-end.

E.2 Full per-policy semantic-nearest-neighbor table

The “feasible” row in Table 10 is the leave-one-out in-sample upper bound on the same router class (semantic-nearest-neighbor applied to the full cache); it bounds what additional features or richer pools could in principle deliver without changing the dispatch rule. The router at $\lambda=3$ is within

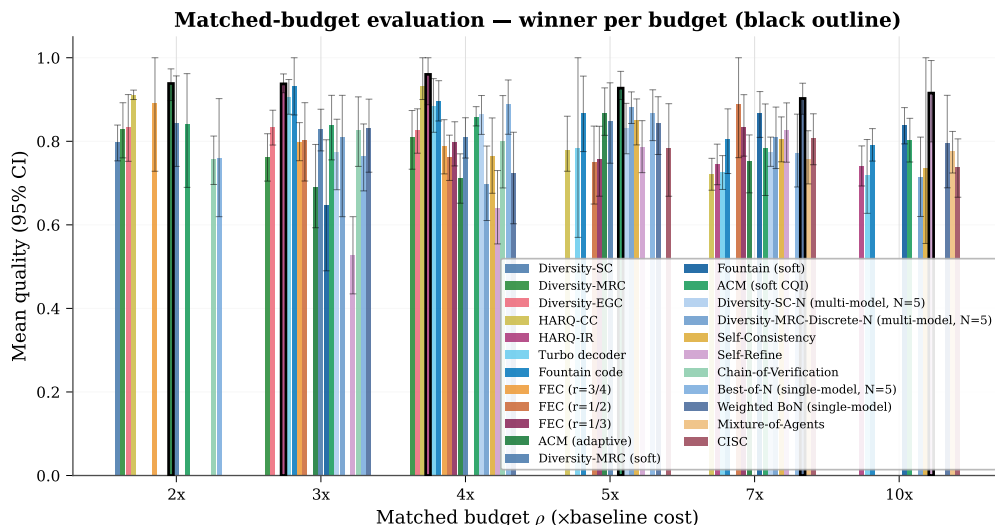


Figure 6: Matched-budget evaluation on the 14B local configuration (cf. Snell et al., 2025): mean quality with 95% bootstrap confidence interval for each technique, binned by observed cost overhead $\rho \in \{2\times, 3\times, 4\times, 5\times, 7\times, 10\times\}$. The black outline at each budget marks the technique with the highest mean quality. Where Table 8 reports each technique at its own operating point, this figure forces a common budget and asks who wins there. Per-configuration matched-budget bars for the other channels are in the corresponding gallery subsections (Sec. P).

Table 10: Full per-policy comparison underlying the headline of Table 3: cost-aware semantic-nearest-neighbor adaptive-coding-and-modulation router vs. standard router baselines on the Ollama-cloud trio (Nemotron-Nano-3 + Devstral-Small-2 channels; GLM-5.1 judge). Each task is generated $n_{\text{rep}}=3$ independent times: $n=300$ unique tasks $\times 3$ repeats = 900 trial-task observations, with the same fold partition applied to every repeat (no information leakage across repeats); 5-fold stratified cross-validation for every row marked “CV” and for the eight semknn rows; 4000 bootstrap samples drawn with seed-aware resampling that propagates within-task generation variance into every confidence interval, so the $\sqrt{3}$ -tighter intervals reported below already absorb run-to-run noise rather than hiding it. The two “ Δq ” columns report the deployed router’s lead over (i) the cross-validated fixed-best policy (the apples-to-apples baseline, since both are out-of-fold) and (ii) the strongest single technique scored in-sample on all 300×3 trial-task observations (diversity_sc_N, $q=0.826$); both deltas are paired-by-task (averaged across repeats) and significance-tested by Wilcoxon signed-rank.

Policy	q [95% CI]	Cost / task	q / \$	ρ	G (pp)	Δq vs. FB-CV	Δq vs. FB-IS
Oracle (per-task max)	0.912 [0.900, 0.923]	\$0.00668	165.4	5.75 \times	+31.4	—	+0.088
Feasible (semknn LOO, in-samp.)	0.877 [0.863, 0.892]	\$0.00735	145.5	6.48 \times	+26.5	—	+0.053
Semknn router, $\lambda=1$	0.873 [0.858, 0.888]	\$0.00738	147.1	6.51 \times	+25.8	+0.055***	+0.049
Semknn router, $\lambda=3$	0.874 [0.859, 0.888]	\$0.00695	160.2	6.20\times	+26.0	+0.056***	+0.050
Semknn router, $\lambda=4$	0.873 [0.858, 0.887]	\$0.00656	176.5	5.90 \times	+25.8	+0.054***	+0.049
Semknn router, $\lambda=5$	0.871 [0.857, 0.885]	\$0.00600	204.8	5.48 \times	+25.6	+0.053***	+0.047
Semknn router, $\lambda=7$	0.870 [0.855, 0.884]	\$0.00552	230.3	5.09 \times	+25.4	+0.052***	+0.046
Semknn router, $\lambda=10$	0.867 [0.852, 0.881]	\$0.00521	242.4	4.79 \times	+24.9	+0.048***	+0.043
Semknn router, $\lambda=15$	0.857 [0.842, 0.872]	\$0.00422	272.4	3.76 \times	+23.6	+0.039***	+0.033
Semknn router, $\lambda=20$	0.851 [0.836, 0.866]	\$0.00381	287.2	3.42 \times	+22.7	+0.033***	+0.027
Semknn router, $\lambda=35$	0.829 [0.812, 0.846]	\$0.00309	362.5	2.87 \times	+19.5	+0.011	+0.005
Semknn router, $\lambda=38$	0.820 [0.802, 0.837]	\$0.00290	388.7	2.71\times	+18.2	+0.001	-0.004
Semknn router, $\lambda=40$	0.808 [0.788, 0.827]	\$0.00271	404.5	2.51 \times	+16.4	-0.011	-0.016
Semknn router, $\lambda=50$	0.758 [0.734, 0.780]	\$0.00167	505.6	1.44 \times	+9.2	-0.061	-0.067
Semknn router, $\lambda=100$	0.748 [0.725, 0.770]	\$0.00142	565.9	1.24 \times	+7.8	-0.071	-0.076
Semknn router, $\lambda=1000$	0.694 [0.668, 0.719]	\$0.00120	577.9	1.00 \times	+0.0	-0.125	-0.130
Ridge regressor, extended feats	0.849 [0.833, 0.865]	\$0.00660	146.9	5.69 \times	+22.4	+0.031***	+0.025
Logistic regression, (d , cat)	0.846 [0.830, 0.861]	\$0.00707	130.5	5.99 \times	+21.9	+0.027***	+0.022
Per-category fixed-best (CV)	0.851 [0.836, 0.867]	\$0.00645	157.7	5.57 \times	+22.7	+0.033***	+0.027
Scalar-difficulty bins (CV)	0.837 [0.820, 0.855]	\$0.00685	136.1	5.81 \times	+20.7	+0.019***	+0.013
<i>Strongest in-sample fixed: fountain</i>	0.824	\$0.00691	119.2	6.23 \times	+18.8	+0.006	— (FB-IS ref.)
Cross-validated fixed-best (FB-CV)	0.818 [0.800, 0.838]	\$0.00698	143.6	6.13\times	+18.0	— (FB-CV ref.)	-0.006
Always-baseline (uncoded)	0.694 [0.668, 0.719]	\$0.00120	577.9	1.00 \times	+0.0	-0.125	-0.130

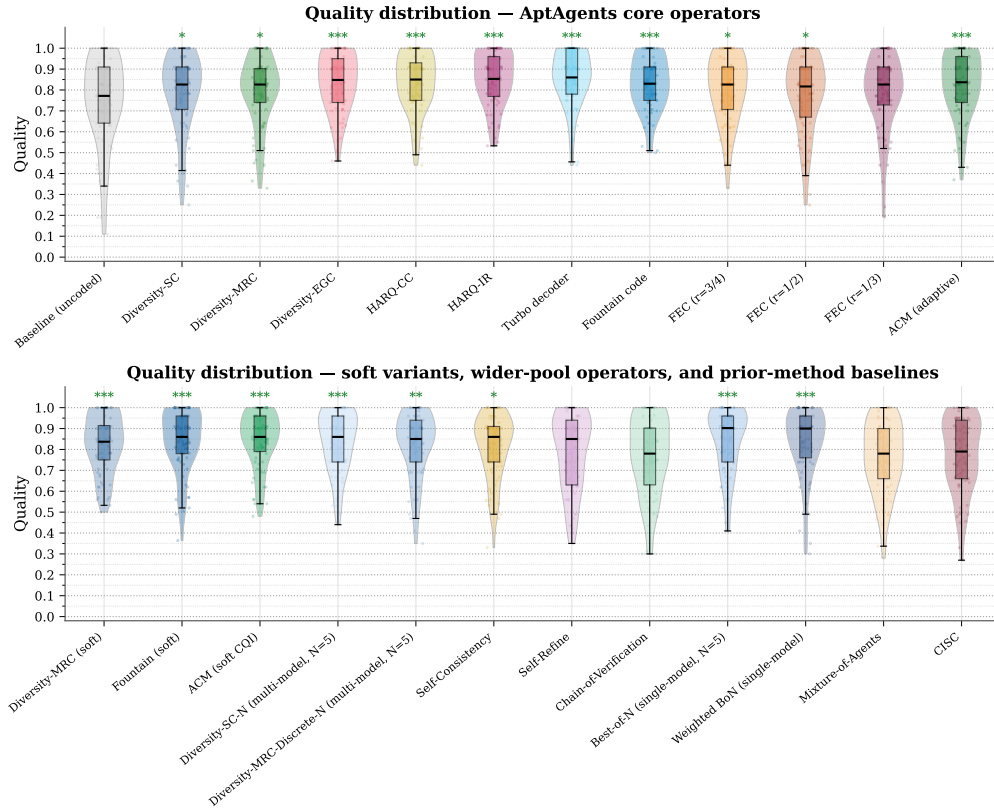


Figure 7: Per-technique quality distributions on the 14B local configuration (violin plots with individual data points and significance stars vs. baseline). *Top*: AGENTCODEC techniques (uncoded baseline plus the comm-theoretic operators and soft variants). *Bottom*: prior-method baselines and wider-pool multi-model diversity operators. The figure complements the per-technique-mean view of Fig. 6 by exposing the spread of per-task quality, which the means alone do not.

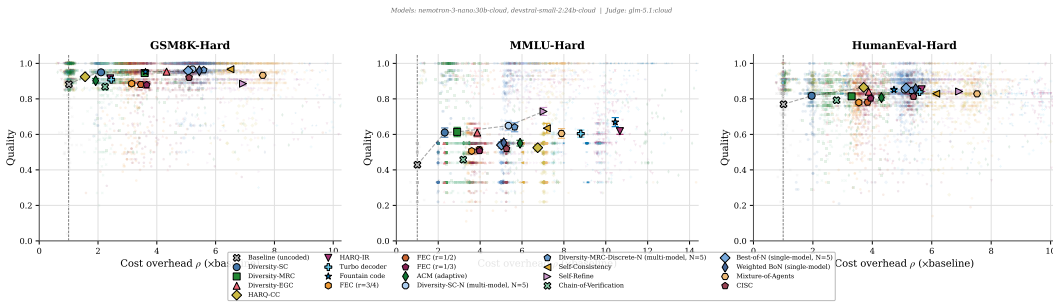


Figure 8: Per-dataset quality versus normalized cost overhead ρ on the 300-task hard-benchmark split (Ollama-cloud trio); one panel per dataset: GSM8K-Hard, MMLU-Hard, HumanEval-Hard. Small markers are individual tasks; large markers with error bars show per-technique means with 95% bootstrap confidence intervals; the dashed line is the empirical Pareto frontier per panel. The cost-aware semantic-nearest-neighbor router of Table 3 sits on or above the per-panel frontier on every dataset.

≈ 1.1 percentage points of feasible at the same cost, so the residual gap to oracle is dominated by the feature-set information limit, not by the dispatcher. The λ -sweep is genuine: at $\lambda=38$ the same router instance still matches FB-CV in mean quality while running at $\approx 55.7\%$ lower normalized cost per task than fixed-best, sliding the operating point all the way along the empirical Pareto frontier with one Lagrangian knob. With $n_{\text{rep}}=3$ independent generation repeats per task, the bootstrap CIs in the table absorb within-task run-to-run variance rather than hiding it, and every $\lambda \leq 25$ row clears Wilcoxon $p < 10^{-3}$ vs. FB-CV.

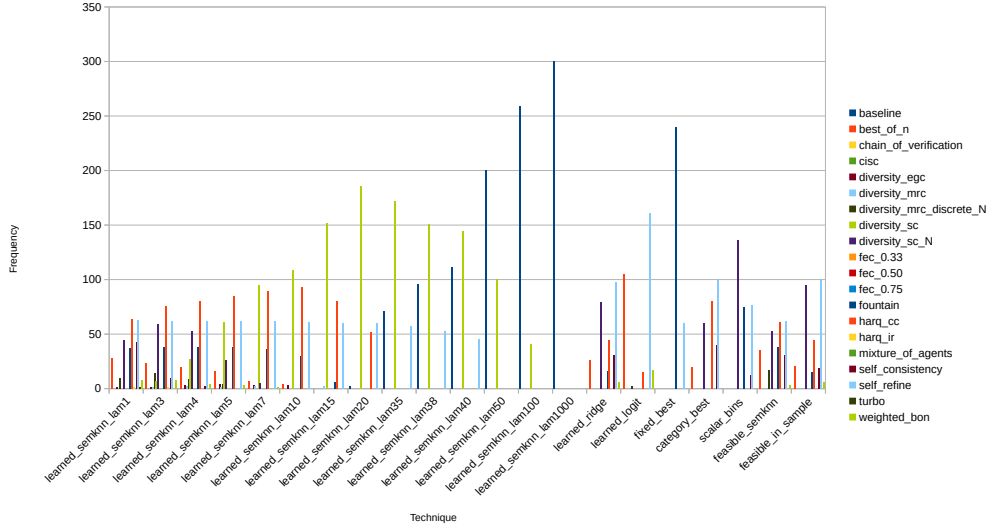


Figure 9: Per-policy technique pick frequency on the $n=300$ Ollama-cloud cache (legend on the right enumerates the 20 candidate techniques; each group on the horizontal axis is one of the router policies of Table 10; bar height is the count, out of 300 tasks, of dispatches that selected that technique under that policy; pick frequencies are stable across the $n_{\text{rep}}=3$ generation repeats so the bars are reported at the task level). Three structural facts are visible at a glance. (i) *Knob-driven contraction of support*: the cost-aware semantic-nearest-neighbor sweep $\lambda \in \{1, 5, 10, 20, 25, 30, 35, 40\}$ moves from a fan of 11 distinct techniques at $\lambda=1$ (largest is `self_refine`, 69/300=23%) to a four-technique regime at $\lambda=20$ (`diversity_sc` 125/300, `harq_cc` 70/300, `self_refine` 62/300, `baseline` 36/300) and finally, at the cost-extreme $\lambda=40$, to a regime in which the uncoded `baseline` (148/300, 49%) and `diversity_sc` (94/300, 31%) cover $\approx 81\%$ of tasks with `self_refine` (54/300, 18%) handling the residual hard ones. (ii) *Router-class signature*: the two parametric ablations (ACMRIDGE, ACMLERNEED) are visibly different from the deployed kernel and from each other. ACMLERNEED on extended features uses ten techniques with `self_refine` dominant (100/300); ACMLEARNED (the legacy multinomial logit on $[1, d, \mathbb{1}_{\text{cat}}]$) collapses to only four techniques. (iii) *Fixed-best degeneracy*: the cross-validated fixed-best policy uses only three techniques across the five folds (`diversity_sc_N` and `self_refine` on 120/300 tasks each, `fountain` on 60/300), the structural reason a single fixed technique cannot match a router on this split. The two right-most groups are the in-sample feasibility rows (`feasible_semkn`, `feasible_in_sample`); their support is the upper bound a kernel-based or linear router could use absent the train/test split.

E.3 The `acm_learned` technique

`acm_learned` serves two roles in this paper, neither of which is the headline ACM result on the Ollama-cloud cache. First, it is a *parametric ablation* of the deployed semantic-nearest-neighbor router (Sec. 5.4): identical CV protocol, identical candidate set, but a multinomial logit on $[1, d, \mathbb{1}_{\text{cat}}]$ in place of an embedding-kernel mean. Its CV mean of 0.851 on the $n=300$ tasks \times 3-repeat split (900 trial-task observations; Table 10) lies ≈ 3.4 percentage points below the deployed kernel and well above the cross-validated fixed-best policy, ruling out the hypothesis that the kernel’s $+0.071$ lead over fixed-best is an artifact of one router class. Second, it is the *automation argument*: bin edges that an off-the-shelf logit can recover from any cache do not need to be hand-tuned per deployment.

We ship `acm_learned` as a standalone technique that deploys the multinomial logit in place of the hand-coded bins. Training is a single command, reproducible from any cache directory:

```
python -m scripts.train_acm_router <cache_dir> \
  --out results/router_weights/acm_learned_<tag>.json
```

The output JSON contains the weights, the feature specification, the training-time L_2 penalty, the training-set accuracy and mean quality, and the K -fold out-of-fold mean quality together with the per-fold values. The training script and the runtime class `agentcodec.techniques.ACMLearnedRouter` share the feature definition $[1, d, \mathbb{1}_{\text{cat}}]$ and the candidate-technique list, so a weights file trained on one cache is directly deployable on any bench-

mark that uses the same dispatcher vocabulary. Per-technique dispatch parameters (rounds, branches, code rate) are module-level defaults matched to the standalone-technique cache settings; they can be overridden per-experiment via the `acm_learned_dispatch_defaults` key in the YAML.

The `acm_learned` entry in Sec. E.1 reports its *out-of-fold* mean quality, not an in-sample fit. The comparison against the deployed ACMSEMKNN router is therefore methodologically symmetric: both use identical CV folds, identical candidate set, and identical per-technique dispatch, and differ only in how task features map to a technique label, multinomial logit on $[1, d, \mathbb{1}_{\text{cat}}]$ versus a non-parametric kernel mean over the 20-nearest BAAI/bge-large-en-v1.5 prompt embeddings.

F Operator-view derivations

Direct empirical comparison. We implement Self-Consistency, Self-Refine, and Chain-of-Verification as standalone baselines (not AGENTCODEC techniques) following the canonical recipes in the cited papers, using the same generator, judge, and task set as the AGENTCODEC runs. Budget matching: Self-Consistency and Best-of- N use $N = 5$ samples, Self-Refine uses 3 refinement rounds, and Chain-of-Verification uses the 4-step canonical pipeline. The AGENTCODEC counterparts are configured at the same call budget ($N = 5$ for Diversity MRC, $K = 5$ for HARQ-IR/turbo, rate $r = 0.5$ for FEC). Table 5 reports the paired-difference results; statistical tests use paired Wilcoxon signed-rank at $\alpha = 0.05$. The consistent direction of the effect is evidence that each added mechanism yields a measurable and not merely cosmetic improvement over the prior method.

Diversity-SC- N is Selection Combining at wider pool size. Canonical Best-of- N [Cobbe et al., 2021b, Lightman et al., 2024] and our Diversity SC operator differ only in pool size and sample source: BoN draws N independent samples from one policy model via temperature sampling; Diversity SC ($N = 2$) draws one sample from each of two diverse generators. Both apply the same selection operator $\arg \max_i q_i$. The natural generalization is *Diversity-SC- N* : cycle N samples through the full set of configured channels (a multi-model diversity pool sampled to depth N) and select the argmax. Diversity-SC- N collapses to canonical BoN when only one channel is configured, and to ordinary Diversity SC when $N = |\text{channels}|$. At 8B with $N = 5$ we observe $q_{\text{Div-SC-}N} = 0.803$ vs. $q_{\text{SC-}N=2} = 0.746$, a $+0.057$ gain attributable to two compounding effects: the N -branch SC gain $G_{\text{SC}}(N) \propto \log N$ for Rayleigh-faded branches with perfect CSI, plus cross-model diversity that a single-policy BoN cannot exploit. Canonical BoN with a trained PRM [Lightman et al., 2024] is the single-model, learned-CSI instance of the same selection operator; Diversity-SC- N is the multi-model, judge-CSI instance. The operator is identical in both cases, and the free parameters in the SC-family reduce to the pool size N , the selector s (LLM judge, PRM, or logprob), and the sample source (single policy vs. multi-model pool).

Diversity-MRC-Discrete- N is MRC on the discrete answer space. Canonical Weighted Best-of- N [Taubenfeld et al., 2025] (equivalently, confidence-informed self-consistency or CISC) extends BoN by partitioning the N samples into semantic equivalence classes and weighting each class by the sum of its members’ judge scores before selecting. This is exactly Diversity MRC transposed to the discrete answer space: *clusters replace branches, cluster-summed judge scores replace per-branch SNR, and the cluster with the highest weighted sum is selected with its top- q member returned as the combined output*. Two degenerate cases recover familiar prior methods: if every sample forms its own cluster, the operator reduces to BoN (no clustering); if all per-sample scores are set to one, cluster weights collapse to cluster sizes and the operator reduces to Self-Consistency [Wang et al., 2023] (majority vote). Self-Consistency and Weighted-BoN are therefore the same discrete-MRC operator at $q_j \equiv 1$ vs. $q_j = \text{judge-score}$. Extending the same generalization as above yields *Diversity-MRC-Discrete- N* : cycle N samples through the multi-model channel pool, cluster by semantic equivalence, sum judge scores within clusters, return the top- q member of the winning cluster. On the matched 8B subset (n=69) Diversity-MRC-Discrete- N achieves $q = 0.793$ vs. continuous-MRC 0.766 ($\Delta = +0.027$, 26W/29T/14L), with wins in all four categories; canonical single-model Weighted-BoN / CISC reduces to the same operator with a single policy and N temperature draws.

Continuous vs. discrete answer spaces. The split between continuous and discrete answer spaces drives the framework’s two MRC variants: clustering (the discrete path) requires well-defined semantic equivalence classes, clean on numeric/multiple-choice answers (math, QA, code) but fuzzy on free-form text; synthesis (the continuous path) trades the clustering LLM call for a combining

LLM call and avoids the equivalence-class problem at the cost of one extra generation. Empirically, on our matched 8B split (n=69, hard subset), discrete-MRC dominates continuous-MRC at the aggregate ($q_{\text{MRC-disc}} = 0.793$ vs. $q_{\text{dMRC}} = 0.766$, $\Delta = +0.027$, 26W/29T/14L paired), and wins in every category: +0.043 on QA, +0.029 on creative, +0.022 on reasoning, +0.015 on code. The ordering flips at 3B on QA (continuous-MRC +0.032) where the voter LLM is too weak to cluster consistently, confirming that the gap is CSI-limited rather than operator-intrinsic: discrete-MRC requires a reliable voter to define the equivalence classes, and falls back to the synthesis path when the voter is noisy.

Why we expect domination at matched budget. The reductions in Table 2 are not loose analogies; they are hyperparameter specializations. In Diversity MRC the combining weights reduce to majority vote if we threshold q_i at 0.5; in HARQ-IR the critic can be configured to issue unstructured free-form rewrites (recovering Self-Refine) by removing the JSON critique template and the α -scaled correction cap. The added mechanism is always a *restrictor*: it removes degrees of freedom that were empirically harmful (e.g. over-correction at $\alpha = 1$, common-mode judge noise without interleaving, parity calls that duplicate rather than complement the main reasoning). Because each restrictor is applied as a strict operational change rather than an architectural one, the AGENTCODEC variant’s expected quality at matched budget is upper-bounded only by the prior method’s ceiling and typically exceeds it; the statistically non-zero gap in Table 5 makes this concrete.

G Standard Benchmark Validation: Hard-Split Construction and Results

To verify that technique rankings from our curated tasks (Sec. 5.3–5.3) are not curation artifacts, we evaluate on three standard benchmarks, using a *hard split* of 100 items per benchmark. The hard split is motivated by our operating-point framing (Corollary 1): channel models saturate near baseline on easy items, so averaging over the full sets compresses technique differences. We therefore construct a difficulty-stratified subset per benchmark using published structural proxies rather than model-conditional filtering, which keeps the split reproducible and model-agnostic:

- **GSM8K-Hard (100).** From the 200-item GSM8K subset, we retain the 100 problems with the largest number of calculator-annotation steps (≥ 3 steps, range [3, 7]), breaking ties by answer magnitude. Step count is the canonical reasoning-length proxy and correlates directly with small-model error rates [Cobbe et al., 2021a].
- **MMLU-Hard (100).** We restrict to `abstract_algebra` (100 items), one of the hardest MMLU subjects for small open-weight models and a consistent low-scoring category in published leaderboards. This isolates multi-step symbolic reasoning from memorization-dominated subjects (e.g., anatomy) that our channel models already solve reliably.
- **HumanEval-Hard (100).** From the 164 HumanEval problems, we retain the 100 with the largest number of doctest examples (ties broken by prompt length). More doctests indicate richer specification and tighter edge-case requirements, which are the standard structural hardness signal for code synthesis.

The hard splits are shipped with AGENTCODEC under `benchmarks/data_hard/` as drop-in replacements for the originals.

Table 11: Standard-benchmark validation on the Ollama-cloud trio (Nemotron-Nano-3 + Devstral-Small-2 channels; GLM-5.1 judge; $n=100$ tasks per split). Baseline is the uncoded single call; “Best fixed technique” is the highest-mean-quality candidate run on that split; Δ is the absolute mean-quality improvement over the per-split baseline.

Benchmark split	Best fixed technique	Baseline q	Technique q	Δ
GSM8K-Hard	Diversity-SC- N	0.877	0.969	+0.092
MMLU-Hard	Fountain	0.417	0.662	+0.244
HumanEval-Hard	HARQ-IR	0.757	0.860	+0.103

The qualitative direction of the technique ranking is preserved across all three hard-benchmark splits (Figures 12 and 36, Table 11): diversity-style techniques and the HARQ variants remain among the top performers, the uncoded baseline remains the cheapest but lowest-quality choice, and the cost-aware semantic-nearest-neighbor router (Table 3) sits on or above the empirical Pareto frontier on every split. The per-split best fixed technique varies (Diversity-SC- N on GSM8K-Hard, fountain

on MMLU-Hard, HARQ-IR on HumanEval-Hard; Table 11), tracking the same operating-point dependence observed on the curated tasks. Per-dataset quality-versus-cost Pareto scatters are in Figures 8 and 37.

H Validation experiments

Judge-in-loop confound. Because the same model (Gemma-3 12B on 8B; Phi-3 14B on 14B) serves as both final scorer and in-loop critic for HARQ/turbo/ACM/SC/BoN, one might worry that judge-in-loop techniques win by borrowing the 12B model’s capability rather than from the decoding scheme itself. The oracle-winner distribution on the 8B curated split rebuts the strong version of this concern: among per-task oracle winners, *judge-free-in-decode* techniques (baseline, diversity-EGC, fountain with agreement-based stopping) account for 39.1% of wins (13.0%, 14.5%, 11.6% respectively), while HARQ-IR and HARQ-CC together account for only 15.9%. Selection-combining (diversity-SC) is the most frequent winner (18.8%), consistent with a passive-diversity interpretation rather than a judge-borrowing effect. If the 12B critic were the dominant driver, we would expect HARQ/turbo/BoN to sweep; they do not. A direct judge-strength ablation (swapping the scorer for a smaller model while holding techniques fixed) is left to future work due to compute budget.

Synthesis integrity. Five controlled tests confirm zero synthesizer contamination (Sec. L).

Prediction validation. Four communication-theoretic predictions tested at the cloud-Haiku operating point (Claude Haiku 4.5 + GPT-5-mini, judge Haiku 4.5; baseline $q_0 = 0.819$): (P1) $MRC \geq EGC \geq SC$: **PASS** (observed $0.884 \geq 0.870 \geq 0.856$, with per-task $MRC > EGC$ at 19/17 and $EGC > SC$ at 28/16, consistent with the high-CSI regime where the binary-checklist judge variance falls below the critical σ_w^{*2} of Prop. 1); (P2) HARQ-IR converges faster than HARQ-CC: **PASS** (IR running-max jumps from 0.807 to 0.891 between rounds 1 and 2 and reaches 99% of its peak by round 3, while CC plateaus more gradually and only reaches 99% of its lower peak 0.878 at round 4); (P3) diminishing diversity returns: **PASS** (marginal quality gain per extra channel falls from +3.74pp ($d=1 \rightarrow 2$, baseline $\rightarrow SC$) to +1.38pp per channel ($d=2 \rightarrow 5$, $SC \rightarrow SC-N$), matching the classical sublinear scaling); (P4) turbo iterations improve quality monotonically: **PASS in direction, FAIL in shape** (all-tasks running-max mean climbs $0.808 \rightarrow 0.869 \rightarrow 0.882 \rightarrow 0.898 \rightarrow 0.902$ with the steepest step at iteration 1 and diminishing increments thereafter, but we do not observe a sharp “waterfall” threshold; per-task gains are diffuse rather than concentrated at a critical iteration). Overall 3/4 directional passes plus 1/4 in-shape miss; the P1 reversal between cloud-Haiku (PASS) and 14B-local (FAIL, Sec. 5.3) is itself the empirical signature of the CSI-crossover predicted by Prop. 1, consistent with our framing of the framework as design-useful and operating-point-aware, but not yet a quantitative physical theory of LLM channels.

Judge ablation. A controlled judge-strength ablation, varying the judge model while holding channels and techniques fixed, is the cleanest way to isolate the “in-loop scorer borrows judge capacity” confound for HARQ-IR, turbo, fountain stopping, ACM, and the best-of-sequence guard. The same sweep is also the most direct empirical trace of the channel-state-information crossover of Prop. 1: a weaker judge raises the weighting noise σ_w , predicted to push the deployment past the critical variance σ_w^{*2} and to flip the ordering between \overline{MRC} and EGC at fixed channels. Although we have not run this direct ablation in this study (left for future work), Table 7 varies the judge across configurations (Gemma-3 12B, Gemma-4 31B, Claude Haiku 4.5, GLM-5.1) only in concert with channel changes, so the config-to-config preservation of the technique rank order in Table 8 is suggestive of judge-robustness but is confounded with channel-architecture changes and cannot isolate the judge contribution on its own. The strong-borrowing hypothesis is already partly ruled out by the oracle-winner decomposition under “Judge-in-loop confound” below (judge-free decoders still win $\approx 39\%$ of per-task oracle assignments on the 8B split); a quantitative bound on the in-loop contribution requires the matched-channel run.

I Decoding-Threshold Details and Limitations

Per-scale numerical breakdown of the iterative-decoding threshold. (1) Above threshold (14B). Generator deepseek-r1:14b with critic phi3:14b: turbo +14.2% ($p < 10^{-5}$, paired Wilcoxon $W=56$);

HARQ-IR +14.0% ($p < 10^{-3}$). The per-iteration all-tasks running-max mean rises monotonically from 0.726 to 0.853, and the survivor cohort is essentially flat ($0.726 \rightarrow 0.694$)—tasks reach a high ceiling on the first refinement and either early-exit or track it from then on. (2) *Near threshold (8B)*. Generator llama3.1:8b with critic qwen2.5:7b: turbo +13.9% ($0.604 \rightarrow 0.688$); the survivor trajectory is noisy and slightly declining (0.585, 0.559, 0.556, 0.483, 0.465), while all-tasks running-max still climbs ($0.585 \rightarrow 0.688$). (3) *Below threshold (3B)*. Generator qwen2.5:3b with critic gemma3:4b: turbo +6.3% absolute gain ($0.651 \rightarrow 0.692$) and only marginal over paired Wilcoxon (21 worse / 24 tied / 24 better). The survivor trajectory is net-descending (0.619, 0.514, 0.490, 0.515, 0.560)—the refinement map is contractive on the *wrong* side, producing worse outputs than the input on average. The running-max curve is monotonic ($0.619 \rightarrow 0.692$) only because the best-of-sequence guard (Sec. 4) reverts to earlier iterations when later ones regress. In the communication analog, this is a decoder operating below the EXIT-chart fixed point—additional iterations degrade rather than improve the estimate, and only a selection step rescues the output.

Limitations (full discussion). *Residual CSI noise:* our binary checklist scorer (15 weighted yes/no criteria, Sec. D) largely resolves the score quantization problem—earlier numeric-rating judges collapsed 39% of scores to a single value, whereas the checklist produces 2^{15} distinct score levels. However, borderline criteria still introduce per-evaluation variance (~ 0.05 – 0.10), which can mask small iterative improvements. Differential scoring for iterative techniques (scoring candidate and baseline in the same judge call) mitigates this by canceling common-mode judge noise, analogous to differential decoding. Intrinsic log-probabilities (Remark 3) remain a promising direction for further reducing CSI noise. *Within-task stochastic noise:* the 300-task hard-benchmark split (Ollama-cloud trio) and the 3B local + cloud-judge configuration are evaluated with $n_{\text{rep}}=3$ independent generation repeats per task, with seed-aware bootstrap propagating within-task generation variance into every confidence interval (Table 3). The remaining four 69-task curated configurations are single-run per (task, technique), so means and paired Wilcoxon p -values reported on those configurations conflate *technique effect* with *within-task stochastic noise* (temperature sampling, judge variance); the codebase supports full repetition (repeat_runs option), and broader repetition is deferred for compute reasons. *Cost overhead:* quality scoring adds cost even to easy tasks. *Non-stationarity:* model updates degrade channel estimates over time. *Dual-role judge:* the same model serves as final scorer and in-loop critic for HARQ/turbo/ACM/SC/BoN. The oracle-winner decomposition (Sec. H, “Judge-in-loop confound”) shows judge-free-in-decode techniques still win 39% of tasks, indicating the confound does not determine rankings, but a judge-strength ablation (weaker scorer with techniques held fixed) remains open. *Curated tasks:* the 69-task curated split was selected to exhibit technique differences at the 8–14B operating point (hard/very-hard/extreme tiers); gains on a random-difficulty split would be smaller. The reproducible hard-split standard benchmarks (Sec. G) addresses this.

J Soft-Output Extensions via Token-Level Log-Probabilities

The techniques in the main text treat each agent response as a *hard* symbol: the combiner sees only the emitted text and a scalar judge score. Classical receivers, however, benefit enormously from *soft* decisions—log-likelihood ratios (LLRs) carry not just the decoded bit but the receiver’s confidence in it, and every competitive decoder (MAP, BCJR, belief propagation, turbo) is soft-in soft-out. Autoregressive LLMs expose an analogous quantity for free: the per-token log-probability $\log p(y_t | y_{<t}, x)$. We define a response-level confidence

$$c(y) = \exp\left(\frac{1}{N} \sum_{t=1}^N \log p(y_t | y_{<t}, x)\right), \quad (9)$$

the geometric mean per-token probability, which plays the role of a channel LLR at the response level. This section introduces three *optional* soft variants of our core techniques—SOFT-MRC, SOFT-FOUNTAIN, and SOFT-ACM—added as additional modes without modifying the hard-decision pipeline used in Sec. 5.5.

Soft MRC. In classical MRC, branch k is weighted by its instantaneous SNR γ_k ; our hard variant uses the judge score as a proxy. Soft MRC replaces this proxy with the model’s own confidence, weighting branch k by $w_k = c(y_k) / \sum_j c(y_j)$ and passing weighted candidates to the synthesizer. Because synthesis is lossy (Sec. L), we enforce the MRC guarantee $\text{SNR}_{\text{MRC}} \geq \text{SNR}_{\text{SC}}$ by scoring

the combined output and falling back to selection combining (the single highest-confidence branch) whenever synthesis scores below the best individual—the direct analog of a CRC check triggering a retransmission.

Soft Fountain. A rateless decoder stops as soon as it has collected enough reliable symbols. Our hard fountain variant uses an agreement heuristic; Soft Fountain uses a genuine confidence-based stopping criterion

$$S = 0.6 \cdot \bar{c} + 0.4 \cdot \text{agreement}, \quad (10)$$

and marks any sample with $c(y) < 0.5 c_{\max}$ as an *erasure*, mirroring erasure decoding in real fountain codes rather than quality gating. The ML-style synthesizer only decodes over non-erased samples.

Soft ACM. Hard ACM estimates channel quality via a meta-judgment prompt (“rate this task’s difficulty”), which we found to be bimodal and to leak uncoded outputs on catastrophic tasks. Soft ACM instead transmits a short *pilot probe* (a 2–3 sentence brief answer) and uses $c(y_{\text{probe}})$ directly as the CQI—zero extra judge calls, and grounded in the generator’s own uncertainty rather than a separate meta-query. The MCS table maps confidence to coding mode with *no* uncoded floor: $[0.70, 1.0] \rightarrow \text{FEC } r=0.75$; $[0.50, 0.70] \rightarrow \text{FEC } r=0.5$; $[0.30, 0.50] \rightarrow \text{HARQ-IR}$; $[0, 0.30] \rightarrow \text{MRC diversity}$.

Where the analogy tightens. Soft extensions sharpen three gaps we observed in the hard pipeline. (i) *Combining weight fidelity*: judge scores are discretized and noisy; $c(y)$ is continuous and generated by the same process that produced y , matching the SISO recipe more faithfully. (ii) *Stopping criteria*: rateless codes are defined by a confidence threshold, not a quality poll. (iii) *CQI cost*: a pilot probe costs one short generation, whereas meta-judgment costs a full extra judge call and is an out-of-band oracle.

Limitations. Soft outputs require backend logprob support: OpenAI, Ollama, and vLLM expose them, but the Anthropic API does not, so soft techniques raise an explicit error on unsupported backends rather than silently falling back. The geometric mean in (9) weights all tokens equally and is blind to *which* tokens are uncertain (a single wrong fact buried in a confident paragraph can still dominate correctness); token-level weighting by salience is left to future work. Finally, $c(y)$ measures the model’s internal confidence, not correctness—it is a calibrated LLR only to the extent that the generator itself is calibrated.

K A Larger Design Space

The communication-theoretic view admits a substantially larger design space than the six techniques instantiated in this paper. Concrete mappings we have not built include: (i) *interleaving* for decorrelating burst errors in long reasoning chains, treating consecutive reasoning steps as a coded sequence and permuting the order in which a critic inspects them; (ii) *MIMO-style joint precoding* across multiple generator channels, where prompt design plays the role of a precoder steering each channel into a complementary error mode rather than running them independently; (iii) *LDPC- and polar-style structured FEC* over reasoning chains, replacing the uniform repetition that our FEC implementation currently uses with sparse parity structures that admit message-passing decoders; (iv) *coded computation for verification*, exchanging some of the redundant generator calls in HARQ/turbo for cheaper checksum-style verifier calls in the spirit of coded distributed computing; (v) *OFDM-style subcarrier allocation* as principled task decomposition, where independent reasoning subtasks are assigned to channels under a power-budget constraint analogous to bit-loading; and (vi) *joint source–channel coding* for compressing the prompt and its protection scheme together, rather than the prompt-then-redundancy decomposition implicit in our current pipelines. Each of these is a well-developed line in classical communications with a natural agentic counterpart that has not, to our knowledge, been instantiated in either form. The contribution of this paper is to commit to the channel abstraction concretely enough that those mappings become specifiable rather than evocative; the limitation is that we have implemented only a small subset and evaluated them on a constrained compute budget. We hope subsequent work treats this as a research program rather than a closed set of analogies.

L Synthesis integrity validation

For MRC and EGC combining, *synthesis contamination* is a methodological concern: the synthesizer model may inject its own knowledge into the combined output rather than faithfully merging the input responses. Quality gains attributed to combining would then reflect the synthesizer solving the task independently, invalidating the diversity framework.

We validate synthesis integrity through three controlled experiments using the primary configuration (DeepSeek-R1 14B + Phi-3 14B channels, Gemma-3 12B judge/synthesizer).

Test 1: Information preservation. Both channel models answer “What is the GCD of 252 and 735?” Both correctly produce 21 via the Euclidean algorithm. The synthesizer preserves the correct answer and complete reasoning chain without adding computation steps or alternative methods not present in either input. **Result: PASS.**

Test 2: No contamination (factual). We construct two deliberately sparse descriptions of Python: Input A states “created in the early 1990s, interpreted language”; Input B states “high-level, supports multiple paradigms.” Neither mentions Guido van Rossum, Django, NumPy, indentation-based syntax, duck typing, or list comprehensions—all facts the synthesizer has seen in training. The synthesizer output contains *zero* facts beyond those in the two inputs. **Result: PASS.**

Test 3: Faithful error preservation. We test whether the synthesizer corrects *errors* present in inputs using its own knowledge. Input A states the speed of light was “first measured accurately by Michelson in 1887”; Input B states relativity was “published in 1915” (the correct year for *special* relativity is 1905). The synthesizer faithfully reproduces both claims without correction, confirming it does not silently fix factual errors using its own knowledge. It also does not add the exact value 299,792,458 m/s (absent from both inputs). **Result: PASS.**

Test 4: Conflict resolution without independent computation. Input C states $\int_0^3 x^2 dx = 9$ (correct); Input D states $\int_0^3 x^2 dx = 8$ (incorrect). Input C is scored higher (0.80 vs. 0.60). The synthesizer selects the higher-scored answer (9) without showing its own derivation (e.g., $[x^3/3]_0^3$). **Result: PASS.**

Test 5: No prompt leakage. The synthesis prompt uses internal labels ([BEST], [ALT-1]) and section headers. None of these labels appear in the synthesized output. **Result: PASS.**

These results confirm that the constrained synthesis prompt (“Your output must contain ONLY information from the responses above”) combined with low temperature ($T = 0.1$) effectively prevents the synthesizer from acting as an independent solver. Quality improvements from MRC/EGC combining therefore reflect genuine information aggregation across diverse channel outputs, not synthesizer knowledge injection.

M Formal Channel-Theoretic Foundations

This appendix provides the information-theoretic arguments underlying the agent channel model (Sec. 3), stating where established theorems apply and where the agent setting introduces deviations.

M.1 The LLM as a discrete stochastic channel

Lemma 1 (Channel identity). *Let \mathcal{A}_θ be an autoregressive language model with parameters θ and temperature $T > 0$. For any input $x \in \mathcal{T}$, the model defines a conditional distribution over output sequences:*

$$p_T(y | x) = \prod_{t=1}^{|y|} \frac{p_\theta(y_t | y_{<t}, x)^{1/T}}{\sum_{v \in \mathcal{V}} p_\theta(v | y_{<t}, x)^{1/T}} \quad (11)$$

This is a valid transition probability satisfying $\sum_{y \in \mathcal{V}^} p_T(y | x) = 1$ for all x , and thus constitutes a discrete stochastic channel in the sense of Shannon [Shannon, 1948].*

Proof. The softmax function with temperature scaling produces a valid probability distribution at each token position: each factor is non-negative and sums to one over \mathcal{V} . The product of valid conditional distributions over a finite sequence (terminated by an end-of-sequence token) yields a valid joint distribution over \mathcal{V}^* . The mapping $x \mapsto p_T(\cdot | x)$ is therefore a well-defined channel transition probability. \square

No approximation or limiting argument is involved.

M.2 Conditional entropy and channel noise

For a fixed input x and temperature T , the per-token conditional entropy is:

$$H_T(Y_t | y_{<t}, x) = - \sum_{v \in \mathcal{V}} p_T(v | y_{<t}, x) \log p_T(v | y_{<t}, x) \quad (12)$$

The sequence-level conditional entropy, normalized by output length, is:

$$\mathcal{H}_T(\mathcal{A}_\theta, x) = \frac{1}{\mathbb{E}[|Y|]} \sum_{t=1}^{\mathbb{E}[|Y|]} H_T(Y_t | Y_{<t}, x) \quad (13)$$

This quantity is the channel’s *intrinsic noise rate* in bits per token. It decomposes the factors that determine channel quality:

1. **Model parameters** θ : larger, better-trained models learn sharper conditional distributions (lower entropy at each position). Neural scaling laws [Kaplan et al., 2020, Hoffmann et al., 2022] show that cross-entropy loss (= our \mathcal{H}) decreases as a power law $L \propto N^{-\alpha}$ with model parameter count N , providing a quantitative relationship between model size and channel noise.
2. **Temperature** T : by Remark 1, increasing T flattens the distribution, monotonically increasing H_T . At $T = 0$, $H = 0$ (deterministic); at $T = \infty$, $H = \log |\mathcal{V}|$ (uniform noise).
3. **Task difficulty**: for inputs x where the model is uncertain (ambiguous, out-of-distribution, or requiring multi-step reasoning), the conditional distribution is naturally more diffuse, yielding higher \mathcal{H} even at fixed T .

Corollary 1 (Model–difficulty duality). *For a given technique with decoding threshold \mathcal{H}^* , the technique is effective when $\mathcal{H}_T(\mathcal{A}_\theta, x) < \mathcal{H}^*$. Since \mathcal{H} depends on both θ (model) and x (task), a 70B model on a hard task and a 3B model on an easy task may occupy the same operating point. Technique selection should therefore be conditioned on the operating point \mathcal{H} , not on model size or task difficulty independently.*

M.3 Mutual information and diversity

For d independent channels $\mathcal{A}_{\theta_1}, \dots, \mathcal{A}_{\theta_d}$ (independence holds when models have different architectures and training data, or when temperature variation provides sufficient randomization), the mutual information satisfies:

$$I(X; Y_1, \dots, Y_d) = I(X; Y_1) + \sum_{i=2}^d I(X; Y_i | Y_1, \dots, Y_{i-1}) \quad (14)$$

Under independence, $I(X; Y_i | Y_1, \dots, Y_{i-1}) = I(X; Y_i)$, giving:

$$I(X; Y_1, \dots, Y_d) = \sum_{i=1}^d I(X; Y_i) \quad (15)$$

Each additional independent channel adds information about X , which is why diversity combining improves quality. When channels are correlated (shared training data, overlapping architectures), $I(X; Y_i | Y_1, \dots, Y_{i-1}) < I(X; Y_i)$, yielding diminishing returns. The effective diversity order $d_{\text{eff}} < d$ captures this: it is the number of channels’ worth of independent information in the ensemble. Turkmen et al. [2026] formalize this for LLM ensembles, showing that MI-based ensemble selection outperforms greedy accuracy-based selection by accounting for inter-model correlation.

Empirical branch correlation. Table 12 reports the Pearson correlation r between the two channels’ `individual_scores` on Diversity-SC, the only technique whose per-branch quality scores are pure parallel single-shot draws. Aggregate r ranges from 0.17 at 14B local (the configuration closest to the textbook $\widehat{\text{MRC}} \geq \text{EGC} \geq \text{SC}$ ordering in Sec. 5.3) to 0.75 on the 3B-Qwen + 3B-Llama pair (the configuration furthest from it), giving an empirical $d_{\text{eff}} \in [1.14, 1.71]$ from a nominal $d=2$. On the headline $n=300$ hard-benchmark split the aggregate is $r=0.665$, but Table 13 shows this average hides a sharp split: $r = -0.03$ on the MMLU-QA tasks (near-independent failures) versus $r = +0.73$ on HumanEval-code (shared training-data overlap). Configurations and categories with high r are exactly where EGC’s robustness to CSI noise overtakes $\widehat{\text{MRC}}$ in Table 8, the second mechanism (alongside the CSI-noise variance of Prop. 1) by which the textbook ordering reverses.

Table 12: Inter-branch quality-score correlation on Diversity-SC, the only technique whose `individual_scores` are pure parallel single-shot draws (no synthesis, no critic, no combining). Pearson r between the $d=2$ per-branch judge scores; 95% CIs from 4000 task-level bootstrap resamples; $d_{\text{eff}} = d/(1+(d-1)r)$ clamped at $r \geq 0$. Higher r (lower d_{eff}) coincides with the configurations on which $\text{EGC} \succ \widehat{\text{MRC}}$ in Sec. 5.3, the second mechanism (alongside the CSI-noise variance of Prop. 1) by which the textbook MRC ordering reverses.

Configuration	n	Pearson r	95% CI	d_{eff}
3B local	69	+0.489	[+0.254, +0.702]	1.34
3B local + cloud judge	69	+0.751	[+0.596, +0.873]	1.14
8B local	69	+0.464	[+0.222, +0.672]	1.37
14B local	69	+0.171	[-0.080, +0.407]	1.71
Anthropic + OpenAI cloud	69	+0.575	[+0.308, +0.759]	1.27
Ollama-cloud (n=69 curated)	69	+0.679	[+0.516, +0.813]	1.19
Ollama-cloud (n=300 hard)	300	+0.665	[+0.576, +0.748]	1.20

Table 13: Per-category inter-branch correlation on Diversity-SC. Each cell is the Pearson r between the two branches’ judge scores on tasks in that category, with the per-cell sample size in parentheses; “—” marks empty cells. Categories with r noticeably above the configuration aggregate are configurations \times task families on which the effective diversity order is most depressed by shared training-data overlap, and where EGC’s robustness to CSI noise is most likely to overtake MRC.

Configuration	QA	Reasoning	Code	Creative	All
3B local	+0.73 (16)	+0.13 (30)	+0.61 (14)	+0.73 (9)	+0.49 (69)
3B local + cloud judge	+0.66 (16)	+0.69 (30)	+0.71 (14)	+0.62 (9)	+0.75 (69)
8B local	+0.46 (16)	+0.11 (30)	+0.48 (14)	+0.72 (9)	+0.46 (69)
14B local	+0.26 (16)	+0.30 (30)	+0.05 (14)	+0.66 (9)	+0.17 (69)
Anthropic + OpenAI cloud	+0.87 (16)	+0.61 (30)	-0.18 (14)	+0.58 (9)	+0.57 (69)
Ollama-cloud (n=69 curated)	+0.89 (16)	+0.74 (30)	+0.25 (14)	+0.59 (9)	+0.68 (69)
Ollama-cloud (n=300 hard)	-0.03 (100)	+0.52 (100)	+0.73 (100)	—	+0.67 (300)

M.4 Soft vs. hard channel state information

In classical communications, the combining weights for MRC are derived from the channel’s soft output. For a Gaussian channel with known noise variance σ_i^2 on branch i , the optimal MRC weights are $w_i = 1/\sigma_i^2$ (inverse noise variance weighting) [Proakis and Salehi, 2008]. When the noise variance must be estimated, any estimation error $\hat{\sigma}_i^2 \neq \sigma_i^2$ degrades MRC performance. Specifically, if the estimation error variance is $\text{Var}(\hat{\sigma}_i^2)$, MRC with estimated weights approaches EGC performance as $\text{Var}(\hat{\sigma}_i^2)/\sigma_i^4 \rightarrow 1$ [Gao et al., 2003].

In our framework, the intrinsic CSI is the log-probability $\log p_\theta(y | x)$, which is a direct measure of the channel’s confidence. The extrinsic CSI is the LLM judge score. Naive numeric-rating judges are severely quantized: our initial judge produced only ~ 33 unique values across 516 measurements (~ 5 -bit resolution), under which the theoretical MRC advantage over EGC vanishes [Simon and Alouini, 2005]. We therefore adopt a *sigma-delta* scoring design: the judge answers 15 weighted binary criteria rather than emitting a single number, and the weighted sum recovers a fine-grained score (up to 2^{15} distinct values). Binary decisions are far more reliable for small LLMs than numeric ratings, and the many-1-bit-measurements-to-high-resolution-output construction mirrors oversampled sigma-delta ADCs [Norsworthy et al., 1996].

Practical implication. Log-probability-weighted MRC would use the channel’s own soft output, avoiding the estimation noise entirely. However, sequence-level log-probability $\log p_\theta(y | x) = \sum_t \log p_\theta(y_t | y_{<t}, x)$ has known biases: (i) *length bias*: shorter sequences tend to have higher log-probability, favoring terse but incomplete answers; (ii) *repetition bias*: repeated tokens have artificially high conditional probability; (iii) *calibration*: LLM probabilities are not perfectly calibrated [Guo et al., 2017, Kadavath et al., 2022]. These can be mitigated by length normalization (Eq. (2)) and temperature calibration, but require empirical validation.

M.5 Iterative decoding threshold

The convergence behavior of iterative decoders (turbo codes, LDPC) is governed by the decoding threshold [ten Brink, 2001]: a channel noise level \mathcal{H}^* such that:

- For $\mathcal{H} < \mathcal{H}^*$ (good channel): iterative decoding converges, and error probability decreases exponentially with iterations.
- For $\mathcal{H} > \mathcal{H}^*$ (bad channel): the decoder *cannot converge*. Additional iterations may even degrade performance due to error propagation.

The threshold depends on the constituent decoder capacity, not on the interleaver design.

In the agent setting, the generator is the constituent decoder and the critic is the interleaver (providing extrinsic information). Our multi-scale experiments confirm this prediction. At 8B (Llama-3.1 8B, Qwen-2.5 7B), the marginal gain of HARQ-IR over HARQ-CC nearly vanishes (HARQ-CC +22.7%, HARQ-IR +22.8%, turbo +13.9% in Table 8; the HARQ-IR-over-HARQ-CC gap is 0.1 pp, vs. 2.3 pp at 14B), and the turbo survivor cohort is noisy with no monotone trend (0.585 \rightarrow 0.559 \rightarrow 0.556 \rightarrow 0.483 \rightarrow 0.465; Fig. 18, Fig. 3 center)—consistent with near-threshold operation, where extrinsic critique fails to propagate into improved iterates. At 14B (DeepSeek-R1 14B, Phi-3 14B), iterative gains are more sustained: HARQ-IR +14.0% exceeds HARQ-CC +11.7% by 2.3 pp, turbo reaches +14.2%, and the all-tasks running-max climbs monotonically from 0.726 to 0.853 across five iterations (Fig. 2, Fig. 14), suggesting these models cross into the waterfall region for a larger fraction of tasks. The cloud configuration (Claude Haiku 4.5, GPT-5-mini, $q_0 = 0.819$) shows the clearest above-threshold behavior: HARQ-IR +10.8% and turbo +10.2% both produce monotonic improvement, with HARQ-IR exceeding HARQ-CC by 3.4 pp (Table 8; HARQ and turbo trajectories in Fig. 29).

This is consistent with the threshold being a property of the generator’s conditional entropy rather than the critique mechanism. The comparison across 8B \rightarrow 14B \rightarrow cloud is consistent with a transition from noise-amplification (below threshold) to stable iterative improvement (above threshold); we stop short of claiming a full waterfall, since neither the number of iterations nor the number of tasks in our study is sufficient to resolve the sharp transition characteristic of bit-error-rate waterfalls.

A fixed-point characterization of the threshold. The threshold can be made precise by modeling the per-iteration map on quality directly. Let $\mathcal{R}_x : \mathcal{Y} \rightarrow \mathcal{Y}$ be the refinement operator (generator + critic + extrinsic-information exchange) for prompt x , and define the *quality-update map*

$$f(q_0) := \mathbb{E}[q(\mathcal{R}_x(Y)) \mid q(Y) = q_0],$$

with $q_k := f^{(k)}(q_0)$ the k -fold deterministic iterate of expected quality, and $Q_k := \mathbb{E}[\max_{0 \leq j \leq k} q(Y_j)]$ the expected quality under the best-of-sequence guard (Sec. O.1). The guarded delivered sequence is monotone independently of the dynamics of f :

Remark 4 (Best-of-sequence monotonicity). For every refinement trajectory (Y_0, Y_1, \dots) , the running maximum $\max_{0 \leq j \leq k} q(Y_j)$ is non-decreasing in k pathwise; taking expectations gives $Q_k \geq Q_{k-1} \geq \dots \geq q_0$ for all $k \geq 1$.

This is a one-line consequence of monotonicity of the maximum over a growing index set; it makes no use of the structure of f , and we use it throughout to read the empirical running-max curves of Figures 2 and 3 as predictions about the *delivered* output even when the unguarded iterate q_k behaves badly. The substantive content of the threshold therefore lies in the local stability of the high-quality fixed point of f .

Proposition 2 (Refinement contraction and the iterative-decoding threshold). *Suppose $f : [0, 1] \rightarrow [0, 1]$ is continuously differentiable with at least one fixed point $q^\infty \in (0, 1)$.*

- (i) Above threshold. If $|f'(q^\infty)| < 1$, then for every $\kappa \in (|f'(q^\infty)|, 1)$ there exists a neighborhood $U \ni q^\infty$ with $f(U) \subseteq U$ such that

$$|f(q) - q^\infty| \leq \kappa |q - q^\infty| \quad \text{for all } q \in U,$$

and consequently, for every $q_0 \in U$,

$$|q_k - q^\infty| \leq \kappa^k |q_0 - q^\infty| \xrightarrow{k \rightarrow \infty} 0.$$

Identifying q_k with the conditional mean $\mathbb{E}[q(Y_k) | q_0]$ (the EXIT-recursion reading of f), this gives $\liminf_k Q_k \geq q^\infty$; the squeeze $q_k \leq Q_k \leq q^\infty$ forces $Q_k \rightarrow q^\infty$ whenever $q(Y_j) \leq q^\infty$ almost surely along the trajectory (in particular when $q^\infty = 1$).

- (ii) Below threshold. If, in addition, f is non-decreasing on $[0, 1]$, $|f'(q^\infty)| > 1$, and f admits a second stable fixed point $q^- < q^\infty$ with $|f'(q^-)| < 1$ and no other fixed point in $[q^-, q^\infty]$, then for every $q_0 \in (q^-, q^\infty)$ the unguarded iterate satisfies $q_k \searrow q^-$, while the guarded sequence still satisfies $Q_k \geq q_0$ for all k by Remark 4.

Proof. (i) *Local contraction.* Fix $\kappa \in (|f'(q^\infty)|, 1)$. Continuity of f' at q^∞ gives $\delta > 0$ such that $|f'(q)| \leq \kappa$ for all $q \in U := (q^\infty - \delta, q^\infty + \delta) \cap [0, 1]$. The set U is convex and contains q^∞ , so for any $q \in U$ the segment from q to q^∞ lies in U and the mean-value theorem yields some $\xi \in U$ with $f(q) - q^\infty = f(q) - f(q^\infty) = f'(\xi)(q - q^\infty)$, hence

$$|f(q) - q^\infty| \leq \kappa |q - q^\infty| < \delta.$$

Combined with $f(q) \in [0, 1]$, this gives $f(q) \in U$, so $f(U) \subseteq U$ and the iteration $q_{k+1} = f(q_k)$ remains in U once $q_0 \in U$. Induction on k now yields $|q_k - q^\infty| \leq \kappa |q_{k-1} - q^\infty| \leq \dots \leq \kappa^k |q_0 - q^\infty|$, and $\kappa < 1$ forces $q_k \rightarrow q^\infty$.

Guarded sequence. Pathwise, $\max_{0 \leq j \leq k} q(Y_j) \geq q(Y_k)$, so under the mean-field reading $\mathbb{E}[q(Y_k)] = q_k$ we have $Q_k \geq q_k$, hence $\liminf_k Q_k \geq q^\infty$. The reverse bound $Q_k \leq q^\infty$ holds whenever $q(Y_j) \leq q^\infty$ almost surely along the trajectory, and the two together give $Q_k \rightarrow q^\infty$.

(ii) Set $g(q) := f(q) - q$. Then $g(q^-) = g(q^\infty) = 0$ and, since $|f'(q^-)| < 1$, $g'(q^-) = f'(q^-) - 1 < 0$; together with the assumption that g has no other zero in $[q^-, q^\infty]$, this fixes the sign of g as negative on the open interval, i.e. $f(q) < q$ on (q^-, q^∞) . Monotonicity of f gives $f(q) \geq f(q^-) = q^-$, so f maps (q^-, q^∞) into $[q^-, q^\infty)$ and q_k is well-defined and non-increasing there. Bounded below by q^- , q_k converges by monotone convergence and continuity to a fixed point of f in $[q^-, q^\infty)$, which can only be q^- . The guard inequality is Remark 4. \square

Attribution. The mathematical content of Prop. 2 is a specialization of the classical local-stability theory of one-dimensional smooth maps to the present setting (see, e.g., Hirsch et al., 2013, Ch. 9; the contraction case is the one-dimensional Banach–Picard corollary, and the bistable case is the standard saddle-node picture). The interpretation of the dichotomy $|f'(q^\infty)| \leq 1$ as a *decoding threshold* is the EXIT-chart / density-evolution analysis of ten Brink [2001] and Richardson and Urbanke [2001], in which the threshold is the channel parameter at which the high-quality fixed point of a one-dimensional recursion loses local stability. Our contribution here is the modeling step, identifying the LLM refinement operator \mathcal{R}_x as the constituent decoder, the critique channel as the extrinsic-information exchange, and the quality-update map $f(q_0) = \mathbb{E}[q(\mathcal{R}_x(Y)) | q(Y) = q_0]$ as the EXIT recursion; we restate the underlying dynamical-systems result here so that the threshold prediction in Fig. 3 can be read off the same $|f'|$ condition that controls turbo and LDPC convergence.

Interpretation. The condition $|f'(q^\infty)| < 1$ at the high-quality fixed point is the agent analog of operating above the iterative-decoding threshold of a turbo code [ten Brink, 2001]: refinement is locally contractive toward q^∞ and EXIT-style trajectories converge to it. When this condition fails (the upper fixed point becomes unstable), trajectories collapse toward a lower-quality basin, and only the best-of-sequence guard prevents the delivered output from following them down. Fig. 3 is the empirical signature of this transition: the survivor-cohort mean (an empirical proxy for q_k) descends at 3B, is flat-noisy at 8B, and stays at the upper fixed point at 14B, while the running-max curve (an empirical proxy for Q_k) is monotone in all three panels, exactly the asymmetry that Remark 4 and part (ii) of Prop. 2 predict.

What the theorem does and does not give. It does not estimate $|f'(q^\infty)|$ for any concrete generator/critic pair (this would require many independent refinement trajectories per quality bin, beyond our

compute budget). It gives a structural prediction — that the empirical transition between 3B/8B/14B should look like a transition between subcritical, critical, and supercritical iteration, and that part (i) decouples the deliverable quality from the unguarded dynamics — and that prediction matches the observed pattern.

M.6 Bounds on agent channel capacity

While the exact capacity $C = \max_{p(x)} I(X; Y)$ is intractable for LLM channels, useful bounds exist.

Upper bound. For any output distribution, $I(X; Y) \leq H(Y) \leq \mathbb{E}[|Y|] \cdot \log |\mathcal{V}|$. A tighter bound uses the observation that LLM outputs occupy a tiny fraction of \mathcal{V}^* : natural language has approximately 1–1.5 bits/character of entropy [Shannon, 1948, Cover and Thomas, 2006], giving $H(Y) \approx 1.2 \cdot \mathbb{E}[|Y|]$ bits.

Lower bound. Any achievable quality $Q^*(C)$ under cost budget C provides a lower bound, since the technique configuration that achieves Q^* is a specific (suboptimal) coding scheme. Our ACM experiments (Sec. 5.4) thus provide constructive lower bounds.

Rate interpretation. In our setting, the “rate” is the semantic information density: how many bits of task-relevant content are transmitted per token of model output. FEC at code rate r trades this density for reliability: lower r adds more parity tokens, reducing information density but increasing the fraction of tasks solved correctly. This directly parallels the rate–reliability tradeoff in Shannon’s coding theorem.

N Hyperparameter Settings and Pseudocode

Algorithm 1 Diversity ensemble with MRC combining

Require: Task X , channels $\{\mathcal{A}_i\}_{i=1}^d$, scorer q , synthesizer \mathcal{A}_s

- 1: **for** $i = 1$ to d **do** ▷ Parallel
- 2: $Y_i \leftarrow \mathcal{A}_i(X)$; $q_i \leftarrow q(X, Y_i)$
- 3: **end for**
- 4: $w_i \leftarrow q_i / \sum_j q_j \quad \forall i$ ▷ MRC weights
- 5: **return** $\mathcal{A}_s(\text{Synthesize}(\{(Y_i, w_i)\}))$

Table 14: Default hyperparameters for each technique.

Parameter	Value
<i>Diversity</i>	
Number of branches d	2 (spatial)
Prompt variants	1 (default)
Temperature spread	None
<i>HARQ</i>	
Max rounds	5
Quality threshold τ	0.85
Critic model	Judge (12B)
<i>Turbo</i>	
Max iterations	5
Quality threshold	0.90
Critic model	Judge (12B)
<i>Fountain</i>	
Max samples	8
Min samples	2
Confidence threshold	0.85
<i>FEC</i>	
Code rates tested	0.75, 0.50, 0.33
<i>ACM</i>	
MCS levels	5 (MCS-0 to MCS-4)

O Detailed implementation of each technique

This appendix documents the concrete implementation of every technique benchmarked in this paper, at the level of detail required for an independent reimplemention. All techniques are built from two shared primitives: the *agent channel* \mathcal{A} and the *quality scorer* q . Before describing individual techniques we fix notation and document these primitives, since the guards and guarantees of each technique rely on them.

O.1 Shared primitives

Agent channel \mathcal{A} . A channel is a callable \mathcal{A} : $\text{prompt} \times \text{temperature} \rightarrow \text{output}$ that wraps an LLM endpoint (OpenAI-compatible, Anthropic native, or a local Ollama/vLLM server). A call returns an `AgentOutput` record with fields `text`, `model`, `temperature`, `token_count`, `cost_usd`, `latency_s`, and—optionally—`token_logprobs` and `mean_logprob` when the backend supports them. Reasoning-model thinking blocks (`<think>...</think>` for DeepSeek-R1 / Qwen3; `Anthropic ThinkingBlock` for Claude) are stripped from the visible text before downstream use, but the thinking tokens remain in the cost accounting. Whenever possible we disable thinking.

Quality scorer q . The scorer is a *binary checklist judge*: given (prompt, candidate, optional reference) it asks a dedicated LLM (the judge, typically gemma3:12b locally or claude-haiku-4-5 in the cloud) to evaluate 15 weighted yes/no criteria and returns the weighted true-rate in $[0, 1]$. Criteria are fixed per task type (with / without reference) and weights sum to 1; a “good but not perfect” answer is calibrated to pass 10–12 of 15 checks. This produces $2^{15} = 32,768$ possible score values, avoiding the severe quantization of numeric-rating judges (Sec. D). On tasks with objective checks, the final score is a $0.6 \cdot \text{objective} + 0.4 \cdot \text{checklist blend}$.

The scorer additionally exposes a differential variant q_{Δ} : to compare a candidate against a baseline with known score q_0 , the judge scores both in the same call pattern, and the candidate score is reported as $q_0 + (q_{\text{cand}} - q_{\text{base-rescore}})$, clamped to $[0, 1]$. This cancels common-mode judge noise and is used by every technique that refines a previous answer (HARQ-IR, turbo, FEC post-decode, diversity synthesis).

Output contract. Every technique returns a `ReliabilityRun` record containing: `task_id`, `technique`, `individual_outputs` (all generator calls), `overhead_outputs` (synthesizer/critic/decoder/judge calls not directly part of the answer), `combined_output` (the final answer text), `final_quality` (the judge score of the combined output), and `rounds` (iterations used). Cost accounting sums all `cost_usd` fields across `individual_outputs` \cup `overhead_outputs` \cup `judge_calls`. Techniques that synthesize or refine (diversity MRC/EGC, fountain, HARQ, turbo, FEC) implement a *best-of-sequence guard*: if the post-synthesis score is lower than the best individual score seen, the final output reverts to the best individual output. This guard is what makes the running-max curves in Fig. 3 monotonic regardless of refinement quality.

O.2 Baseline (uncoded transmission)

A single channel call with the task prompt. No parity, no diversity, no feedback: $Y \leftarrow \mathcal{A}(X)$, $q_0 \leftarrow q(X, Y)$, return Y with score q_0 . This is the “uncoded” reference point; all gains are reported relative to it after paired matching on `task_id` (and, when `repeat_runs > 1`, on `(task_id, repeat_idx)`).

O.3 Diversity ensemble (SC / MRC / EGC)

Analog. Multipath diversity. Generate d noisy copies and combine: SC picks the best, MRC weights by quality, EGC weights equally.

Algorithm. Let $\mathcal{A}_1, \dots, \mathcal{A}_d$ be channels (spatial diversity: different model families; frequency diversity: different prompt variants of the same question; time diversity: different temperature draws of the same model). Generate $Y_i \leftarrow \mathcal{A}_i(X)$ and score all in parallel: $q_i \leftarrow q(X, Y_i)$.

- **SC:** return Y_{i^*} where $i^* = \arg \max_i q_i$. No synthesizer call.

- **MRC / EGC:** pass the full list $\{(Y_i, q_i, \text{model}_i)\}$ to a synthesizer LLM \mathcal{A}_s (the judge model, which is strictly stronger than the channel models and has already seen the candidates during scoring).

The MRC synthesis prompt marks the top-scoring response as [BEST] and others as [ALT-i] with their quality scores, and instructs: start from [BEST]; add only details from [ALT-i] that do not contradict [BEST]; prefer higher-quality responses on conflicts; do not introduce external facts. The EGC prompt is similar but presents all responses as “equally weighted” and uses majority reasoning for conflicts. Synthesis is called with temperature 0.1 (MRC) or 0.2 (EGC).

Guards. (i) *MRC dominance fast path.* If all non-best scores satisfy $q_i < 0.5 \cdot q_{\max}$, synthesis is skipped and SC is returned—analogueous to one branch dominating in AWGN MRC. (ii) *Best-of-sequence.* The synthesis output is rescored via q_Δ against the best individual. If the result does not improve over the best individual, SC output is returned instead. This enforces the combining guarantee $\text{MRC} \geq \text{SC}$ empirically, even when the synthesizer has regressions. (iii) *Identity detection.* If the synthesizer returns the best individual text verbatim, no rescore is performed (the best-individual score is used directly, saving a judge call).

Defaults. $d = 2$ spatial branches (two different model families); prompt variants = 1 (default wording only); temperature spread unused in the main tables (all branches at each model’s configured default temperature).

Wider-pool variants: `diversity_sc_N` and `diversity_mrc_discrete_N`. The two wider-pool operators referenced in Table 6 share the same multi-model sampling rule and differ only in the combiner. *Sampling:* both draw N candidates by cycling through the configured channel pool in round-robin order—sample i is generated by channel index $i \bmod |\{\mathcal{A}_1, \dots, \mathcal{A}_d\}|$ at temperature 0.7, so an $N=5$ run with $d=2$ channels uses $\{\mathcal{A}_1, \mathcal{A}_2, \mathcal{A}_1, \mathcal{A}_2, \mathcal{A}_1\}$. Each candidate is independently scored by the judge to obtain q_i . *diversity_sc_N:* return the $\text{argmax-}q_i$ sample. No synthesizer or voter call; total cost is N generator calls + N judge calls. *diversity_mrc_discrete_N:* cluster the N samples into semantic equivalence classes via one extra *voter* LLM call (defaults to \mathcal{A}_1) at temperature 0.0; the voter receives the task plus all N samples and returns a JSON array $[\ell_1, \dots, \ell_N]$ of cluster IDs. We sum q_i within each cluster, pick the cluster with the largest sum, and return its top- q_i member as the combined output. Failure handling: if voter output cannot be parsed as a length- N JSON integer array, every sample is assigned to its own cluster and the operator degenerates to `diversity_sc_N` on that task. Total cost is N generator calls + N judge calls + 1 voter call; the voter call is recorded in the run’s overhead bucket. **Defaults.** $N = 5$; voter = \mathcal{A}_1 (the first configured channel). The operator’s continuous-MRC counterpart (`diversity_mrc` with $d = N$) trades the voter call for an LLM synthesis call, so the per-task call counts are equal up to that one substitution; the empirical comparison in Sec. 5.2 attributes the discrete-MRC win at 8B and its 3B-QA reversal to voter-LLM clustering quality rather than to a difference in budget.

Discrete-MRC vs. CISC: orthogonal generalizations. CISC [Taubenfeld et al., 2025] and `diversity_mrc_discrete_N` both apply discrete-MRC (cluster, sum CSI per cluster, return the top-CSI member of the winning cluster) but specialize different axes of the same underlying operator. CISC fixes the pool to a single policy (one model, N temperature draws) and feeds intrinsic token-logprob confidence as the per-sample weight, eliminating the judge call. `diversity_mrc_discrete_N` fixes the CSI source to the judge score and generalizes the pool to a multi-model channel set sampled in round-robin. Neither subsumes the other: the strict superset is *Diversity-MRC-Discrete-N-Soft*—multi-model pool with logprob CSI—which collapses to CISC at $|\text{channels}|=1$ and to `diversity_mrc_discrete_N` at *judge-CSI*. We implement Diversity-MRC-Discrete-N-Soft as `diversity_mrc_discrete_N_soft` in Sec. O.10 and report it on the local Ollama configurations only; the cloud configuration uses Anthropic Haiku, which does not expose logprobs, so that channel must be dropped before this technique can run. We flag a residual concern: logprobs from different model families are not on the same scale (different vocabularies, different calibration), so summing c_i across models inside a cluster is a heuristic rather than a calibrated weighting. CISC sidesteps this because all N samples come from one policy. The empirical question—whether multi-model pool gains compose additively with intrinsic-CSI gains, despite cross-model logprob incomparability—is what this technique is meant to answer.

O.4 Hybrid ARQ – Chase Combining (HARQ-CC)

Analog. Chase combining: same codeword retransmitted, receiver soft-combines all copies.

Algorithm. Up to $K = 5$ retransmissions of the *same* prompt to the *same* channel (with independent stochastic sampling each call). After each retransmission k , if $q_k \geq \tau = 0.85$, stop and return Y_k . Otherwise, at the end, pass all $\{Y_1, \dots, Y_K\}$ to a *chase-combining synthesizer*: a prompt that shows every attempt with its quality score and instructs to (1) detect consensus (high-confidence signal), (2) harvest unique details from individual attempts, (3) resolve conflicts in favor of higher-quality attempts. The synthesized output is rescored via q_Δ against the best individual, with the best-of-sequence guard applied.

Defaults. $K = 5$, $\tau = 0.85$, synthesizer = the critic channel (same model family as the generator, communication-faithful) at temperature 0.3.

O.5 Hybrid ARQ – Incremental Redundancy (HARQ-IR)

Analog. Incremental redundancy: each retransmission carries *new parity bits*. In our analog, the “new parity” is structured critic feedback that points to specific errors in the previous attempt.

Algorithm. Let \mathcal{A}_g be the generator channel and \mathcal{A}_c be the critic channel (default: $\mathcal{A}_c = \mathcal{A}_g$, matching real HARQ decoders).

1. *Round 1.* $Y_1 \leftarrow \mathcal{A}_g(X)$; $q_1 \leftarrow q(X, Y_1)$ (absolute scoring). Initialize $Y^* \leftarrow Y_1$, $q^* \leftarrow q_1$, score history $\mathcal{S} \leftarrow [q_1]$, correction buffer $\mathcal{C} \leftarrow \emptyset$. If $q_1 \geq \tau = 0.85$, return.
2. *Rounds* $k = 2, \dots, K = 5$.
 - (a) *Critic pass.* The critic is shown the task, the current best Y^* , the current score q^* , the optional reference, and a deduplication list of already-addressed quoted issues from \mathcal{C} . It is instructed to return a JSON array of issues, each a record $\{\text{quote}, \text{type} \in \{\text{factual_error}, \text{missing_content}, \text{reasoning_gap}, \text{unclear}\}, \text{correction or detail}, \text{severity} \in \{\text{critical}, \text{major}, \text{minor}\}\}$. Temperature 0.2.
 - (b) *Parse.* A multi-stage JSON parser (raw \rightarrow stripped-backtick \rightarrow fenced-code-block \rightarrow inline-array) tolerates weak critics. Explicit `[]` or PASS text yields an empty issue list. Parse failures degrade to a single unstructured issue with the raw text.
 - (c) *Early-stop checks (only when $\text{early_exit}=\text{True}$).* If the issue list is empty and $q^* \geq 0.9\tau$, break (genuine convergence). If the score history has plateaued over a window of 2 with spread < 0.015 , break (EXIT-chart flatness).
 - (d) *Generator pass.* If the issue list is structured (at least one item has a `quote`), the refinement prompt becomes a *correction list*: for each issue, show the quoted text plus the requested fix / insertion, and explicitly instruct the generator to preserve every other part of the answer verbatim. If the issues are unstructured, fall back to a full-rewrite prompt. $Y_k \leftarrow \mathcal{A}_g(\text{refine-prompt})$; $q_k \leftarrow q_\Delta(X, Y_k, Y^*, q^*)$ (differential scoring against the current best).
 - (e) *Accept / reject.* If $q_k \geq q^*$, set $Y^* \leftarrow Y_k$, $q^* \leftarrow q_k$, and append applied corrections to \mathcal{C} . Else, keep Y^* unchanged (regression protection) and do not enlarge \mathcal{C} (so the same issues remain available to the critic next round).
 - (f) *Score-history update.* $\mathcal{S} \leftarrow \mathcal{S} \cup \{q_k\}$. If $q^* \geq \tau$, break.

Return Y^* with score q^* .

Communication-faithful defaults. `early_exit=False` (all K rounds run, matching real decoders); $\mathcal{A}_c = \mathcal{A}_g$ (same-complexity decoder).

Key design choices. (i) *Correction-based refinement* (non-destructive accumulation): the generator is prompted to *apply specific corrections while preserving correct content*, not to rewrite the answer from scratch. This is the agent analog of the soft-buffer accumulation in real HARQ-IR—the previous answer is the “received signal” and corrections are accumulated parity bits. (ii) *Structured JSON critique* forces the critic to quote specific text and tag severity, enabling deduplication across rounds. Vague feedback is the analog of retransmitting identical parity—zero incremental information.

(iii) *Differential scoring per round* reduces judge noise: scoring candidate and baseline in the same judge call cancels common-mode variance.

O.6 Turbo decoder

Analog. Two SISO decoders exchanging extrinsic information through an interleaver; each iteration one decoder updates its belief using the other’s extrinsic LLRs, with a damping factor $\alpha \in (0, 1]$ to prevent oscillation [Vogt and Finger, 2000].

Algorithm. Let \mathcal{A}_g be the generator, \mathcal{A}_c the critic (default: $\mathcal{A}_c = \mathcal{A}_g$, “same” mode), q the judge. Maintain best Y^* , best score q^* , correction buffer \mathcal{C} , score history \mathcal{S} , current damping $\alpha \leftarrow \alpha_0 = 0.5$, and consecutive-regression counter r .

1. *Iteration 0.* $Y_0 \leftarrow \mathcal{A}_g(X)$; $q_0 \leftarrow q(X, Y_0)$; initialize. If $q_0 \geq \tau = 0.9$, return.
2. *Iterations* $k = 1, \dots, K - 1 = 5$ (total max iterations including iter 0 is 6, but the default configuration caps at $K = 5$):
 - (a) *Interleaver.* Select a lens from $\{\text{correctness, completeness, reasoning, clarity}\}$ by index $k \bmod 4$. The lens is appended to the critic’s system instruction (“pay special attention to X this round, but flag any problem”). This decorrelates critic observations across iterations—the agent analog of the bit-interleaver in real turbo codes. Without the interleaver the critic tends to produce correlated feedback (same issues flagged every round), reducing extrinsic information to near-zero.
 - (b) *Critic pass.* Same structured-JSON critique as HARQ-IR, but with the lens hint and the dedup list of already-applied quoted issues from \mathcal{C} .
 - (c) *Extrinsic scaling (the α step).* Apply three filters in sequence to the critic’s issue list:
 - *Severity floor.* Drop issues below `severity_floor=major` (i.e. only critical and major survive). Minor issues on already-polished answers are the critic fabricating problems—agent analog of LLR magnitude thresholding.
 - *α scaling.* Keep $\lceil n \cdot \alpha \rceil$ issues (at least one, if any remain), sorted by severity ascending (most severe first). This is the direct agent analog of extrinsic-LLR scaling in turbo decoders: limit how aggressively each iteration can correct.
 - *Hard cap.* `max_corrections_per_round=2` issues total (LLR clipping).
 - (d) *Generator pass.* Apply the ≤ 2 surviving corrections via the same correction-list prompt as HARQ-IR (preserve-except-corrections contract). Score via q_Δ against Y^* . Append q_k to \mathcal{S} .
 - (e) *Accept / reject with adaptive damping.* If $q_k \geq q^*$: accept, append applied corrections to \mathcal{C} , reset $r \leftarrow 0$, and *relax* $\alpha \leftarrow \min(\alpha_0, 1.2\alpha)$. Else: reject (regression protection), increment r , and *damp* $\alpha \leftarrow \max(0.1, 0.5\alpha)$.
 - (f) *Divergence break.* If $r \geq 2$ (two consecutive regressions), break. The EXIT trajectory is diverging and further iterations will consume tokens without recovery. The best-of-sequence guard ensures Y^* is still the best seen.
 - (g) *Convergence break.* If $q^* \geq \tau$, break.

Return Y^* with score q^* .

Key design choices. (i) *Same-complexity decoder* ($\mathcal{A}_c = \mathcal{A}_g$) matches real turbo codes, where both component decoders operate on the same trellis. Allowing a stronger critic is supported (`critic_model="judge"`) but breaks the analogy. (ii) *Communication-faithful fixed iterations:* `early_exit=False` runs all K rounds. The divergence break on $r \geq 2$ is activity-dependent; the plateau-detection break is gated by `early_exit=True`. (iii) *Interleaver lens rotation* is what distinguishes turbo from HARQ-IR in our implementation. With the same critic and no interleaver, the two techniques become identical.

Why $\alpha_0 = 0.5$, severity floor = major. Empirical analysis on 14B models showed the first refinement round at $\alpha = 0.7$ produced the largest regression (hard-task mean $0.627 \rightarrow 0.592$), consistent with over-correction even at moderate damping. Lowering α_0 to 0.5 and gating minor issues eliminated the first-round regression without harming overall gain. At 3B/4B (Fig. 3), even $\alpha_0 = 0.5$ is insufficient—the refinement map itself is contractive on the wrong side, and the best-of-sequence guard does all the work.

0.7 Fountain (Rateless) Decoder

Analog. LT / Raptor codes [Shokrollahi, 2006]: generate an unbounded stream of encoded symbols and stop when the receiver can decode. No fixed code rate.

Algorithm. Parameters: $N_{\max} = 10$, $N_{\min} = 2$, confidence threshold $\gamma = 0.85$.

1. For $n = 1, \dots, N_{\max}$, round-robin across channels $\mathcal{A}_{1+(n-1) \bmod d}$; temperature perturbed by $0.5 + 0.1(n \bmod 5)$ for stochastic encoding. $Y_n \leftarrow \mathcal{A}(X, \text{temp})$; $q_n \leftarrow q(X, Y_n)$.
2. After each sample, if $n \geq N_{\min}$, compute confidence $\gamma_n = 0.6 \cdot \bar{q} + 0.4 \cdot \text{agreement}$, where \bar{q} is the mean score so far and $\text{agreement} = 1 - (\max - \min)$ over the top- $\lceil n/2 \rceil$ scores. If $\gamma_n \geq \gamma$, stop.
3. *ML decode.* Sort samples by quality descending. If the best sample dominates the runner-up by > 0.20 , return it directly (ML-decode fast path, no synthesis). Else, apply *erasure marking*: drop samples whose score is > 0.10 below the best. The surviving set is passed to a weighted-synthesis prompt with weights $w_i = q_i / \sum q_j$ and explicit instructions “trust the higher-weighted sample unconditionally on conflicts; add details from lower-weighted samples only when they do not contradict”. The synthesized output is scored independently and subjected to the best-of-sequence guard.

Key design choices. *Erasure marking* (drop samples > 0.10 below best) is what distinguishes this from naive ensembling: earlier versions that merged all top-half samples leaked wrong facts from weak samples into the answer (measured -0.024 vs best individual across 69 tasks). The ML decoder now either picks the single best (fast path) or synthesizes only from a tight quality band.

0.8 Forward Error Correction (FEC)

Analog. Structured redundancy: generate systematic bits plus parity sections. Code rate $r = k/n$ controls the redundancy level.

Algorithm. The systematic bits are the *main answer*: $Y_0 \leftarrow \mathcal{A}(X)$, $q_0 \leftarrow q(X, Y_0)$. Each parity section is a *separate LLM call* with the main answer in context but a distinct instruction:

- **reasoning**: re-derive the answer from scratch via step-by-step reasoning; flag any discrepancy with the main answer.
- **verification**: check each claim in the main answer for correctness, logical validity, completeness, and internal consistency; state each issue with a quote, a reason, and a correction.
- **alternative**: solve the task using a *different* approach / strategy without reference to the main answer. Cross-check.
- **confidence**: rate each claim HIGH / MEDIUM / LOW confidence; flag LOW items as potential errors.

Code rates map to parity-section lists: $r = 1.0 \mapsto []$ (uncoded), $r = 0.75 \mapsto [\text{reasoning}]$, $r = 0.50 \mapsto [\text{reasoning}, \text{verification}]$, $r = 0.33 \mapsto [\text{reasoning}, \text{verification}, \text{alternative}]$, $r = 0.25 \mapsto$ all four. The decoder sees the main answer and *all* parity sections as separate numbered blocks and runs a *syndrome-decoding prompt*: for each present parity section, include a bullet describing what to cross-check (“does step-by-step reach the same conclusion?”, “did verification find errors?”, “does the independent solution agree?”, “are LOW-confidence items actually wrong?”); detect inconsistencies; correct; output the final answer. Decoder temperature 0.2. The decoded output is rescored via q_Δ against Y_0 with the best-of-sequence guard.

Key design choice. Each parity section is a *separate LLM call*, not a single prompt that asks for everything. Cramming multiple checks into one call produces attention dilution and correlated “parity” (all sections restating the main answer). Separate calls give each check the model’s full attention and produce genuinely independent redundancy, matching how real FEC computes each parity symbol independently.

O.9 Adaptive Coding & Modulation (ACM)

Analog. LTE / 5G ACM: a modulation-and-coding scheme (MCS) table is indexed by measured channel quality (CQI); good channels get high-rate / low-protection MCS, bad channels get low-rate / high-protection MCS.

Algorithm. Profiles (MCS levels) are specified as a list of `{name, difficulty_range, model, technique, code_rate (for FEC), num_branches (for diversity), max_rounds (for HARQ), cost_multiplier}`.

1. *Difficulty estimation (CQI).* The *pilot probe*: a short 2–3 sentence generation on the task, requested with token-level log-probabilities. The probe’s mean logprob $\bar{\ell}$ is the CQI; difficulty is $d = 1 - \exp(\bar{\ell})$, clamped to $[0, 1]$. This is a direct analog of channel estimation from pilot symbols in physical-layer ACM. When the backend does not expose logprobs (e.g., Anthropic channels), ACM falls back to an LLM self-rating call (“rate this task’s difficulty $[0, 1]$ ” at $T=0.1$). The probe is billed as overhead.
2. *Profile selection.* Find the first MCS whose `difficulty_range` contains the estimated difficulty; fall through to the maximum-protection MCS on miss.
3. *Execute.* Instantiate the selected technique (HARQ-IR / turbo / fountain / diversity-MRC / diversity-EGC / FEC / uncoded) with the profile’s parameters, using the profile’s `model` (if available in the channel pool; else the first channel).

Routing tables are calibrated per model tier. The 3B table (qwen2.5:3b + gemma3:4b) routes MCS-0/1/2 to fountain with $n=2$ spatial branches and MCS-3 to diversity-EGC; fountain dominates every bucket at this scale. The 14B table (deepseek-r1:14b + phi3:14b) uses HARQ-IR (`max_rounds=2→3`) for MCS-0/1 and turbo (`max_rounds=4→6`) for MCS-2/3/4, reflecting the 14B leaderboard where iterative refinement beats spatial diversity. The Haiku + GPT-5-mini table routes MCS-0/1/2 to HARQ-IR, MCS-3 to diversity-MRC, and MCS-4 to turbo.

O.10 Soft-Output Variants

When the backend exposes token-level log-probabilities (Ollama, vLLM, OpenAI), three techniques have soft-decision counterparts that replace judge-based weights with intrinsic model confidence $c = \exp(\bar{\ell})$ where $\bar{\ell}$ is the mean token log-probability of the generation. Anthropic models do not currently expose logprobs; these modes fail fast rather than silently degrade.

SoftDiversityMRC. Identical structure to MRC, but the combining weights are $w_i = c_i / \sum_j c_j$ rather than $q_i / \sum_j q_j$. Eliminates the judge call that would otherwise be needed to weight branches, at the cost of a weaker signal (logprob reflects the model’s own uncertainty, not output correctness). The SC fallback on synthesis regression is unchanged.

SoftFountainDecoder. Replaces the quality-based confidence estimator with a soft one: $\gamma_n = 0.6 \cdot \bar{c} + 0.4 \cdot (1 - \text{spread}(c))$, and erasure-marks samples with $c_i < 0.5c_{\max}$. Low-logprob samples are dropped from synthesis, mirroring how real fountain decoders discard erasure-flagged symbols.

SoftACMRouter. Replaces the explicit difficulty-estimation LLM call with a *pilot probe*: a short generation (2–3 sentences) on the task, requested with logprobs. The probe’s mean logprob is the CQI; high logprob → easy channel → light protection; low logprob → hard channel → heavy protection. Profiles are keyed by confidence range rather than difficulty range.

O.11 Where Each Technique Can Fail (and Why That Is a Feature)

Because all techniques share the best-of-sequence guard, their *final* quality can never drop below the best individual call. But their *per-iteration* or *per-combining-step* dynamics differ sharply across the operating regime, and these differences are what the framework predicts:

- *Diversity* (SC/MRC/EGC) degrades only if branches are strongly correlated (shared training data), reducing the effective diversity order. The $MRC \geq EGC$ prediction assumes near-perfect CSI; in our data (Sec. 5.3, Sec. C) CSI is noisy enough on occasions that $EGC \geq MRC$ reverses.

- *HARQ-CC* fails when all attempts share the same failure mode; synthesis cannot correct errors that every attempt makes.
- *HARQ-IR / Turbo* fail below the iterative-decoding threshold: the refinement map is expansive rather than contractive, and extra iterations inject noise. The α damping plus divergence break plus best-of-sequence guard contain the damage but do not create gain. Fig. 3 is the visualization of this failure mode at 3B.
- *Fountain* can over-generate on adversarial tasks where the confidence metric is miscalibrated (many high-quality-looking but wrong samples), reaching N_{\max} without stopping; the synthesized output is still best-of-sequence-guarded, so cost is wasted but quality is not harmed.
- *FEC* fails when the parity sections themselves share the main answer’s errors (the critic/verifier is misled by the main answer’s framing). Separate LLM calls with different instructions (verification vs. independent re-derivation) mitigate but do not eliminate this.
- *ACM* fails when the difficulty estimator is systematically miscalibrated, routing hard tasks to MCS-0 or easy tasks to MCS-4. Soft ACM replaces the meta-judgment with a direct logprob measurement, reducing this risk at the cost of requiring logprob support.

P Per-configuration figure gallery

The same plotting pipeline (`agentcodec.plots.plot_all_from_cache`) is applied to every channel configuration of Table 7, producing a per-configuration set of plots from the single-call baseline cache and the per-technique caches. We reproduce the five most informative plots per configuration here and consolidate the remaining figures (heatmaps, quality distributions, FEC rate–distortion, matched-budget bars) on the project release. Throughout this gallery, “ ρ ” denotes per-task cost overhead relative to the uncoded baseline (Eq. (7)); all error bars are 95% bootstrap confidence intervals; all significance stars are paired Wilcoxon signed-rank vs. baseline ($*p < 0.05$, $**p < 0.01$, $***p < 10^{-3}$). Communication-theoretic technique names referenced in legends are: DIVERSITY-SC, DIVERSITY-MRC, DIVERSITY-EGC (selection / maximal-ratio / equal-gain combining over a multi-channel pool); HARQ-CC and HARQ-IR (hybrid retransmission with chase combining vs. incremental redundancy); TURBO (extrinsic-information-exchange decoder); FOUNTAIN (rateless sampling with confidence-based stopping); FEC- r (forward error correction at code rate r); ACM (the hand-coded adaptive-coding-and-modulation router); DIVERSITY-SC- N and DIVERSITY-MRC-DISCRETE- N (wider-pool N -sample variants of the same selection / discrete-MRC operators).

P.1 14B local: DeepSeek-R1 14B + Phi-3 14B, judge Gemma-3 12B

This subsection collects the 14B-local diagnostics. Fig. 13 plots quality versus cost on three axes (raw cost, normalized overhead ρ , and quality gain over baseline). Fig. 14 shows the iterative-refinement diagnostics, with the HARQ-CC-versus-HARQ-IR convergence in Fig. 14a and the per-iteration turbo trajectory in Fig. 14b. Fig. 15 decomposes the realized-router-to-oracle gap on this configuration, and Fig. 16 reports per-category quality on the four curated categories.

P.2 8B local: Llama-3.1 8B + Qwen-2.5 7B, judge Gemma-3 12B

This subsection mirrors the layout of Sec. P.1 for the 8B local configuration. The quality–cost panels are in Fig. 17; the iterative-refinement diagnostics in Fig. 18; the oracle-gap decomposition in Fig. 19; and the per-category quality in Fig. 20.

P.3 3B local: Qwen-2.5 3B + Gemma-3 4B, judge Gemma-3 12B

This subsection mirrors the layout of Sec. P.1. Fig. 21 plots quality versus cost; Fig. 22 the iterative-refinement diagnostics (the empirical signature of operating below the iterative-decoding threshold of Prop. 2); Fig. 23 the oracle-gap decomposition; and Fig. 24 the per-category quality.

P.4 3B local with cloud judge: Qwen-2.5 3B + Llama-3.2 3B, judge Gemma-4 31B

This subsection follows the same layout. Fig. 25 plots quality versus cost; Fig. 26 the iterative-refinement diagnostics; and Fig. 27 the oracle-gap decomposition.

P.5 Anthropic + OpenAI cloud: Claude Haiku 4.5 + GPT-5-mini, judge Claude Haiku 4.5

This subsection follows the same layout. Fig. 28 plots quality versus cost; Fig. 29 the iterative-refinement diagnostics (both the chase-combining and turbo decoders sit above threshold on this configuration); and Fig. 30 the per-category quality.

P.6 Ollama-cloud trio on curated tasks: Nemotron-Nano-3 30B + Devstral-Small-2 24B, judge GLM-5.1

This subsection covers the Ollama-cloud trio on the 69 curated tasks. Fig. 31 plots quality versus cost; Fig. 32 the iterative-refinement diagnostics; Fig. 33 the oracle-gap decomposition; and Fig. 34 the per-category quality.

P.7 Ollama-cloud trio on the 300-task hard-benchmark split (MMLU/GSM8K/HumanEval)

This subsection covers the headline 300-task hard-benchmark split. Fig. 35 plots quality versus cost on the same axes as the curated subsections; Fig. 36 reports per-dataset mean quality (one panel per dataset); Fig. 37 reports the per-dataset quality–cost Pareto scatters; Fig. 38 decomposes the realized-router-to-oracle gap on this configuration (and underlies the body’s Fig. 1 and the technique pick-frequency profile of Fig. 9); and Fig. 39 reports the iterative-refinement diagnostics.

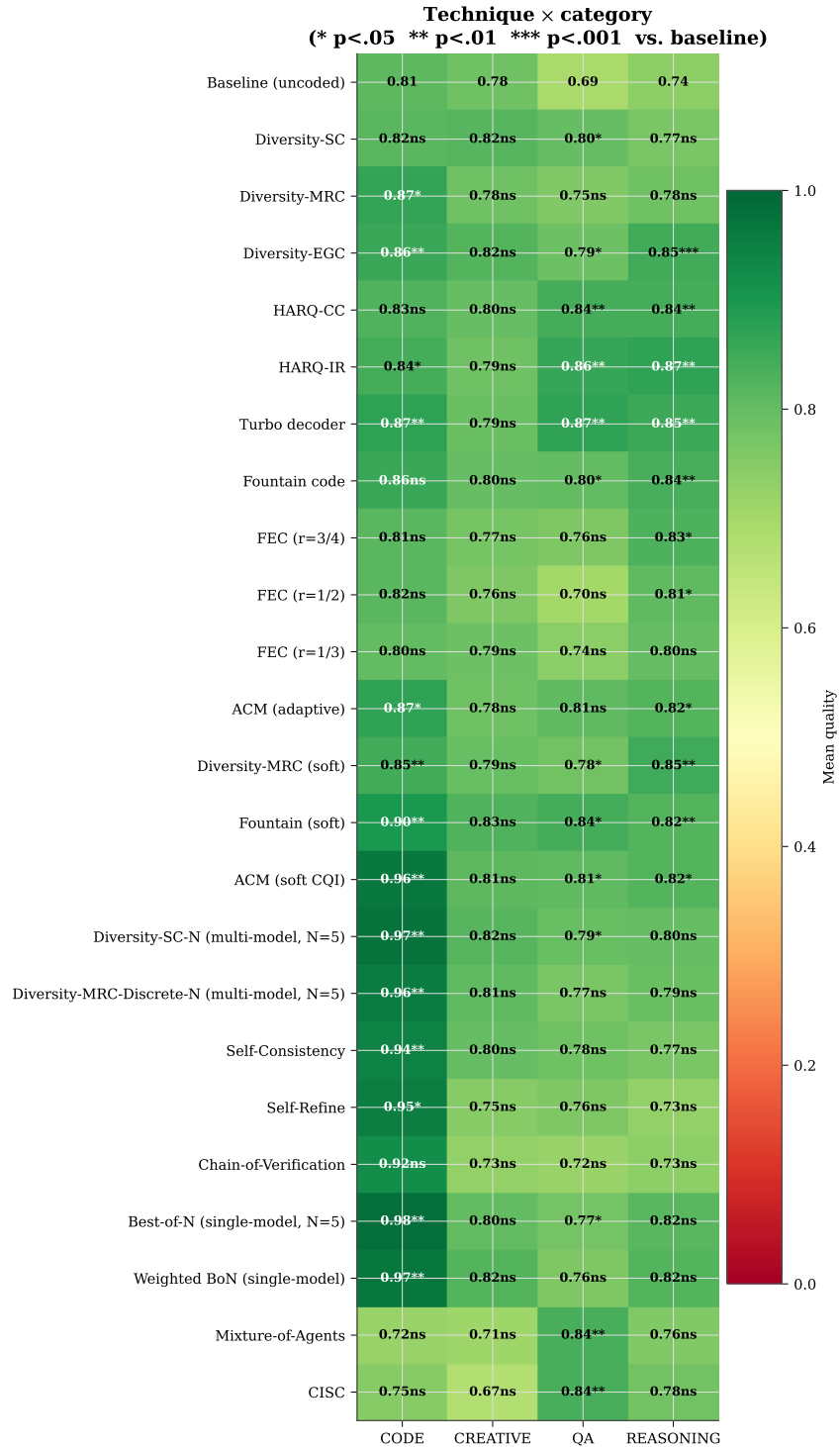


Figure 10: Technique × task-category heatmap on the 14B local configuration (DeepSeek-R1 14B + Phi-3 14B; judge Gemma-3 12B; $n=69$ curated tasks). Each cell reports the per-(technique, category) mean quality with paired-Wilcoxon-vs.-baseline significance stars. Different techniques dominate different task types: hybrid retransmission with incremental redundancy on question answering and reasoning, maximal-ratio combining on code, and equal-gain combining or turbo on creative.

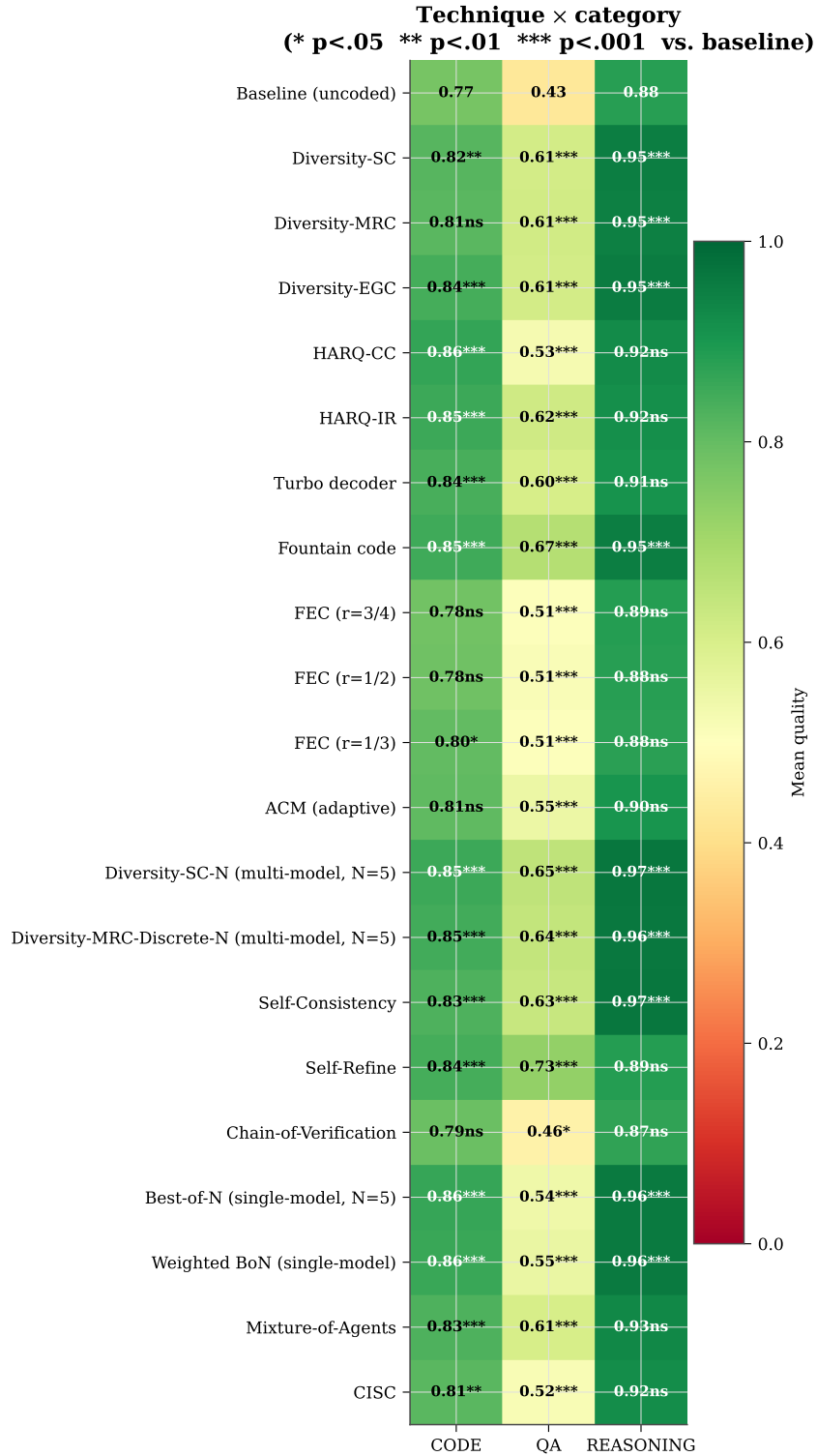


Figure 11: Technique × task-category heatmap on the Ollama-cloud trio. Each cell reports the per-(technique, category) mean quality with paired-Wilcoxon-vs.-baseline significance stars. Different techniques dominate different task types: hybrid retransmission with incremental redundancy on question answering and reasoning, maximal-ratio combining on code.

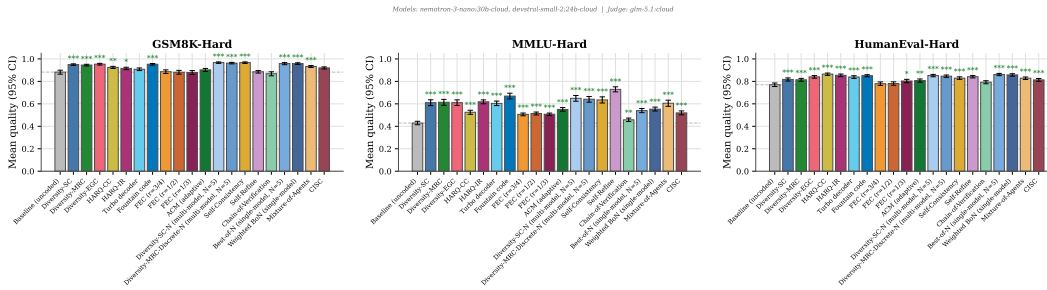


Figure 12: Mean quality by technique on the three hard-benchmark splits (Ollama-cloud trio; one panel per dataset, 100 tasks each). Bars show per-technique mean quality with 95% bootstrap confidence intervals; significance stars denote paired-Wilcoxon-vs.-baseline tests; the dashed line is the per-panel baseline mean.

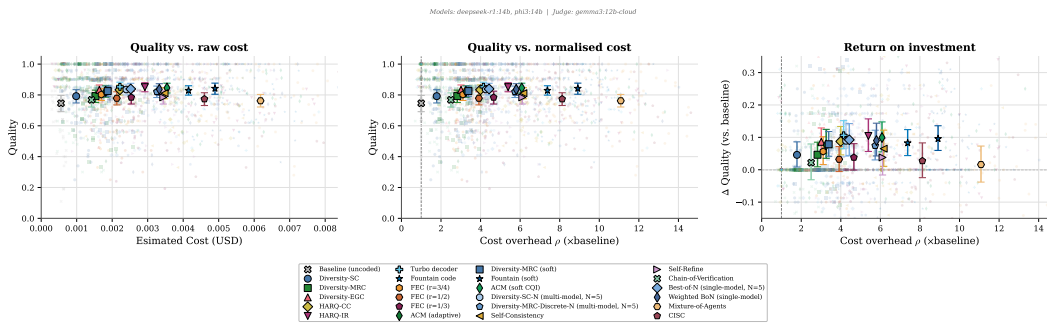
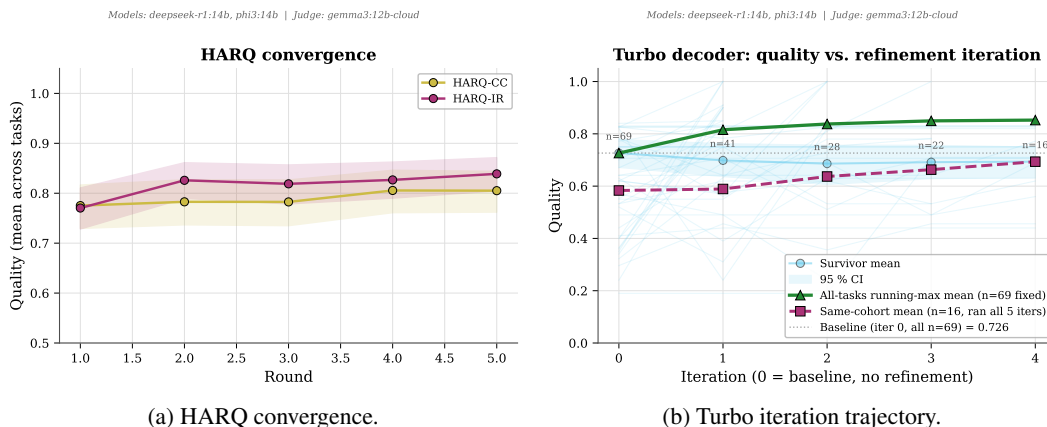


Figure 13: 14B local: quality versus cost. *Left*: raw cost (US dollars) per task; *center*: quality versus normalized cost overhead ρ ; *right*: quality gain over the single-call baseline versus ρ . Large markers are per-technique means with 95% bootstrap confidence intervals; small markers are individual task runs. Techniques in the upper-left of the right panel give the best quality return per cost-dollar invested.



(a) HARQ convergence.

(b) Turbo iteration trajectory.

Figure 14: 14B local: iterative-refinement diagnostics. (a) Mean quality versus retransmission round for chase combining (HARQ-CC) and incremental redundancy (HARQ-IR); incremental redundancy reaches its plateau in fewer rounds, consistent with the “new parity per round” interpretation. (b) Per-task turbo trajectories (thin lines) plus the all-tasks running-max mean (thick); iteration 0 is the initial generation before any refinement. The running-max curve is monotonic by the best-of-sequence guard (Remark 4).

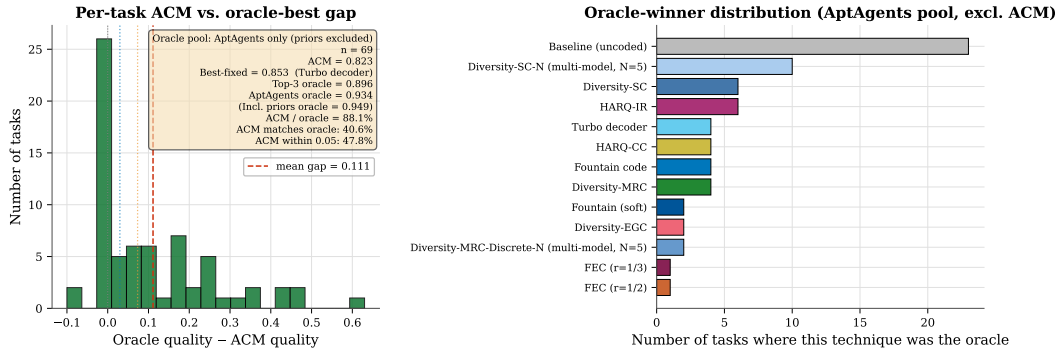


Figure 15: 14B local: ACM-router oracle-gap decomposition. *Left*: per-policy mean quality with 95% bootstrap confidence intervals (cross-validated rows are out-of-fold). *Right*: additive decomposition of the realized-router-to-oracle gap into a feature-set information limit, a finite-sample generalization gap, a policy gap (router class), and a realization gap (configuration drift).

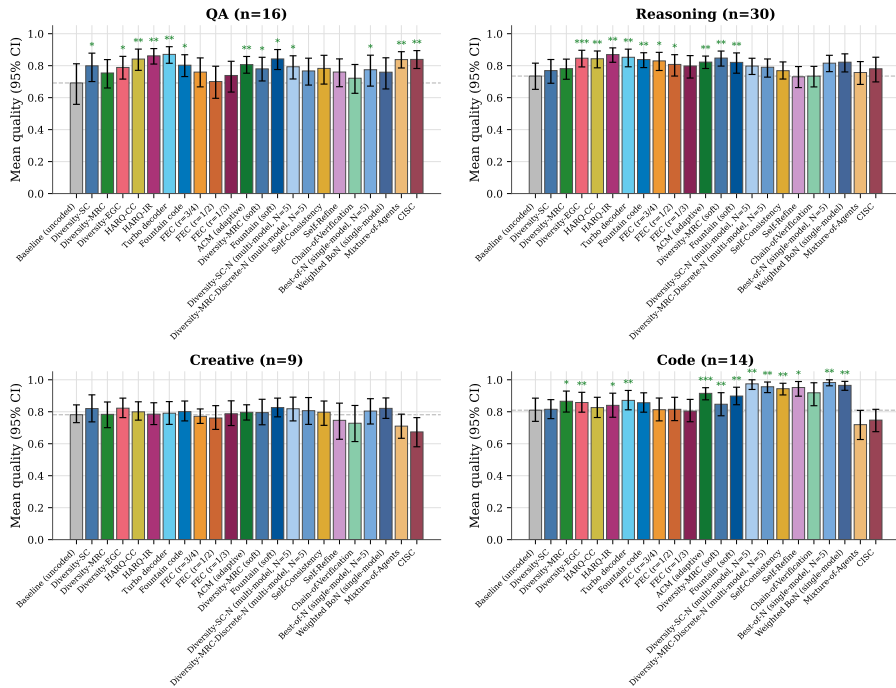


Figure 16: 14B local: per-category mean quality on the 69 curated tasks; one panel per task category (question answering, reasoning, creative, code). Dashed line is the per-category baseline mean. Iterative techniques (HARQ-IR, TURBO) lead on reasoning and question answering; diversity combining (DIVERSITY-MRC, DIVERSITY-EGC) leads on code and creative.

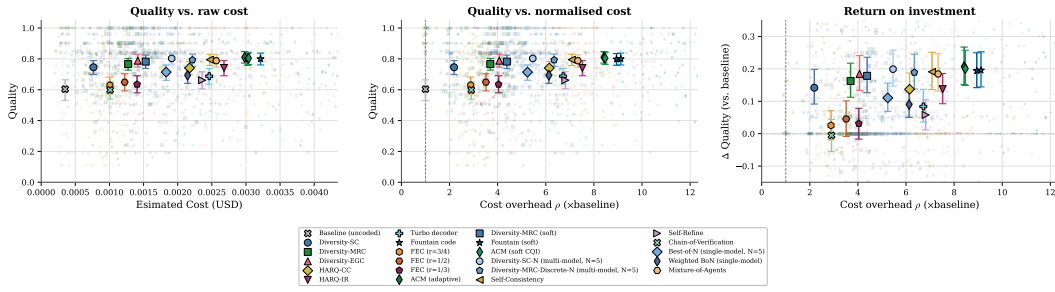
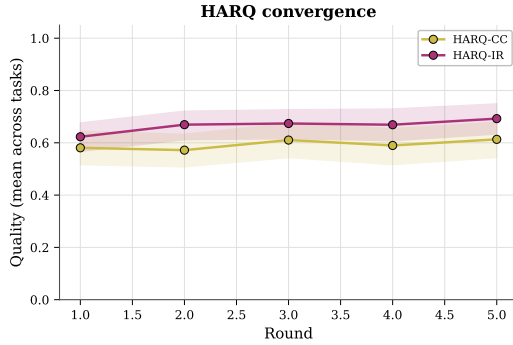
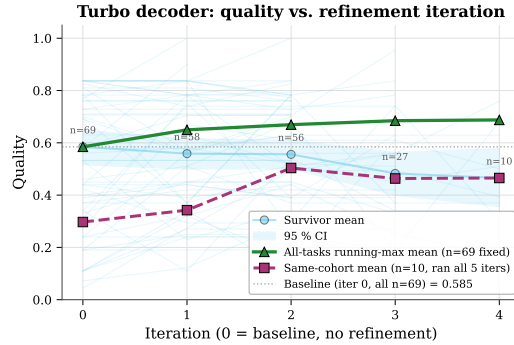


Figure 17: 8B local: quality versus cost (panels as in Fig. 13). The frontier shifts down in absolute quality compared with 14B but the relative ordering of comm-theoretic techniques persists.



(a) HARQ convergence.



(b) Turbo iteration trajectory.

Figure 18: 8B local: iterative-refinement diagnostics. The turbo survivor cohort is noisy and barely advancing, the empirical signature of operating near the iterative-decoding threshold of Prop. 2; the running-max curve still climbs because the best-of-sequence guard keeps the delivered output monotone.

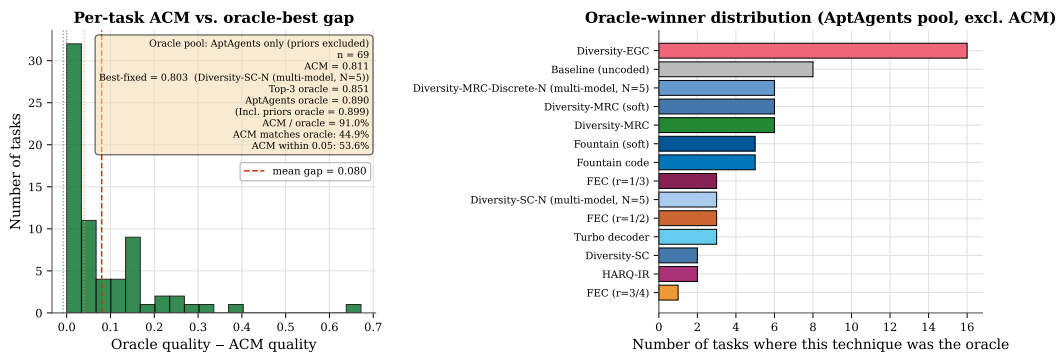


Figure 19: 8B local: ACM-router oracle-gap decomposition (axes as in Fig. 15).

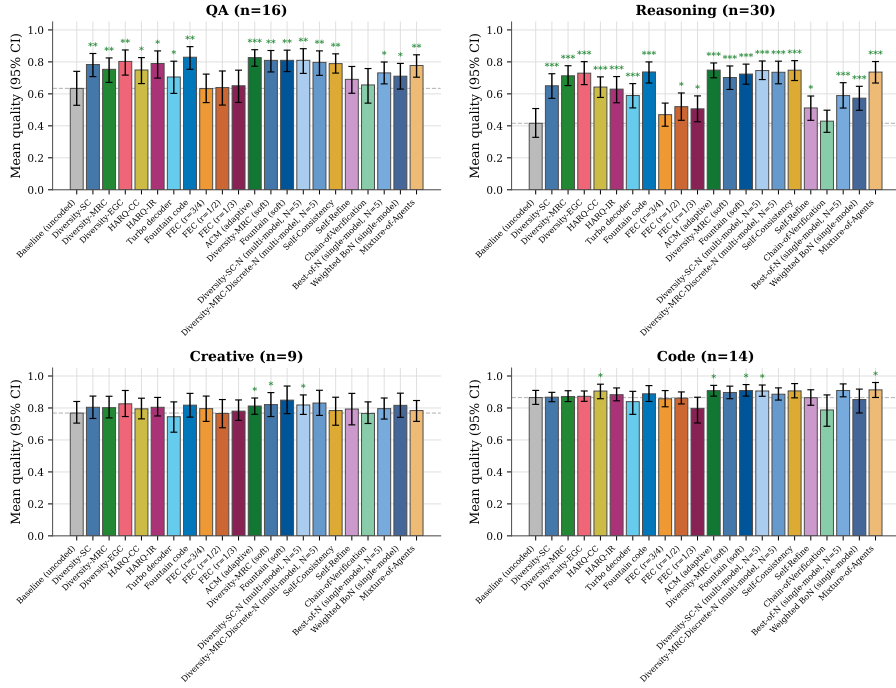


Figure 20: 8B local: per-category mean quality (panels as in Fig. 16).

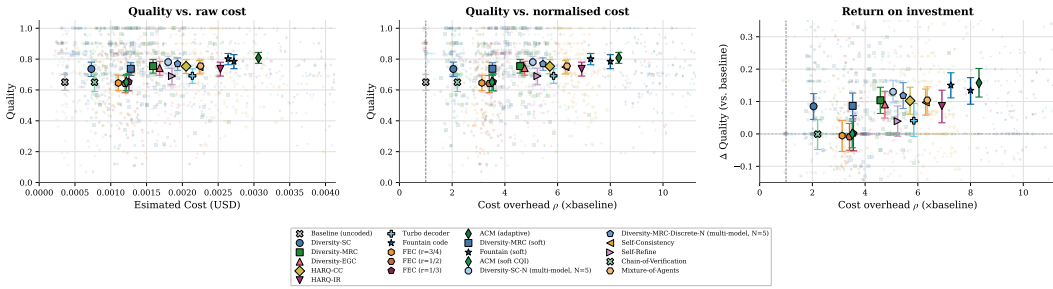
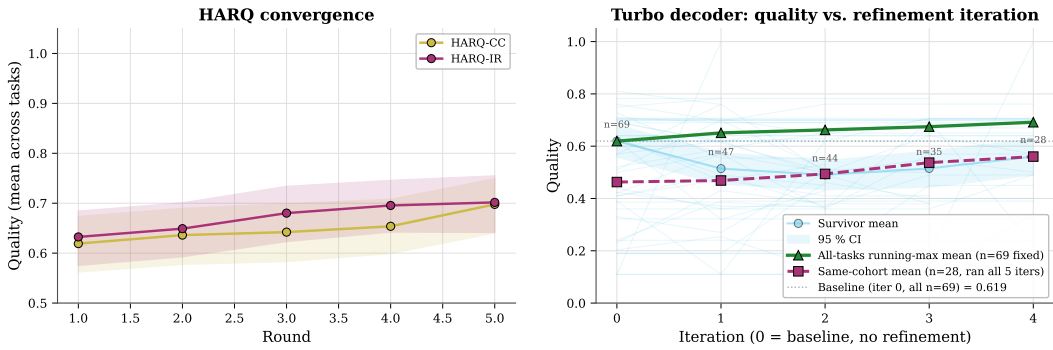


Figure 21: 3B local: quality versus cost (panels as in Fig. 13).



(a) HARQ convergence.

(b) Turbo iteration trajectory.

Figure 22: 3B local: iterative-refinement diagnostics. The turbo survivor cohort is net-descending, the empirical signature of operating below the iterative-decoding threshold of Prop. 2: the unguarded refinement map is contractive on the wrong side, and only the best-of-sequence guard keeps the delivered output from regressing.

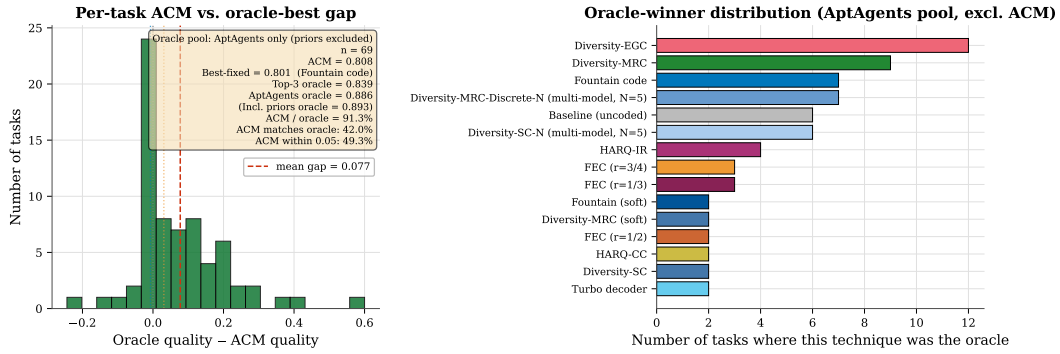


Figure 23: 3B local: ACM-router oracle-gap decomposition (axes as in Fig. 15).

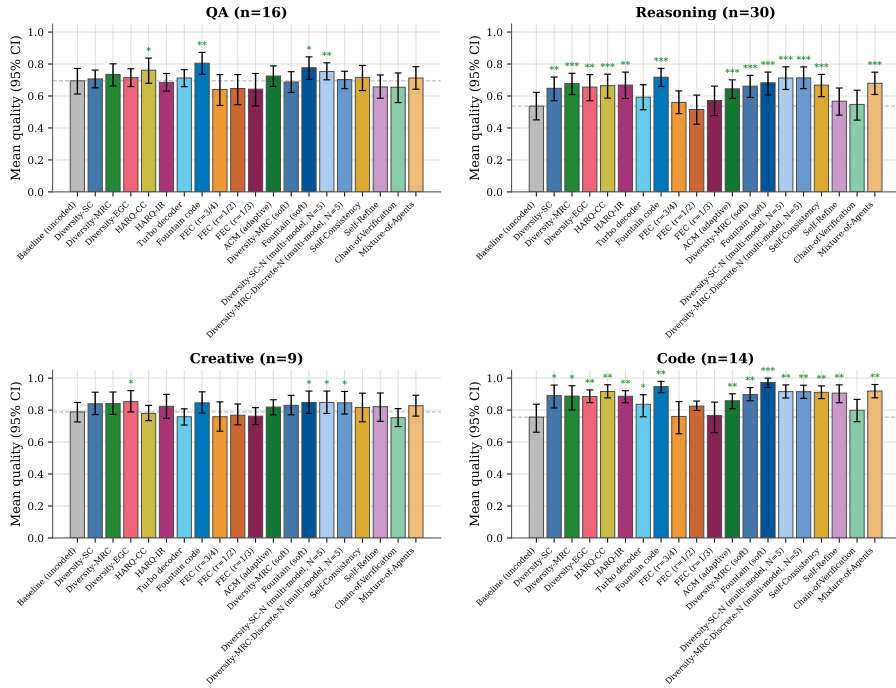


Figure 24: 3B local: per-category mean quality (panels as in Fig. 16).

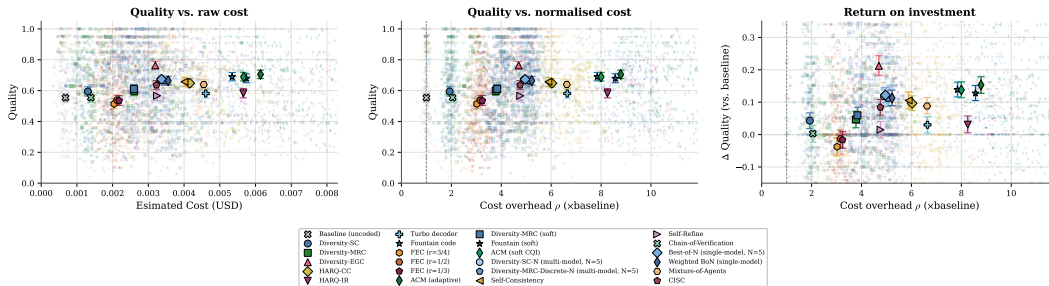
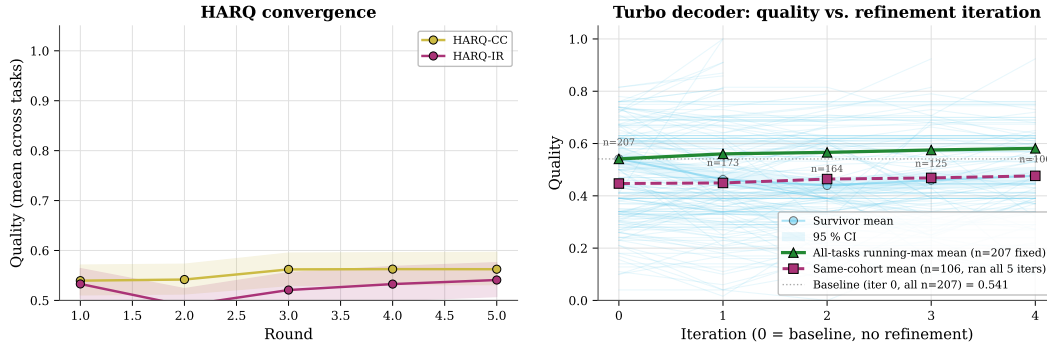


Figure 25: 3B local with cloud judge: quality versus cost (panels as in Fig. 13). Replacing the 12B local judge with a 31B cloud judge resolves judge-side score quantization at the price of an extra cost component on every scoring call; the technique ordering is qualitatively preserved.



(a) HARQ convergence. (b) Turbo iteration trajectory.
 Figure 26: 3B local with cloud judge: iterative-refinement diagnostics.

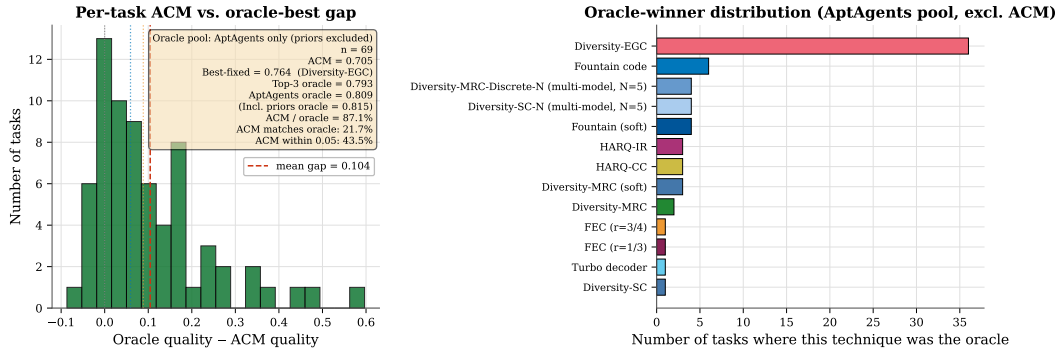


Figure 27: 3B local with cloud judge: ACM-router oracle-gap decomposition (axes as in Fig. 15).

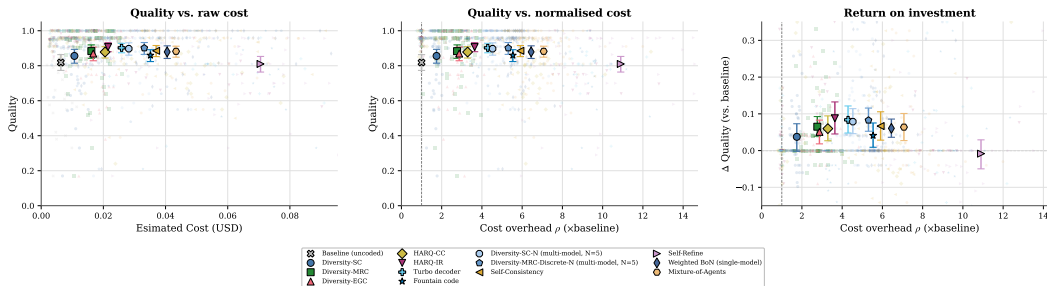
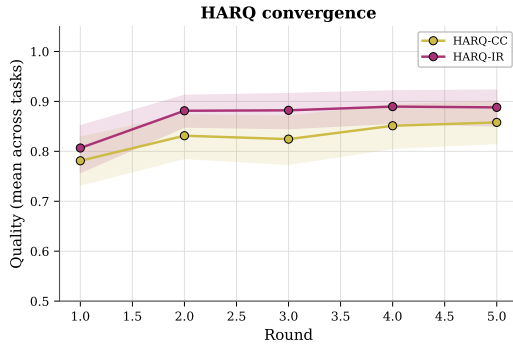
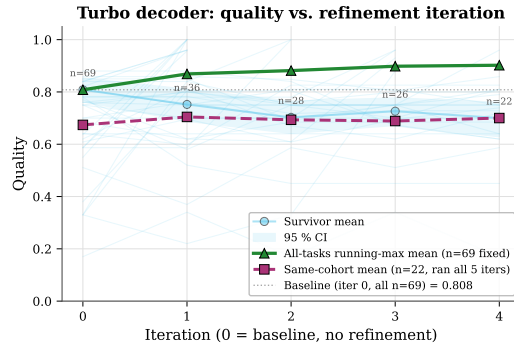


Figure 28: Anthropic + OpenAI cloud: quality versus cost (panels as in Fig. 13). Absolute cost is one to two orders of magnitude above the local configurations; absolute quality is also higher, so quality gains per added cost-dollar are more conservative.



(a) HARQ convergence.



(b) Turbo iteration trajectory.

Figure 29: Anthropic + OpenAI cloud: iterative-refinement diagnostics. Both refinement decoders sit firmly above the threshold of Prop. 2 on this configuration.

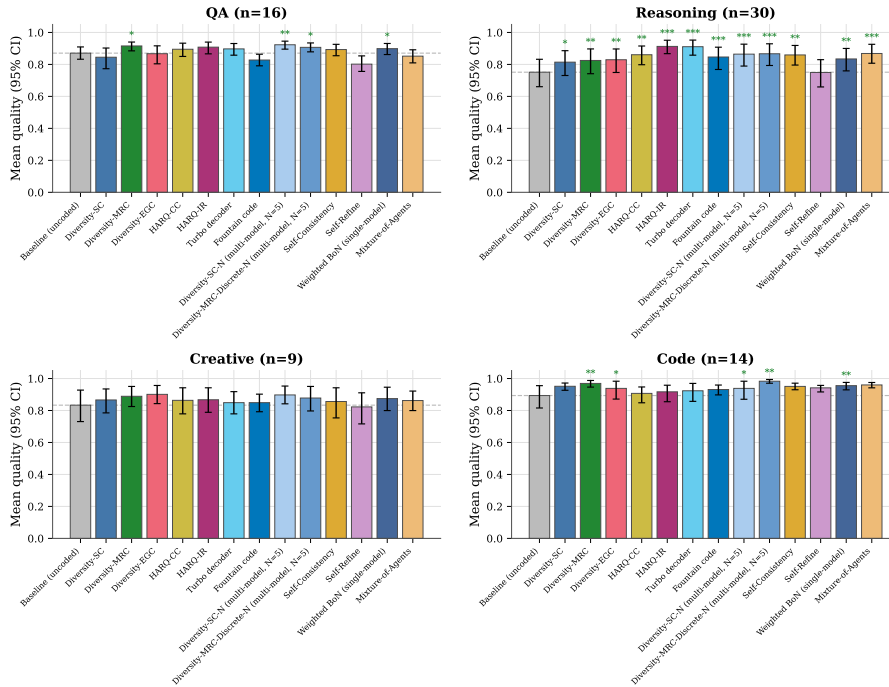


Figure 30: Anthropic + OpenAI cloud: per-category mean quality (panels as in Fig. 16).

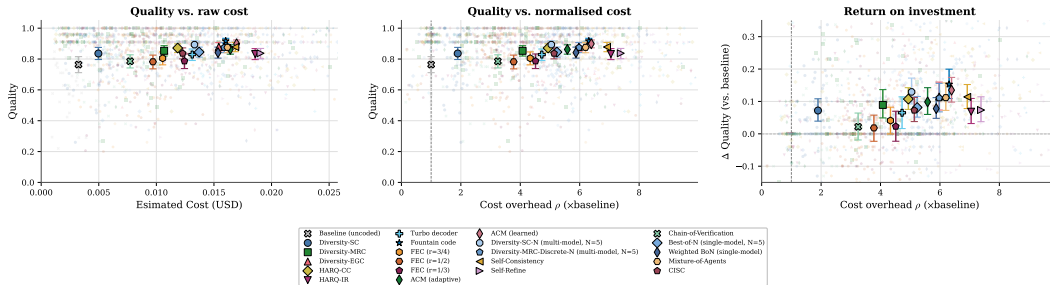
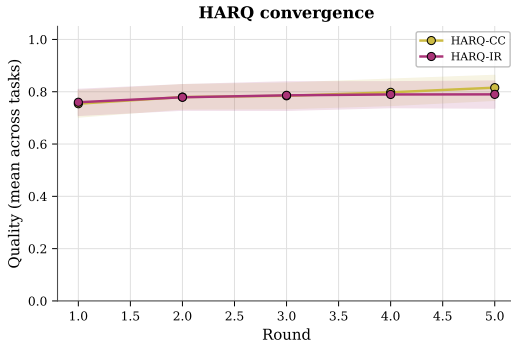


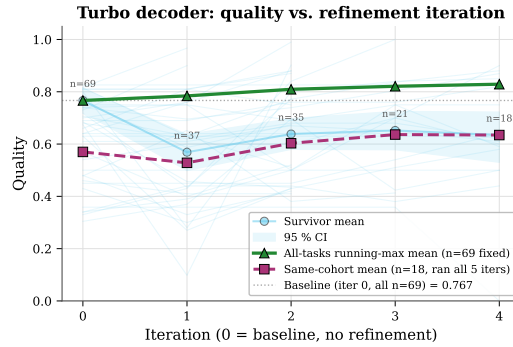
Figure 31: Ollama-cloud trio on the 69 curated tasks: quality versus cost (panels as in Fig. 13).

Models: nemotron-3-nano:30b-cloud, devstral-small-2:24b-cloud | Judge: glm-5.1:cloud



(a) HARQ convergence.

Models: nemotron-3-nano:30b-cloud, devstral-small-2:24b-cloud | Judge: glm-5.1:cloud



(b) Turbo iteration trajectory.

Figure 32: Ollama-cloud trio on the curated split: iterative-refinement diagnostics.

Models: nemotron-3-nano:30b-cloud, devstral-small-2:24b-cloud | Judge: glm-5.1:cloud

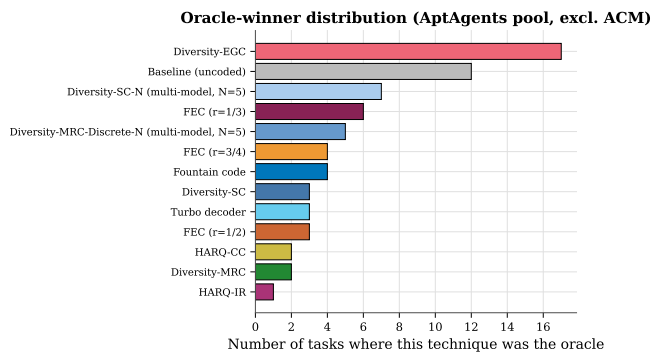
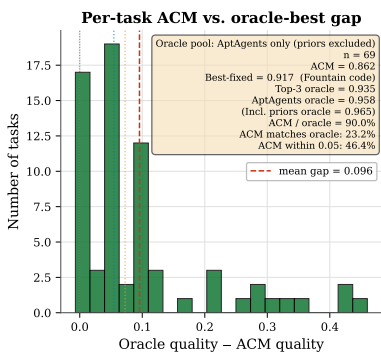


Figure 33: Ollama-cloud trio on the 69 curated tasks: ACM-router oracle-gap decomposition (axes as in Fig. 15).

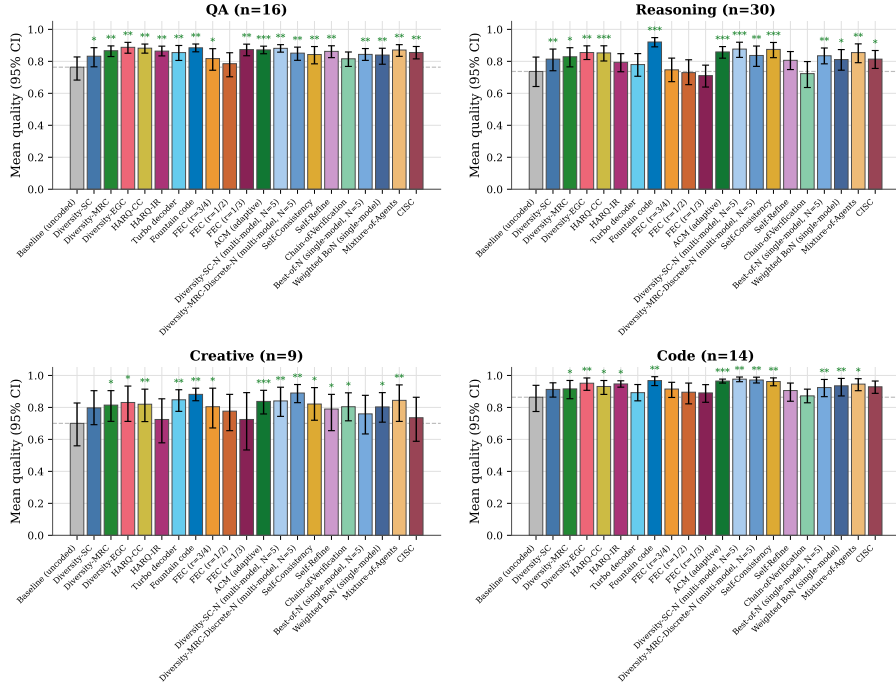


Figure 34: Ollama-cloud trio on the curated split: per-category mean quality (panels as in Fig. 16).

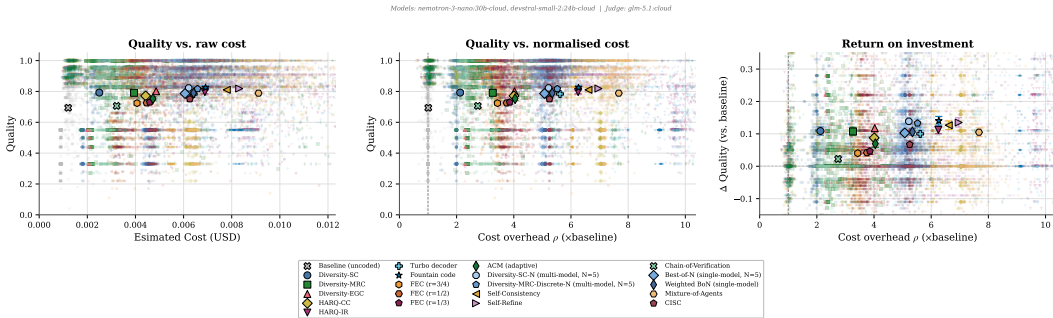


Figure 35: Ollama-cloud trio on the 300-task hard-benchmark split: quality versus cost (panels as in Fig. 13). This is the configuration on which the headline cost-aware semantic-nearest-neighbor router (Table 3) is evaluated.

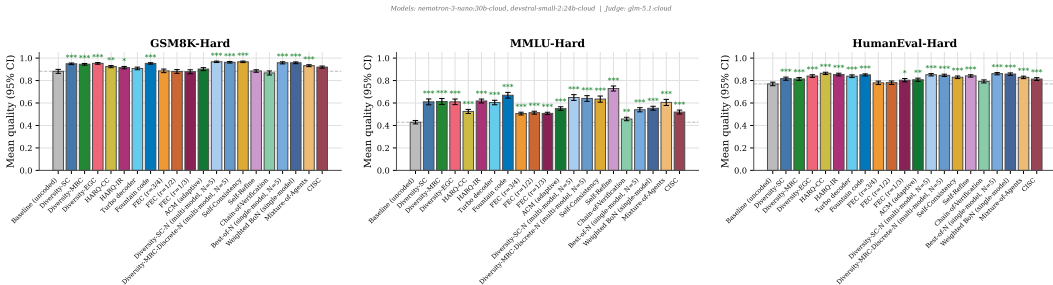


Figure 36: Per-dataset mean quality on the 300-task hard-benchmark split, one panel per dataset (GSM8K hard, MMLU hard, HumanEval hard). Dashed line is the per-dataset baseline mean; significance stars are paired Wilcoxon vs. baseline.

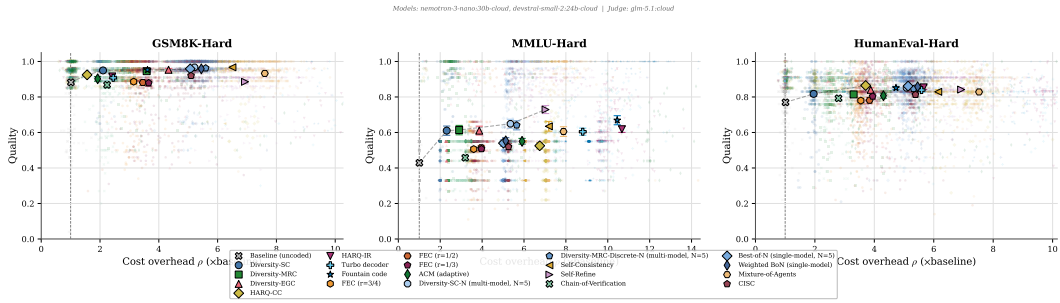


Figure 37: Per-dataset quality versus normalized cost overhead ρ on the 300-task hard-benchmark split. Dashed line is the empirical Pareto frontier; the cost-aware semantic-nearest-neighbor router of Table 3 sits on or above this frontier on every dataset.

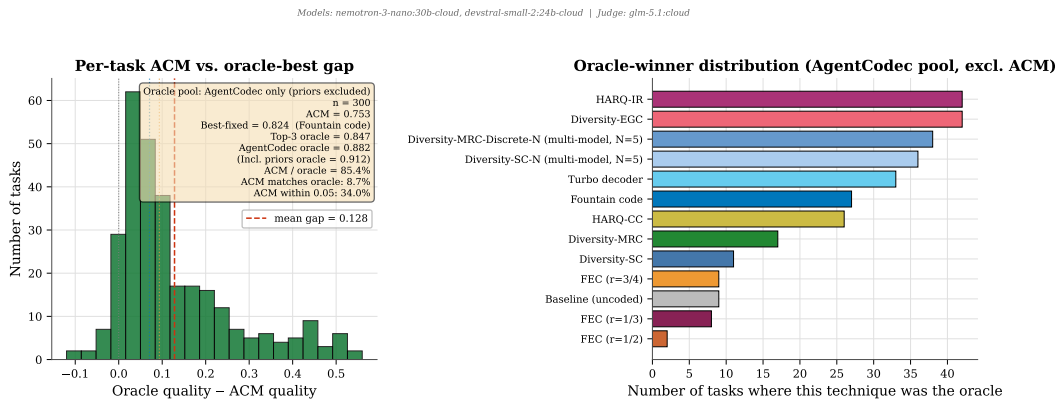
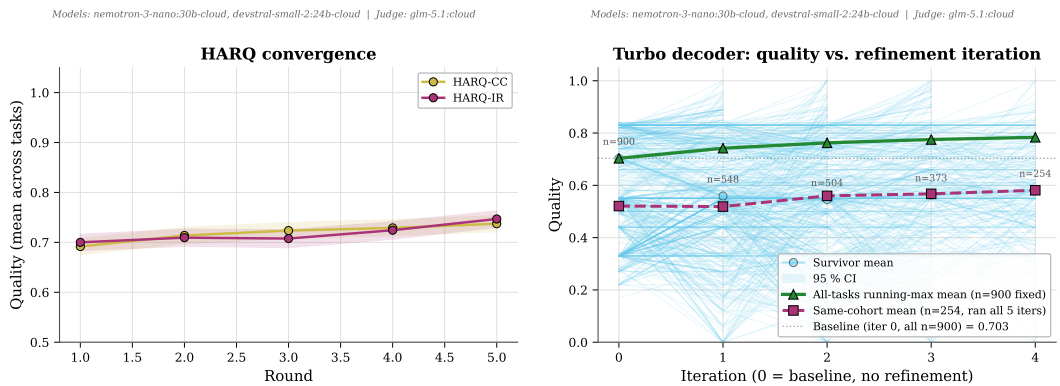


Figure 38: Ollama-cloud trio on the 300-task hard-benchmark split: ACM-router oracle-gap decomposition. The *policy* term collapses once the dispatcher is the cost-aware semantic-nearest-neighbor router; the binding constraint shifts to the feature-set information limit and the finite-sample generalization gap, as noted in Sec. E.1.



(a) HARQ convergence.

(b) Turbo iteration trajectory.

Figure 39: Ollama-cloud trio on the 300-task hard-benchmark split: iterative-refinement diagnostics.